Advanced Control Strategies to Enable a More Wide-Scale Adoption of Single-Phase Photovoltaic Systems

Yang, Yongheng

DOI (link to publication from Publisher):
10.13140/RG.2.2.15106.07367

Publication date:
2014

Document Version
Publisher's PDF, also known as Version of record

YANG, Yongheng

Advanced Control Strategies to Enable a More Wide-Scale Adoption of Single-Phase Photovoltaic Systems

Department of Energy Technology
AALBORG UNIVERSITY

DEPARTMENT OF ENERGY TECHNOLOGY
AALBORG UNIVERSITY

Advanced Control Strategies to Enable a More Wide-Scale Adoption of Single-Phase Photovoltaic Systems

Yongheng YANG

Advanced Control Strategies to Enable a More Wide-Scale Adoption of Single-Phase Photovoltaic Systems

by

Yongheng Yang

A Dissertation Submitted to
the Faculty of Engineering and Science at Aalborg University
in Partial Fulfillment for the Degree of
Doctor of Philosophy in Electrical Engineering

August 2014
Aalborg, Denmark

Aalborg University
Department of Energy Technology
Pontoppidanstraede 101
Aalborg East, DK-9220
Denmark
Phone: +45 99 40 92 40
Fax: +45 98 15 14 11
http://www.et.aau.dk

Printed in Denmark by Uniprint
First Edition (May 2014)
Second Edition (August 2014)

ISBN: 978-87-92846-40-2

Public Defence of PhD Dissertation

Thesis Title:

Advanced Control Strategies to Enable a More Wide-Scale Adoption of Single-Phase Photovoltaic Systems

Ph.D. Defendant:

Yongheng Yang

Supervisor:

Prof. Frede Blaabjerg

Moderator:

Prof. Stig Munk-Nielsen

Assessment Committee:

Prof. Claus Leth Bak (Chairman)

Department of Energy Technology
Aalborg University
Pontoppidanstraede 101
9220 Aalborg, Denmark

Prof. Jorma Kyyrä

Department of Electrical Engineering and Automation
Aalto University
Otakaari 5
00076 Aalto, Finland

Prof. Toshihisa Shimizu

Department of Electrical and Electronic Engineering
Tokyo Metropolitan University
1-1, Minami-ohaswa, Hachioji
Tokyo 192-0364, Japan

Defence Date and Place:

Wednesday, August 20, 2014
Pontoppidanstraede 101, Room 23, Aalborg University

Copyright Statements

Dedicated
to my parents for their exceptional love to the family
and
to my sisters

Preface

This thesis is written according to the project entitled "*Advanced Control Strategies to Enable a More Wide-Scale Adoption of Single-Phase Photovoltaic Systems*". The Ph.D. project is supported mainly by China Scholarship Council (CSC) and partially by the Department of Energy Technology, Aalborg University, Denmark. Acknowledgements are given to the above-mentioned institutions, as well as the Center Of Reliable Power Electronics (CORPE) and Otto Mønsteds Fond, who supported me for conference participation several times through my Ph.D. study. Special thanks to the head of the Department of Energy Technology John K. Pedersen, and Mr. Chenggang Liu from the Embassy of The People's Republic of China in The Kingdom of Denmark for their kind support and tremendous help.

This research project was done under the supervision of Prof. Frede Blaabjerg from the Department of Energy Technology, Aalborg University, Denmark. First and foremost, I would like to express my deepest gratefulness to my supervisor, Prof. Frede Blaabjerg, for his professional and patient guidance with his open-mindedness and earnestness during the Ph.D. project period. I do believe that the encouragement which I received from Prof. Blaabjerg during my Ph.D. study will be of great supportiveness for my career and through my future life.

Also, I place on record, my gratitude to Prof. Prasad Enjeti for his kindness and professional supervision during my study abroad at the Department of Electrical and Computer Engineering, Texas A&M University, TX, USA. Additionally, many thanks to Dr. Keliang Zhou from the School of Engineering, University of Glasgow, Scotland, for his comments and discussions during my Ph.D. period, and also to my friends who I met at Texas A&M University for their tremendous assistance.

In particular, I take this opportunity to record my since gratefulness to all my colleagues from the Department of Energy Technology, Aalborg University, Denmark, for the lively environment and the endless friendship. Especially, I would like to articulate my gratitude to Dr. Huai Wang for his help, sharing research experience and moral support. I also would like thank my friends Dr. Xiao Liu, Dr. Ke Ma, Dr. Xiongfei Wang, Dr. Yang Yang, Dr. Yunqian Zhang, Dr. Chi Su, Mr. Ge Xie, Mr. Dao Zhou, Mr. Jie Tian, Mr. Rui Wu, and Mr. Wenli Yao. Moreover, much special appreciations

are extended to Prof. Remus Teodorescu, Assoc. Prof. Kaiyuan Lu, Assoc. Prof. Dezső Séra, Assoc. Prof. Tamás Kerekes, Tina Lisbeth Larsen, Mette Skov Jensen, Corina Busk Gregersen, Casper Jørgensen, Mads Lund, and Walter Neumayr for their assistance in many different ways. I would also like to express my gratitude to the assessment committee for the Ph.D. defence.

Finally, the most important and the sincerest gratitude to my parents for their exceptional love to the family and their encouragement through my life, to my lovely sisters and their families, and to Ms. Xin Gao for the support, concerns and understanding.

Niels Bohr, a Danish physicist, ever said,

"*Prediction is very difficult, especially about the future*"

After this three-year Ph.D. study, I found out that life is full of miracles, and I can understand what Niels Bohr has said and the true meaning of life much better. I do be of much braveness to face it with what I have learnt from all of you. All the best for our future.

Yongheng Yang

May 20, 2014
Aalborg Øst, Denmark

Abstract

The installations of PhotoVoltaic (PV) systems, including grid-connected PV systems, have experienced a significant increase in the past few decades. More PV capacity is expected for the future power grid to be of intelligence and flexibility. This thriving scenario also raises concerns about the availability, quality and reliability of the whole power grid. Consequently, grid codes/standards are continuously being revised to host more PV energy in the grid. Ancillary services required initially by wind power systems, e.g. fault ride-through and grid support, are becoming more preferable in PV systems today than they were. In addition, achieving high efficiency and high reliability is always of importance for PV systems in order to reduce the cost of energy. Both goals can be enabled by advanced control strategies for PV systems, which are typically based on power electronics technology. In the light of those issues, the Ph.D. project has investigated and evaluated next-generation transformerless inverters for single-phase grid-connected PV systems, and proposed advanced control strategies to enhance the PV penetration with reduced cost of energy. The research work mainly includes two parts: *1) Modelling and Evaluation of Single-Phase PV Systems* and *2) Advanced Control Strategies for Single-Phase PV Systems*.

The first part, including Chapters 2 and 3, describes the entire models of the most promising transformerless PV candidates (models of PV modules, inverters, and filters) in Chapter 2. Then, a thorough evaluation of those topologies in terms of e.g. efficiency, reliability, leakage current mitigation ability, and reactive power injection capability has been presented in Chapter 3, where a multidisciplinary assessment approach with characterized features of energy production estimation and lifetime prediction based on mission profiles (e.g. solar irradiance level and ambient temperature) has been proposed. Grid detection and synchronization techniques have also been discussed in Chapter 2, since they are of importance in the control of single-phase systems both in normal operation mode with maximum power point tracking and under grid faults.

According to those investigations, advanced control strategies, which are able to ensure a flexible, reliable and efficient power conversion from PV systems in different operation modes, have been proposed and implemented in Chapters 4 to 6. The first discussed advanced control strategy is about the low voltage ride-through control of

single-phase PV systems, which can contribute to the grid voltage stability and the avoidance of energy losses during low-voltage grid faults. Then, a constant power generation control (reduced power control) strategy has been introduced in Chapter 5 with the purpose to accept more PV energy without violating the distribution grid capacity. Other benefits of constant power generation control have also been explored in that chapter. Finally, thermal optimized control strategies are discussed in order to improve the reliability of PV inverters, and thus an extended lifetime of the entire system is expected.

It has been found from the research work that the penetration level of PV systems will be much higher with the demand of clean power generation, leading to an evolution of grid standards. The presented verification results reveal that the proposed advanced control strategies can underpin the increase of power electronics based PV systems. It is expected that the outcome of this work documented in this thesis would make a contribution to the development and implementation of new single-phase grid standards regarding PV interconnection and novel control strategies in the future. Finally, a more wide-scale adoption of PV energy can be realized with reduced cost of energy.

Danske Abstrakt

Installationen af solcelle (PV) - systemer, herunder nettilsluttede solcelleanlæg, har oplevet en markant stigning i de seneste årtier. I det fremtidige elnet forventes endog mere PV kapacitet og disse systemer skal være både intelligent og fleksible. Dette voksende kapacitets scenarie rejser også bekymringer om tilgængelighed, kvalitet og pålidelighed af hele elnettet. Derfor er net-tilslutnings standarderne løbende blevet revideret for at muliggøre endnu mere PV energi til elnettet. Hjælpefunktioner, som i første omgang har været krævet til vindkraftsystemer, fx fejl ved spændingsdyk og normalt net støtte, forventes også at blive anvendt i solcelleanlæg i fremtiden. Hertil kommer at høj effektivitet og høj pålidelighed altid er vigtig for solcelleanlæg for at kunne reducere prisen på den producerede energi. Begge mål kan realiseres ved nye avancerede styre strategier for solcelleanlæg, som baserer sig på effektelektronik. I lyset af disse udfordringer, har Ph.D. projektet undersøgt og evalueret den næste generation af transformerløs invertere til en-fasede nettilsluttede solcelleanlæg, og har foreslået nye avancerede kontrol- strategier til at forbedre PV udbredelsen med reducerede omkostninger til energien. Arbejdet i afhandlingen omfatter primært to dele: *1) Modellering og evaluering af en-fasede solcelleanlæg* og *2) Avancerede kontrol strategier for en-fasede solcellesystemer.*

Den første del, som er beskrevet i kapitel 2 og kapitel 3, omhandler beskriver modellene af de mest lovende transformerløse PV omformere (PV moduler, invertere, og filtre). Derefter er der foretaget en grundig evaluering af disse topologier i form af effektivitet, pålidelighed, lækstrøm, og reaktiv effekt kapacitet i kapitel 3. Desuden er der foretaget en tværfaglig vurdering af de forskellige funktioner i forbindelse med estimering af energiproduktion og levetid forudsigelse baseret på solcelle systemernes mission profiler (f. eks. solstråling og rumtemperatur). Detektion og synkronisering af net-tilslutningen er også diskuteret i kapitel 2, da de er af betydning for kontrol af en-fasede systemer både i normal drift med maksimal power point tracking og under netfejl.

Avancerede kontrol- strategier som vil være i stand til at sikre en fleksibel, pålidelig og effektiv effekt konvertering fra solcelleanlæg i forskellige driftstilstande er blevet foreslået og gennemført i kapitel 4 til kapitel 6. Den første diskuterede kontrol strategi

omhandler styring under lav spænding af en-fasede solcelleanlæg, og som kan bidrage til el-nettets spændings-stabilitet og reduktion af energitabet under denne fejl. Derefter er der foreslået en konstant el-produktion kontrol (reduceret power kontrol) strategi i kapitel 5 med det formål at acceptere mere PV energi uden at overstige el-distributions nettets kapacitet. Andre fordele ved konstant el-produktion kontrol er også blevet undersøgt f. eks. at levetiden forøges. Endelig er termisk optimerede styringsstrategier diskuteret med henblik på at forbedre pålideligheden af PV invertere, og dermed kan forventes en forlænget levetid på hele systemet.

I dette projekt er det konkluderet at udbredelsen af solcelleanlæg vil blive meget højere i fremtiden i forbindelse med at efterspørgslen af mere ren el-produktion er stigende, hvilket samtidig fører til en videreudvikling af eksisterende net-standarder. De præsenterede resultater viser, at de nye foreslåede avancerede kontrolstrategier kan understøtte væksten i effektelektronik baserede solcellesystemer. Det forventes, at resultatet af dette arbejde giver et bidrag til udvikling og implementering af nye en-fasede net standarder vedrørende PV tilslutning til nettet og samt implementering af nye kontrol strategier. Endelig vil en sådan mere storstilet udbredelse af PV energi medføre en yderligere reduktion of energi-prisen for solenergi.

Contents

List of Figures

List of Tables

Report

Part I

Preamble

*This part is the preamble of the documented Ph.D. project, which includes one chapter - **Chapter 1**. Introduction.*

1 Introduction

This chapter firstly presents the background and motivation of this research project. It also includes a short state-of-the-art of grid-connected PhotoVoltaic (PV) technologies, followed by the objectives and limitations of the project. Then, the thesis structure is presented to give a better understanding about the flow of this research work. All the publications related to this work are listed at the end of this chapter.

1.1 Background and motivation

Solar PV energy is of increasing competitiveness and utilization in power generation systems as an alternative to fossil energy resources [1–7]. It has been reported that the global cumulative PV capacity is now more than 136.7 GW as shown in Figure 1.1. This strong market is mainly shared by the European countries, such as Germany, Spain and Italy, in contrast to other countries. Even so, driven by a common target of lowering cost of energy in most countries, electricity generation from PV systems will take a major share in the future.

For instance, recent reports show that many countries have set ambitious goals for the next few decades to accept highly penetrated PV systems as a part of their renewable energy systems. The European Commission has set a "2020" renewable target, in which it is stated that 12% of European electricity demand will be supplied by PV systems by 2020 [1]. Even Denmark, which has quite limited sunshine in the winter, is also accelerating the pace of PV installations and reshaping its future renewable energy

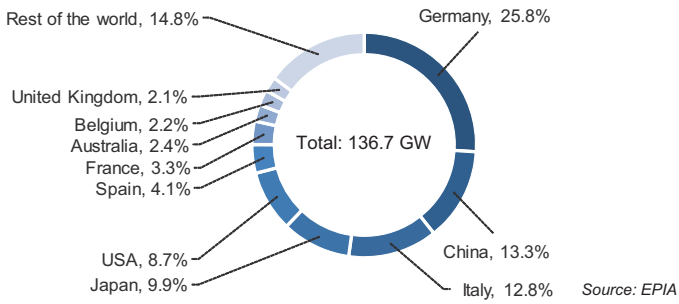

Figure 1.1: *PV cumulative installation capacity world-wide share in 2013 (%).*

structure. Moreover, Japan has set a national goal of 60 GW of PV capacity by 2030, and the total installed PV capacity in U.S. reached 3.3 GW in 2012 [8–11]. Thus, it can be seen that there are increasingly world-wide expectations for energy production by means of solar (PV) energy systems.

Nevertheless, the high penetration level of PV systems especially imposes new challenges for the Distributed System Operators (DSO) and the end-consumers. It may introduce significant impacts on the availability, quality and reliability of the electrical grid, since it makes the distributed networks more decentralized, uncontrollable and heterogeneous [12, 13], leading to discussions of appropriate adoption of PV power systems. Consequently, on one hand, grid regulations are continuously updated so as to enhance the PV hosting capacity in distributed grids [12, 14–28]. On the other hand, it calls for an emerging development of advanced control strategies accordingly.

Current active grid requirements are applied mostly to three-phase systems connected to Medium-Voltage and/or High-Voltage (MV/HV) grids for grid stability concern [14, 29, 30]. Whilst, for single-phase systems, the demands are focused on islanding protection and energy maximization, and there are not so many demands on the Fault Ride-Through (FRT) capability [31–38], which may also induce instability of the entire grid as the PV systems may contribute a large amount of short-circuit power [19–22, 31, 39, 40]. Therefore, it is essential to assess the grid fault effects on the control of single-phase grid-connected PV systems, and also to develop advanced control strategies to further enable an increase of the penetration degree of PV systems with cost-effective solutions. In addition, the basic requirements, related to active power output, frequency control dependent on active power, power quality and voltage stability, should also be fulfilled by every generating system [23, 24, 26, 41]. The major demands for a grid-connected PV system are summarized in Figure 1.2, which shows the requirements at different levels of the system.

As the interface of PV generators (i.e. PV panels) and the grid shown in Figure 1.2, power electronic technology (i.e. PV inverters), is one key to achieve the above require-

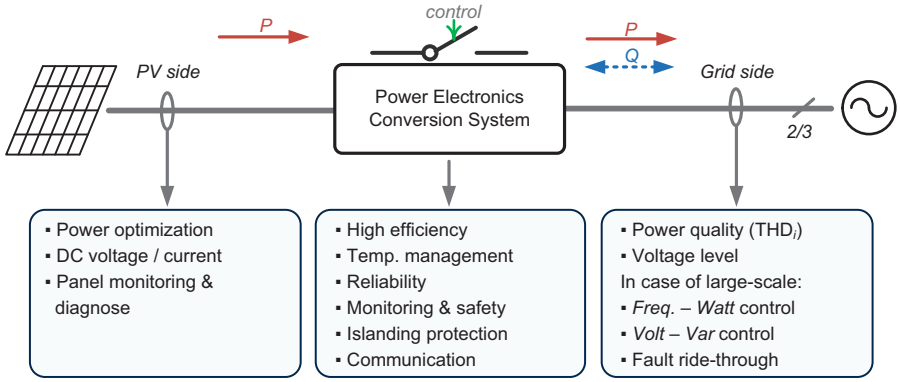

Figure 1.2: *Demands for a grid-connected PV system.*

ments associated by the advanced control strategies, while it has also been one of the most often life-limiting components of PV systems and produces harmonics. Firstly, in order to reduce switching harmonics injection from power converters, an alternative and attractive solution is to use an *LCL*-filter in the PV system [42, 43]. As for the low-order harmonics, advanced control methods could be employed to suppress the injected harmonics [15, 41]. Furthermore, transformerless inverters could be adopted to meet the demands like high efficiency, small size and weight, and low price [12, 16, 44–48]. Moreover, the stresses of those topologies differ with the operating environmental conditions (e.g. mission profiles and voltage sags). By appropriate design and optimization of the DC-link capacitor and the control system, both electrical and thermal stresses on the capacitor and the power electronics devices can be realigned [12, 15, 49]. As the electrical redistributions will affect the power losses, the efficiencies of those topologies are changed. Since the thermal stress is the most observed factor that induces failures of the power electronics system [50–53], improvement of the entire system reliability, being an emerging requirement for PV systems in order to reduce the cost of energy, can be achieved by internal thermal optimization and control.

1.1.1 Overview of grid-connected PV configurations

According to the state-of-the-art technologies, there are mainly four configuration concepts [6, 16, 21] to organize and transfer the PV power to the grid, as it is shown in Figure 1.3. Each of the concepts consists of series of paralleled PV panels or strings, and they are configured by a couple of power electronics converters (DC-DC converters and DC-AC inverters), depending on the output voltage of the PV panels.

A common central inverter is generally adopted for the residential or utility PV systems of tens kWp, in order to achieve lower conversion losses and lower cost. Figure

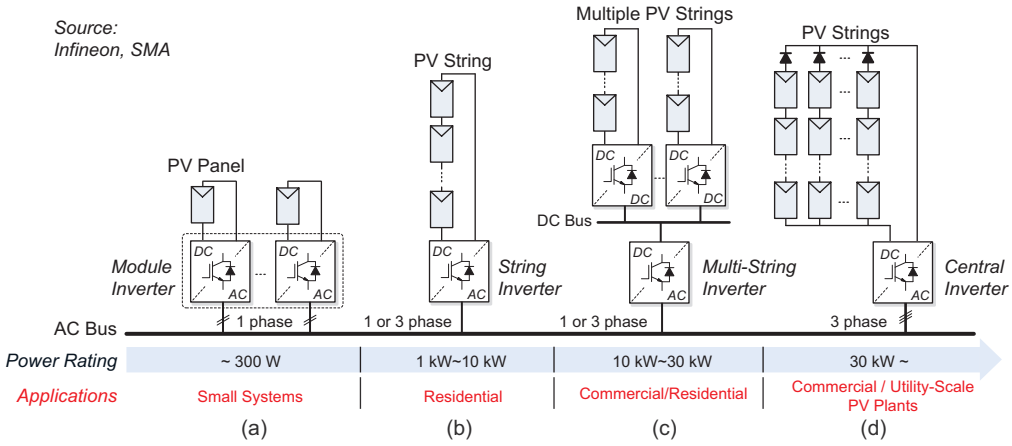

Figure 1.3: *Grid-connected PV systems with: (a) module inverter, (b) string inverter, (c) multi-string inverter, and (d) central inverter [6, 16, 21].*

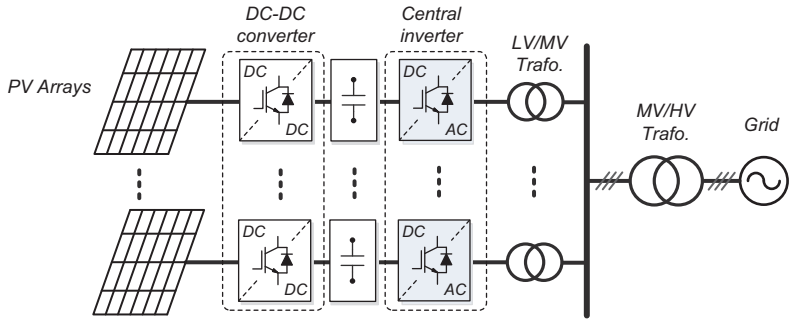

Figure 1.4: *Utility-scale PV power plant configuration based on central inverters.*

1.4 presents an example of large-scale PV power systems for commercial or utility applications with central inverters and DC-DC converters. The major disadvantages of this configuration include that the wiring requires high voltage DC cables (and thus arc protection), and the common Maximum Power Point Tracking (MPPT) for many panels and module mismatching may increase the energy losses [6, 16, 54, 55], especially in a harsh operating environment where the solar irradiance level changes at a rapid rate, and maybe also in dirty areas. In contrast, the string inverter is more promising, because it can achieve MPPT control separately, leading to a better total energy yield. Yet, there are mismatching issues in the PV panels connected in series as well, and thus, the module inverter is introduced, which acts on an individual PV panel with a

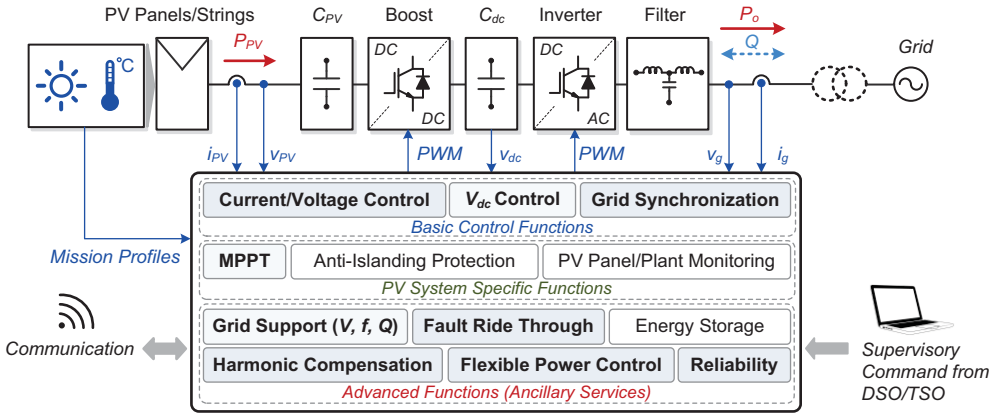

Figure 1.5: *Control functions of a single-phase grid-connected PV system.*

single MPPT. The main disadvantage of a module inverter is the low overall efficiency. Another grid-connected PV technology is an intermediate solution between the string inverter and the module inverter technologies, being multi-string inverter, and it combines the advantages of both technologies. This configuration is flexible with a high overall efficiency because each PV string is controlled separately.

Since PV systems are still dominant in residential applications with much lower power ratings (e.g. several kWs) compared to wind turbine power systems, at present, single-phase topologies are more widely-used solutions for PV applications, where a DC-DC converter is adopted to boost up the PV panel voltage within an acceptable range of the PV inverter, as it is shown in Figure 1.5. The boost converter also extends the operating time when the solar irradiation is very low, and offers the flexibility of extracting the maximum PV power (i.e. MPPT), which is an essential demand for PV systems as shown in Figure 1.2. Hence, the single-phase string-inverter configuration is analyzed in this project, and the focuses are highlighted in Figure 1.5. Notably, even for large-/utility- scale PV power plants, three single-phase configurations with center or string inverters are preferred by some industries for reliability concern [12, 14, 56].

As for grid-connected PV systems, the galvanic isolation for safety is one important issue, and another is related to the conversion efficiency, as shown in Figure 1.2. Traditionally, an isolation transformer can be adopted either at the grid-side with low frequencies or as a high frequency transformer as shown in Figure 1.6(a) and (b). Both PV technologies are available on the market with an efficiency of 93-95% [12]. In contrast, transformerless systems (Figure 1.6(c)) are increasing in popularity because of the achievements in higher efficiency. However, when the transformer is removed from a grid-connected PV system, safety concerns (e.g. leakage current) will arise since the

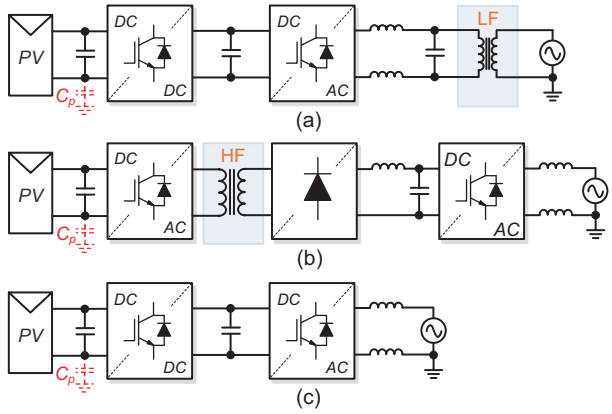

Figure 1.6: *Single-phase grid-connected PV systems: (a) with a low-frequency (LF) transformer, (b) with a high-frequency (HF) transformer, and (c) without transformer.*

lack of galvanic isolations, which leads to the necessity to reduce the leakage current, e.g. by including passive damping components, by modifying the modulations, or by adding extra switching devices to realize the isolation [47, 57, 58]. Besides low conversion losses, transformerless topologies are lighter than their counterparts used in PV systems, which may also lower the cost.

A vast number of different transformerless topologies have been developed [12, 44, 45, 49, 57–60], and the success of them in Europe has also proved the impact of efficiency improvement. It should be pointed out that the first priority of a transformerless inverter is to avoid the generation of leakage currents by means of the aforementioned solutions or with the incorporation of advanced control strategies. In order to further increase the penetration level of PV systems, transformerless topologies will be even more widely adopted in the future. Consequently, those transformerless inverters are required to comply with relevant directives and standards, and thus pave the way for next-generation PV systems to take a major part in electricity generation.

1.1.2 Project motivation

With more national objectives which have been initiated to solve the emerging energy crisis, more distributed generation systems, especially PV systems, are expected to be installed and will be hooked up to the grid. As a result, those PV systems will feed a large portion of fluctuating power into the grid at various connection-points along the distributed electrical lines. Additionally, an increase of PV energy adoption also comes with a set of new challenges for the system operators as discussed above. Hence, new, stringent and specific grid demands are expected to come into force to guide the

integration [5,20–22,47]. Besides, achieving high reliability of power electronics devices is always of paramount interest. This reliability (lifetime) demand for next-generation PV systems will be further strengthened in order to guarantee reliable PV power generation with reduced cost of energy. In those cases, it would be desirable for the inverters to have enhanced functionalities complied with grid codes/requirements by retrofitting existing PV systems or considering a replacement of all PV systems.

However, current active grid standards seem to largely require low power (e.g. several kWs) single-phase PV systems to operate at unity power factor with MPPT control, and disconnect from the grid under grid faults. In the case of a wide-scale penetration of single-phase PV systems in the distributed grid, the disconnection under grid faults may contribute to: a) voltage flickers, b) power outages, and c) system instability. Meanwhile, due to intermittency, the output power will fluctuate, and thus leading to additional maintenance and operational costs, and even early replacement. Those aspects have to be coped with in the design and operation of next-generation PV systems.

Actually, PV systems can make significant contributions to an efficient and reliable electricity generation without violating the conventional grid infrastructure. Key benefits can be obtained from advanced control of PV systems, such as a) mitigation of voltage variations, b) avoidance of PV generation loss due to anti-islanding shutdown, c) improvement of system stability, d) achievement of improved power quality, e) increasing de-centralization of power generation, and f) extension of lifetime of the converter. As the core of a PV power conversion system, the PV inverter has to perform "smart" functionalities imposed by both the system operators and consumers like what the conventional power plants can do. It should be pointed out that, in contrast to the conventional power systems, the PV inverters are inertialess, which may affect the frequency controllability. Nonetheless, those advanced functionalities of next-generation PV inverters can be enhanced by means of intelligent control strategies.

The above considerations initiated the research project. In summary, the major motivation of this project is to examine the appropriation of enabling advanced PV functionalities in order to accept more PV energy, and thus to develop advanced control strategies to ensure a more wide-scale adoption of PV systems in the future grid.

1.2 Project objectives and limitations

1.2.1 Research questions and objectives

In order to enhance the grid integration of PV systems with lowered cost of energy, the PV penetration degree will be further increased in the future energy mix. It also rises emerging challenges that need to be dealt with:

- *What benefits will be brought by an even high penetration of PV systems in addition to carbon-dioxide emission reduction?*

- *Can highly-penetrated single-phase PV inverters be improved to better support the future grid infrastructure?*
- *What control strategies can be developed to cater for more PV installations and also to obtain the potential benefits?*
- *Are there any solutions to further reduce the cost of solar PV energy?*

With those research questions, one objective of this PhD project is to evaluate and improve the performance of single-phase transformerless PV system also including reliability issues when the mission profiles are taken into consideration. The primary goal of this project will be focused on the analysis and control of single-phase transformerless PV systems in different operation modes based on the former evaluation, and consequently, advanced control strategies are proposed to further increase the penetration level of PV systems. The objectives of this project are solved in details by:

Modeling and Evaluation of Transformerless Inverters-
This focuses on an assessment of several mainstream transformerless PV inverters in terms of efficiency, low voltage ride-though capability, and reliability based on real-field mission profiles. To reach this goal, the electrical models of the inverters, the thermal models of the DC-link capacitors and power electronics devices used in transformerless topologies are established. Hence, optimization of the whole systems with reduced cost of energy can be conducted to meet the requirements such as high reliability, high efficiency, small size and weight, and low price.

Propose and Refine Grid Detection and Synchronization Techniques-
In order to guarantee a correct generation of the reference signals for single-phase PV systems in different operation modes, there must be an accurate and fast grid condition monitoring technique. A state-of-the-art synchronization method applied in single-phase PV systems will be done in this project. Proposals or refinement of existing techniques are expected.

Advanced Control of Single-Phase Grid-Connected PV Systems-
A benchmarking of possible control strategies for single-phase PV systems in different operation modes will be carried out. Advanced control strategies will be proposed and developed according to the evaluations and comparisons. The proposed control strategies are supposed to help the PV system to ride-through grid faults, to ensure the power quality and stability in different operation modes, to better support the grid, and as a consequence to further increase the penetration degree of PV systems.

1.2.2 Project limitations

There are many ways and many topologies available in the literature and on the market, but only three mainstream single-phase transformerless topologies are considered in this project. The evaluation methods developed in this project can later be adopted for different topologies and other renewable energy systems, even in three-phase systems,

but minor adaptations and modifications might be necessary with a better knowledge of mission profiles.

All the experiments included in this project were carried out on commercial inverters, which are supplied by DC power sources. This is not a real representation of PV strings or modules. It is effective only when an assumption of an accurate and robust MPPT control is assured. As for the reliability verifications, far more research is required since the lifetime tests are time-consuming, and accelerating lifetime tests have not been done either. The mission profiles used in this project have a sampling period of around 200 ms. The processed data for evaluations may affect the accuracy of the results.

Although the discussions in this project are based on a high penetration level of single-phase PV systems, only a typical residential PV system with the power of several kWs is studied in this project. All the developed control strategies are conducted on this system at this power level. The interactive effect of large-scale aggregated PV systems at a system-level on the power grid also calls for further investigations.

1.3 Thesis outline

The final outcomes of this project are documented in the form of Ph.D. thesis, including a report of the project and a collection of the selected publications through the entire study. In the ***Report***, a summary of this research work is presented, whilst in the ***Selected Publications***, relevant papers derived from this project during the Ph.D. study period are collected selectively. The thesis structure is shown in Figure 1.7.

As shown in Figure 1.7, the ***Report*** consists of seven chapters, which can be divided into four main parts. The first part is the preamble, which includes one chapter - *Chapter 1. Introduction*. The second part- "*Modelling and Evaluation of Single-Phase PV Systems*" covers two chapters. *Chapter 2. Modelling of Single-Phase PV Systems* presents the models of the PV systems, and also the synchronization techniques. A benchmarking of synchronization techniques is also included. *Chapter 3. Evaluation of Single-Phase PV Inverters* is focused on the evaluation of mainstream transformerless PV inverters in terms of efficiency and reliability. The third part is entitled "*Advanced Control Strategies for Single-Phase PV Systems*", covering three chapters. *Chapter 4. Control of PV Systems in Different Operations* presents the basic control and advanced control strategies for single-phase grid-connected PV systems in the normal operation and under grid faults. *Chapter 5. Constant Power Generation Control Concept* is focused on the constant power generation control of single-phase PV systems to enable a wide-scale adoption of PV energy in the line without expanding power grid infrastructure. *Chapter 6. Thermal Optimized Control Strategy* deals with the thermal optimized control method to further increase the reliability of the PV systems and thus to reduce the cost of energy. The ***Report*** is ended with one chapter - *Chapter 7. Summary and Outlook*, which gives the conclusions, summarizes the main contributions, and presents research perspectives enabled by the documented project.

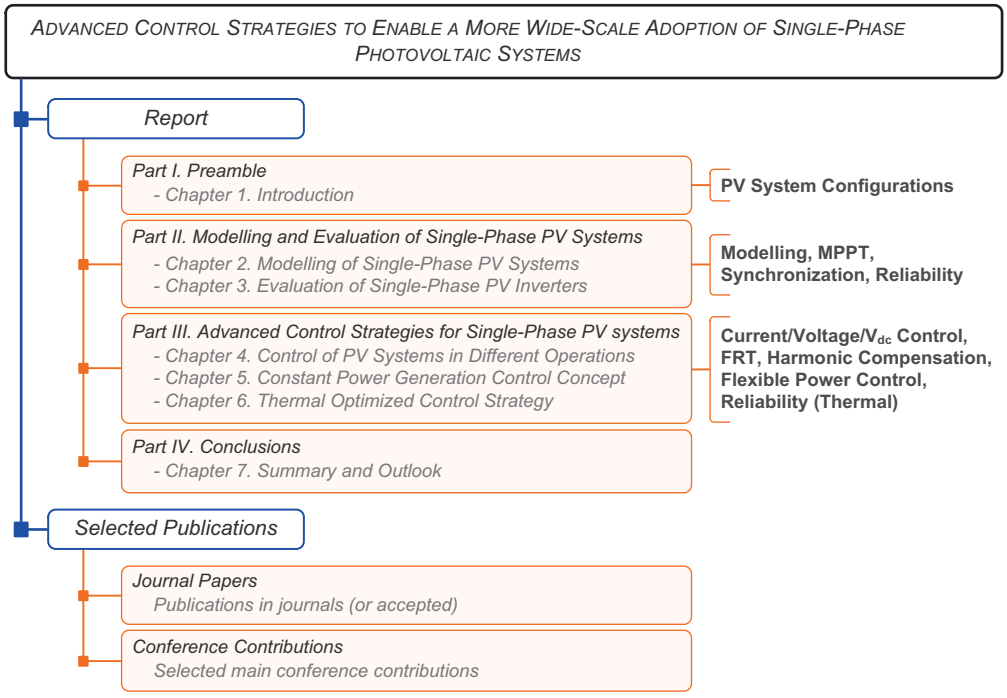

Figure 1.7: *Thesis structure and covered topics of each part in Figure 1.5.*

The ***Selected Publications*** is a collection of relevant disseminations based on this project. It includes several peer-reviewed Journal Papers (published or accepted) and Conference Contributions.

1.4 List of publications

A list of the papers derived from this project, which are published till now or have been submitted, is given as follows:

Journal Papers

J1. **Y. Yang** and F. Blaabjerg, "Low voltage ride-through capability of a single-stage single-phase photovoltaic system connected to the low-voltage grid," *International Journal of Photoenergy*, vol. 2013, 9 pages, 2013. [Open Access]. DOI:10.1155/2013/257487.

J2. **Y. Yang**, F. Blaabjerg, and Z. Zou, "Benchmarking of grid fault modes in single-phase grid-connected photovoltaic systems," *IEEE Trans. Ind. Appl.* (also in *Proc. of ECCE'12*), vol. 49, no. 5, pp. 2167-2176, Sept./Oct. 2013.

J3. **Y. Yang**, F. Blaabjerg, and H. Wang, "Low voltage ride-through of single-phase transformerless photovoltaic inverters," *IEEE Trans. Ind. Appl.* (also in *Proc. of ECCE'13*), vol. 50, no. 3, pp. 1942-1952, May/Jun. 2014.

J4. **Y. Yang**, P. Enjeti, F. Blaabjerg, and H. Wang, "Suggested grid code modifications to ensure wide-scale adoption of photovoltaic energy in distributed power generation systems," *IEEE Ind. Appl. Mag.* (also in *Proc. of IAS Annual Meeting 2013*), vol. 99, no. 99, in press, Sept./Oct. 2015.

J5. **Y. Yang**, H. Wang, and F. Blaabjerg, "Reduced junction temperature control during low-voltage ride-through for single-phase photovoltaic inverters," *IET Power Electron.*, vol. 7, no. 8, pp. 2050-2059, Aug. 2014.

J6. **Y. Yang**, H. Wang, and F. Blaabjerg, "Reactive power injection strategies for single-phase photovoltaic systems considering grid requirements," *IEEE Trans. Ind. Appl.* (also in *Proc. of APEC'14*), vol. 50, no. 6, in press, pp. 1-12, Nov./Dec. 2014.

J7. **Y. Yang**, H. Wang, F. Blaabjerg, and T. Kerekes, "A hybrid power control concept for PV inverters with reduced thermal loading," *IEEE Trans. Power Electron.* (also in part presented at *APEC'14*), vol. 29, no. 12, pp. 6271-6275, Dec. 2014.

J8. **Y. Yang**, K. Zhou, H. Wang, F. Blaabjerg, D. Wang, and B. Zhang, "Frequency adaptive selective harmonic control for grid-connected inverters," *IEEE Trans. Power Electron.*, in press, pp. 1-13, 2015.

Book Chapters

B1. K. Ma, **Y. Yang**, and F. Blaabjerg, "Introduction to renewable energy systems," in *Advanced and Intelligent Control in Power Electronics and Drives*, vol. 531, Springer, pp. 3-40, Jan. 2014.

B2. **Y. Yang**, W. Chen, and F. Blaabjerg, "Advanced Control of Photovoltaic and Wind Turbines Power Systems," in *Advanced and Intelligent Control in Power Electronics and Drives*, vol. 531, Springer, pp. 41-89, Jan. 2014.

B3. K. Ma, **Y. Yang**, H. Wang, and F. Blaabjerg, "Design for reliability of power electronics in renewable energy systems," in *Use, Operation and Maintenance of Renewable Energy Systems - Experiences and Future Approaches*, Springer, pp. 295-338, May 2014.

Conference Contributions

C1. **Y. Yang** and F. Blaabjerg, "A modified P&O MPPT algorithm for single-phase PV systems based on deadbeat control," in *Proc. of IET PEMD'12*, pp. 1-5, Mar. 2012.

C2. **Y. Yang** and F. Blaabjerg, "Synchronization in single-phase grid-connected photovoltaic systems under grid faults," in *Proc. of PEDG'12*, pp. 476-482, June 2012.

C3. **Y. Yang**, F. Blaabjerg, and Z. Zou, "Benchmarking of voltage sag generators," in *Proc. of IECON'12*, pp.943-948, Oct. 2012.

C4. **Y. Yang**, K. Zhou, and F. Blaabjerg, "Harmonics suppression for single-phase grid-connected photovoltaic systems in different operation modes," in *Proc. of APEC'13*, pp. 889-896, Mar. 2013.

C5. **Y. Yang**, H. Wang, and F. Blaabjerg, "Thermal optimized operation of the single-phase full-bridge PV inverter under low voltage ride-through mode," in *Proc. of PCIM Europe'13*, pp. 1055-1062, May 2013.

C6. **Y. Yang** and F. Blaabjerg,"A new power calculation method for single-phase grid-connected systems," in *Proc. of ISIE'13*, pp. 1-6, May 2013.

C7. **Y. Yang**, H. Wang, F. Blaabjerg, and K. Ma, "Mission profile based multi disciplinary analysis of power modules in single-phase transformer-less photovoltaic inverters," in *Proc. of EPE'13 ECCE Europe*, pp. P.1-P.10, Sept. 2013.

C8. **Y. Yang**, F. Blaabjerg, and H. Wang, "Constant power generation of photovoltaic systems considering the distributed grid capacity," in *Proc. of APEC'14*, pp. 379-385, Mar. 2014.

C9. **Y. Yang**, H. Wang, and F. Blaabjerg, "Improved reliability of single-phase PV inverters by limiting the maximum feed-in power," in *Proc. of ECCE'14*, accepted, Sept. 2014.

C10. **Y. Yang**, K. Ma, H. Wang, and F. Blaabjerg, "Mission profile translation to DC-link capacitor stresses in grid-connected photovoltaic systems," in *Proc. of ECCE'14*, accepted, Sept. 2014.

There are also other publications contributed by the results of this project. Those are listed below:

Co-Authored Publications

O1. Z. Zou, Z. Wang, M. Cheng, and **Y. Yang**, "Active power filter for harmonic compensation using a digital dual-mode-structure repetitive control approach," in *Proc. of PEDG'12*, pp. 161-166, Jun. 2012.

O2. H. Wang, **Y. Yang**, and F. Blaabjerg, "Reliability-oriented design and analysis of input capacitors in single-phase transformerless PV inverters," in *Proc. of APEC'13*, pp. 2929-2933, Mar. 2013.

O3. K. Zhou, W. Lu, **Y. Yang**, and F. Blaabjerg, "Harmonic control: A natural way to bridge resonant control and repetitive control," in *Proc. of ACC'13*, pp. 3189-3193, Jun. 2013.

O4. M. Huang, F. Blaabjerg, **Y. Yang**, and W. Wu, "Step by step design of a high order power filter for three-phase three-wire grid-connected inverter in renewable energy system," in *Proc. of PEDG'13*, pp. 1-8, Jul. 2013.

O5. C. Sintamarean, F. Blaabjerg, H. Wang, and **Y. Yang**, "Real field mission profile oriented design of a SiC-based PV-inverter application," in *Proc. of ECCE'13* (also *IEEE Trans. Ind. Appl.*), pp. 940-947, Sept. 2013.

O6. F. Blaabjerg, **Y. Yang**, and K. Ma, "Power electronics – Key technology for renewable energy systems – Status and future," in *Proc. of EPECS'13*, pp. 1-7, Oct. 2013.

O7. R. Pena-Alzola, M. Liserre, F. Blaabjerg, and **Y. Yang**, "Robust design of *LCL*-filters for active damping in grid converters," in *Proc. of IECON'13* (also submitted to *IEEE Trans. Ind. Informatics*), pp. 1248-1253, Nov. 2013.

O8. F. Blaabjerg, K. Ma, and **Y. Yang**, "Power electronics for renewable energy systems - status and trends," in *Proc. of EVER'14* (also submitted to *IEEE Trans. Power Electron.*), pp. 1-11, Mar. 2014.

O9. K. Zhou, **Y. Yang**, F. Blaabjerg, W. Lu, and D. Wang, "Selective harmonic control for power converters," in *Proc. of ECCE'14*, accepted, Sept. 2014.

O10. W. Yao, F. Blaabjerg, X. Zhang, **Y. Yang**, and Z. Gao, "Zero sequence blocking transformers for multi-pulse rectifier in aerospace applications," in *Proc. of ECCE'14*, accepted, Sept. 2014.

O11. L. Hadjidemetriou, E. Kyriakides, **Y. Yang**, and F. Blaabjerg, "Power quality improvement of single-phase photovoltaic systems through a robust synchronization method," in *Proc. of ECCE'14*, accepted, Sept. 2014.

O12. K. Ma, **Y. Yang**, and F. Blaabjerg, "Transient modelling of loss and thermal dynamics in power semiconductor devices," in *Proc. of ECCE'14*, accepted, Sept. 2014.

O13. K. Zhou, **Y. Yang**, F. Blaabjerg, and D. Wang, "Optimal selective harmonic control for power harmonics mitigation," *IEEE Trans. Ind. Electron.*, in press, pp. 1-10, 2015.

Since these papers provide technical explanations and validation results for the ***Report*** of this thesis, the relationship between the publications listed above and the chapters of this thesis is summarized in Table 1.1, in order to give a better understanding of the research project.

Table 1.1: *Relationship between publications and chapters of the report.*

Chapter No.	Relevant Publications
1	J4, B1, O6, O8
2	J2, B1, C1, C2, O2, O11, O12
3	J3, B3, C7, C9, C10, O2, O5, O6
4	J1, J2, J3, J4, J6, J8, B2, C2, C3, C4, C6, O3, O9, O13
5	J7, B2, C8, C9, O8
6	J5, J6, B3, C5, O3
7	-

Part II

Modelling and Evaluation of Single-Phase PV Systems

Referring to Figure 1.5, the second part of the Ph.D. thesis includes two chapters. ***Chapter 2****. Modelling of Single-Phase PV Systems presents both electrical and thermal models of the selected transformerless PV systems as well as synchronization techniques. A benchmarking of synchronization methods is also discussed.* ***Chapter 3****. Evaluation of Single-Phase PV Inverters is focused on an evaluation of three transformerless PV inverters in terms of efficiency, leakage current rejection, and reliability.*

2 Modelling of Single-Phase PV Systems

This chapter focuses on modelling of single-phase PV systems. Firstly, a discussion of the PV module model and commonly-used MPPT algorithms is given, followed by a description of three transformerless topologies, including thermal models for power devices and capacitors, and a basic comparison of grid-side filters. Then, synchronization techniques are discussed and evaluated. A summary is provided at the end.

2.1 PV module model and MPPT control

2.1.1 Modelling of PV panel

As the core and source of a PV power conversion system as shown in Figure 1.5, PV panels are directly or indirectly connected to the DC-AC inverter, where a boost stage may be necessary depending on the input voltage level of the inverter. For grid-connected applications, the typical input voltage is within a range of 200 $\sim$ 800 V, e.g. 400 V for single-phase systems. Thus, a series of PV panels are required to feed string/central

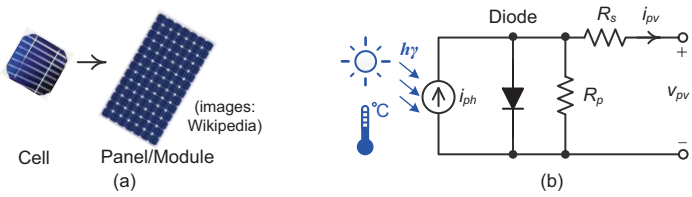

Figure 2.1: *A PV module: (a) from PV cells to module and (b) PV cell model.*

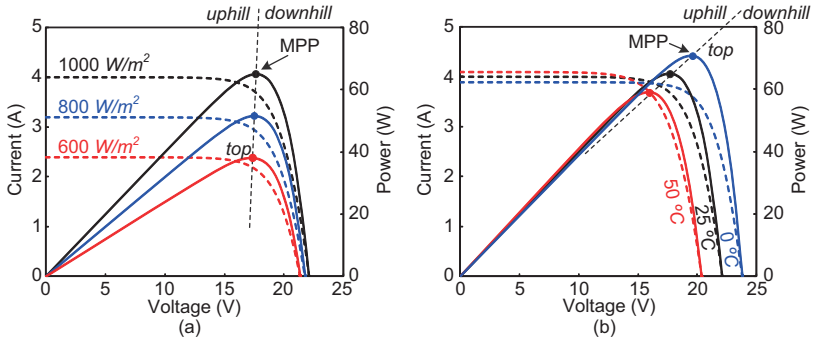

Figure 2.2: *Characteristics of a PV panel (65 W): (a) different solar irradiance levels at 25 °C and (b) different ambient temperatures at 1000 W/m².*

inverters. Likewise, a PV panel/module is an assembly of many PV cells connected in series (increased output voltage) and in parallel (increased output current), as it is shown in Figure 2.1, where a single-diode model of the PV module [61–63] is also given. Thus, the output characteristics of a PV cell can be expressed as,

$$i_{pv} = i_{ph} - i_0 \left[\exp\left(\frac{v_{pv} + i_{pv} R_s}{n k_B T / q}\right) - 1 \right] - \frac{v_{pv} + i_{pv} R_s}{R_p} \tag{2.1}$$

where i_{pv} and v_{pv} are the PV cell output current and voltage, respectively, i_{ph} is the photo-generated current and is proportional to the solar irradiance level, i_0 is the saturation current of the diode, q is the charge of an electron, n is the ideality factor of the $p-n$ junction, k_B is the Boltzmann constant, T is the cell temperature in Kelvin, R_s and R_p are the PV cell series and shunt resistances, respectively, and $R_s \ll R_p$.

As it has been shown in Figure 2.1 and Eq. (2.1), the generated current i_{pv} of a PV panel, and thus the output power, are significantly affected by the solar irradiance level and the ambient temperature. To study those characteristics, the PV panel with the parameters shown in Table 2.1 is adopted in this project. Figure 2.2 shows that the $I-V$ and $P-V$ characteristics are non-linear and also vary with different ambient

Table 2.1: *Parameters of a solar PV panel used in this project [64].*

Rated power (25 °C, 1000 W/m^2)	$P_{mpp} = 65$ W
Voltage at the maximum power point	$V_{mpp} = 17.6$ V
Current at the maximum power point	$I_{mpp} = 3.69$ A
Open circuit voltage	$V_{OC} = 21.7$ V
Short circuit current	$I_{SC} = 3.99$ A

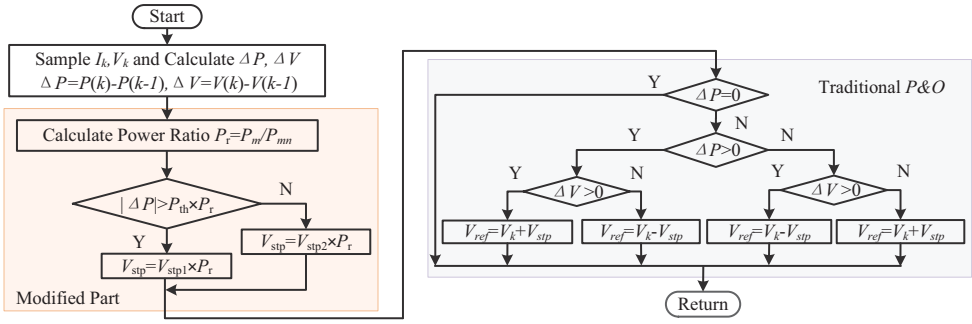

Figure 2.3: *Flowchart of a modified Perturb and Observe (P&O) MPPT algorithm.*

conditions. Due to the non-linear property and the environmental dependency of the PV panel, an MPPT algorithm is necessary to ensure that the maximum solar energy is captured and converted – also for the sake of reduction of cost of energy.

2.1.2 Modified P&O MPPT control

It can be seen in Figure 2.2 that the $P-V$ curve of a PV panel is of "hill" form under a given condition (e.g. 25 °C, 1000 W/m^2). Thus, the $P-V$ curve can be divided into three segments: a) *uphill* – a positive dp/dv, when the PV panel is working as a constant current source, b) *downhill* – a negative dp/dv, and c) *the-top* – $dp/dv = 0$, which corresponds to the Maximum Power Point (MPP) for a given ambient condition [65]. Many MPPT algorithms are proposed based on this "hill" characteristic, such as the Perturb and Observe (P&O) method and the INcremental Conductance (INC) method [62–67]. Those are the most commonly adopted MPPT algorithms. However, the main drawbacks of them are the power oscillations around the MPP in the steady-state condition and poor accuracy under rapid solar irradiation changes.

Hence, a modified P&O MPPT algorithm is introduced to overcome these problems [63]. Figure 2.3 shows the flowchart of the modified MPPT algorithm, where I, V, and $P = IV$ are the instantaneous current, voltage, and power of the PV panels. The operating principle is described as: when $|\Delta P| > P_{th} \times P_r$, the step-size is V_{stp1}; and it could rapidly track the power; otherwise the step-size is V_{stp2} (smaller), and the

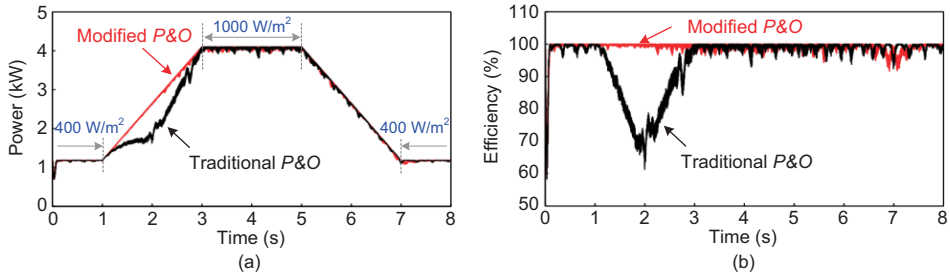

Figure 2.4: *Performance of the modified P&O MPPT algorithm (ambient temperature 25 °C): (a) tracked PV power and (b) MPPT instantaneous efficiency.*

proposed method should be able to offer a more accurate tracking response. Here, P_{th} is the power threshold for selecting different step-sizes, and P_r is the power ratio of the maximum power P_m under different conditions and the nominal maximum power P_{mn}. The power ratio P_r is introduced considering low solar irradiation cases, where a large step-size will contribute to large power variations.

Simulation results of a 4.1 kW single-phase grid-connected PV system [63] with a trapezoidal solar irradiance profile are presented in Figure 2.4. As shown Figure 2.4(a), the modified MPPT algorithm can go back to steady-state quickly and operate around MPP with smaller power variations when compared to the traditional method. Thus, there should be less power losses (higher tracking efficiency as shown in Figure 2.4(b)), and the amplitude of the injected grid current should be more stable. However, it should be pointed out that the characteristics shown in Figure 2.2 are only for an individual PV panel or module. If many PV panels are adopted to increase the output power, the MPPs may be different because of panel mismatch. Moreover, the partial shading of the panels increases the MPPT difficulty [62]. Thus, a robust MPPT algorithm should be able to maximize energy yield even with mismatch and partial shading issues.

2.2 Single-phase transformerless configurations

2.2.1 Single-phase transformerless inverters

Besides the PV panels, the PV inverters are responsible for the power conversion. Among various PV topologies, the single-phase Full-Bridge (FB) inverter is a widely adopted topology due to its simplicity, and it is shown in Figure 2.5, where an *LCL*-filter is used for the power quality concern. According to the discussion in § 1.1.1, either high-frequency or low-frequency transformers can be used for galvanic isolation but at the cost of overall efficiency and system volume. Thus, from an efficiency point of view, transformerless topologies are much more promising for the next generation PV systems, and also will be more widely used in Europe [12, 68].

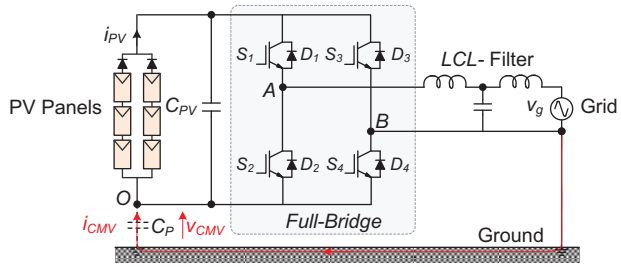

Figure 2.5: *A single-phase single-stage full-bridge (FB) grid-connected PV system.*

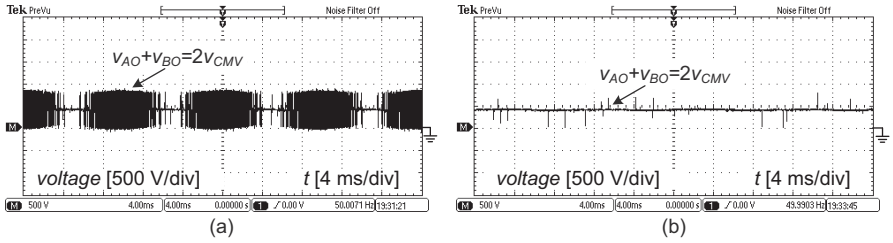

Figure 2.6: *Common mode voltage of a FB inverter with different modulation schemes: (a) unipolar modulation scheme and (b) bipolar modulation scheme.*

However, the lack of galvanic isolation may induce high leakage currents in transformerless PV inverters. To avoid this, the instantaneous Common Mode Voltage (CMV, v_{CMV}) has to be constant, since the CMV will introduce a common mode current i_{CMV} (leakage current). The relationship can simply be described as,

$$i_{CMV} = C_P \frac{dv_{CMV}}{dt} = \frac{C_P}{2} \frac{d(v_{AO} + v_{BO})}{dt} \tag{2.2}$$

in which v_{AO} and v_{BO} are the voltages of the two midpoints of a FB inverter shown in Figure 2.5 and C_P is the stray capacitor between the PV panels and the ground.

A vast of transformerless inverters have been proposed to eliminate or at least reduce the leakage current while maintaining a high efficiency, e.g. by including passive damping components and/or by modifying the modulation methods [14, 44–47, 57, 59, 60]. As for the FB inverter, there are mainly two modulation schemes: a) unipolar modulation scheme and b) bipolar modulation scheme. The former modulation strategy will generate a varying CMV as shown in Figure 2.6, which makes it not suitable for use in transformerless systems. In addition, leakage current elimination can also be achieved either by disconnecting the PV panels from the inverter (bypassing at the DC side) or by providing a bypass leg at the AC side.

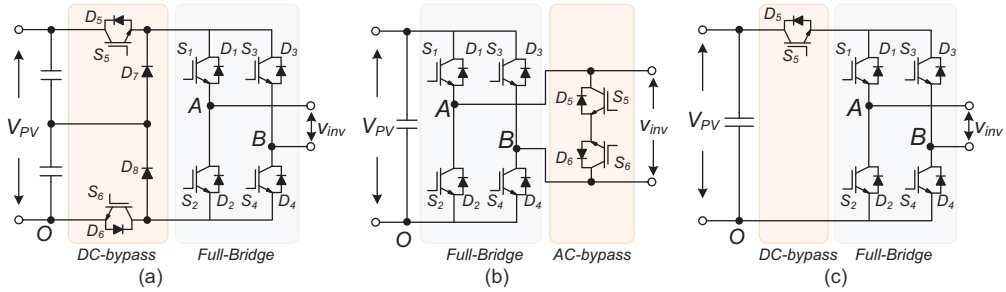

Figure 2.7: *Mainstream single-phase transformerless inverters: (a) H6 inverter, (b) HERIC inverter, and (c) H5 inverter.*

For instance, the H6 inverter patented by Ingeteam [57,69] (shown in Figure 2.7(a)) disconnects the PV panels from the inverter at the DC-side using four extra devices (two switching devices S_5D_5, S_6D_6 and two diodes D_7, D_8), while the Highly Efficient and Reliable Inverter Concept (HERIC inverter shown in Figure 2.7(b)) by Sunways [70] provides an AC bypass using two extra switching devices (S_5D_5 and S_6D_6). Another example of transformerless inverters by providing DC-bypass is the H5 inverter [71] shown in Figure 2.7(c), where it adopts an extra device (S_5D_5) to realize the disconnection. The H5 technology has been successfully implemented in SMA's products. Notably, there have been other transformerless topologies reported in the literature. Some are based on the multi-level topologies [12, 14, 72, 73], and some are derived by optimizing traditional transformerless inverters [72,74]. In this project, the FB inverter with bipolar modulation, the H6 inverter, and the HERIC inverter are chosen for comparison.

2.2.2 Modelling of the FB inverter and grid filters

Considering possible stability and power quality problems, an inverter model (e.g. small-signal models) is important for the control of PV systems in different operation modes [75–81]. Besides, small-signal analysis is also an effective way to get the knowledge of the interactive effect between the paralleled PV inverters. For simplicity, the following derives the mathematical model of a FB inverter with an L filter, as it is represented in Figure 2.8(a), where the bipolar modulation is adopted in order to reduce leakage current. In a switching period, T_{sw}, the state equation can be expressed as,

$$\begin{cases} L\dfrac{di_g}{dt} = v_{dc} - Ri_g - v_g, & 0 \le t < dT_{sw} \\ L\dfrac{di_g}{dt} = -v_{dc} - Ri_g - v_g, & dT_{sw} \le t < T_{sw} \end{cases} \tag{2.3}$$

in which L, R are the inductance and resistance of the L-filter, i_g, v_g are the grid current and voltage, d is the duty cycle, and v_{dc} is the DC-link voltage.

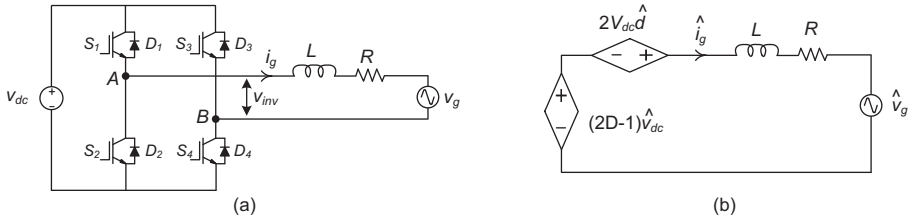

Figure 2.8: *(a) Single-phase FB inverter with an L-filter and (b) small-signal model.*

Then, during this switching interval, the averaged state-space model of Eq. (2.3) can be obtained as Eq. (2.4) by averaging the state equations with the duty cycle as the weighting factor. This averaged state-space model is nonlinear and can be linearized as Eq. (2.5) by applying small-signal perturbations.

$$L\frac{di_g}{dt} = (2d-1)v_{dc} - Ri_g - v_g \tag{2.4}$$

$$\hat{i}_g(s) = \frac{2D-1}{Ls+R}\hat{v}_{dc}(s) + \frac{2V_{dc}}{Ls+R}\hat{d}(s) - \frac{1}{Ls+R}\hat{v}_{dg}(s) \tag{2.5}$$

where "ˆ" denotes the small disturbance term. According to Eq. (2.5), the transfer functions can easily be obtained, e.g. the duty cycle to the current, $G_{id}(s) = \hat{i}_g(s)/\hat{d}(s) = 2V_{dc}/(Ls+R)$. The small-signal model of the FB inverter with an L-filter is shown in Figure 2.8(b). Similar derivations can be applied to the PV inverter with other filters.

Regarding the grid interfaced filters, appropriate design can contribute to a satisfactory Total Harmonic Distortion (THD) of the injected grid current as required by the grid interconnection standards, e.g. *IEEE Std. 929*. Since the input voltage of the filter is a pulse width modulated signal, v_{inv}, which contains switching frequency harmonics, the grid-interfaced filter has to a) reduce the high switching noise and b) convert the pulse width voltage to an almost ripple-free current [54]. As shown in Figure 2.9, there are at least four types of grid interfaced filters. The L-filter is the simplest one, but it has a poor high-order harmonic attenuation performance as it is shown Figure 2.10. The LC-filter with an extra capacitor, C_f, in parallel with the grid is introduced to absorb the high frequency components, but it is effective only the grid impedance is higher than the capacitor impedance [54]. To solve the above issues, high-order filters, e.g. LCL-filter and $LLCL$-filter [43,82], are proposed with reduced size and improved performance. However, in a closed-loop control system, instability may occur due to high-order filter resonances, which requires to be passively or actively damped [42, 83–85].

Compared to the LCL-filter, the $LLCL$-filter can contribute to a smaller grid-side inductance, L_g, and also a better rejection of the switching frequency harmonics [82]. However, the higher (e.g. double-switching) frequency harmonic attenuation ability is degraded as it can be observed in Figure 2.10. Hence, in this project, the LCL-filter is

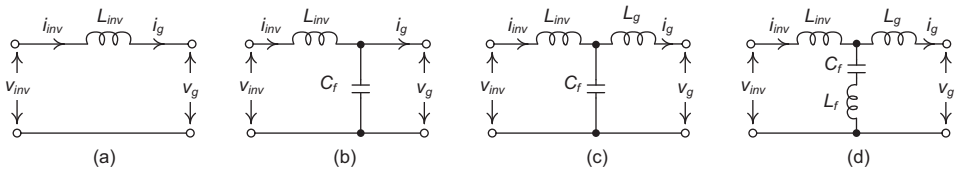

Figure 2.9: *Typical grid interfaced filters: (a) L-filter, (b) LC-filter, (c) LCL-filter, and (d) LLCL-filter.*

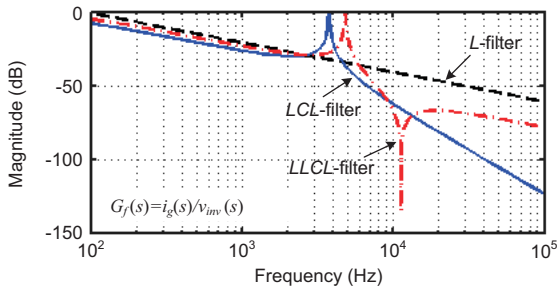

Figure 2.10: *Magnitude response ($G_f(s)$) of three grid-connected filters.*

adopted as the grid interfaced filter for simplicity as well. The design details of those high-order filters are presented in [43], [84] and [85].

2.2.3 Thermal models of power devices and capacitors

Power losses on the power electronics devices are inevitable, which will heat the devices. Temperature changes of the power devices will affect the reliability, as the temperature fluctuation has been one of the most observed factors that cause failures of power devices (e.g. IGBTs) [50, 51, 53]. It has been reported that the power electronics devices and the capacitors are two of the most life limiting components in a PV system [50, 86]. In order to develop reliability-oriented control strategies and thus achieve a reduced cost of energy during lifetime, more efforts should be devoted to the thermal modelling of power devices and capacitors, as the accelerating tests are normally quite time-consuming.

Ideally, all the solar PV energy should be transferred to the power grid. However, there are power losses e.g. on the passive components and the power devices. The power losses, which mainly include switching losses and conduction losses, of the power devices will cause temperature rise at certain points (e.g. the junction inside the device) due to the thermal impedances. In other words, the electrical performance (electrical model) of a power device, and thus a PV inverter, is coupled with its thermal behavior (thermal model) through the power losses, as shown in Figure 2.11. Then, the instantaneous

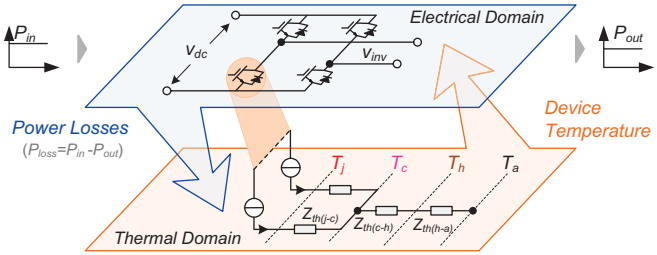

Figure 2.11: *Thermal model of a power device in a FB inverter.*

temperature of the power device can be expressed as,

$$\begin{cases} T_{j(S/D)}(t) & = P_{tot(S/D)}(t) Z_{th(S/D)(j-c)}(t) + T_c(t) \\ T_c(t) & = [P_{totS}(t) + P_{totD}(t)] \cdot [Z_{th(c-h)}(t) + Z_{th(h-a)}(t)] + T_a(t) \end{cases} \tag{2.6}$$

in which,

$T_{j(S/D)}$ is the IGBT/diode junction temperature,
$P_{tot(S/D)}$ is the IGBT/diode total power losses,
$Z_{th(S/D)(j-c)}$ is the thermal impedance from junction to case,
$Z_{th(c-h)}$ is the thermal impedance from case to heat-sink,
$Z_{th(h-a)}$ is the thermal impedance from heat-sink to ambient,
T_c is the case temperature, and
S represents the IGBT and D denotes the diode.

Eq. (2.6) shows that the ambient temperature will also influence the junction temperature. It means that the PV power converters even with low power losses may have high junction temperatures when operating in a harsh environment (e.g. desert).

In respect to the thermal impedance from junction to case ($Z_{th(S/D)(j-c)}$), it can be modelled as a Cauer RC network [64,87], which is a physical-material-based and realistic representation of the impedance, and thus it can reflect the thermal transient behavior of an IGBT module more accurately [87]. However, the Cauer model requires an in-depth material level knowledge. Thus, it is normally converted into a Foster model, of which the thermal parameters can be found in the data-sheets of the power devices. As it is shown in Figure 2.12, the analytical function of the thermal impedance can be described as [88, 89],

$$Z_{th(S/D)(j-c)}(t) = \sum_{i=1,2,3,4}^{n} R_{thi}(1 - e^{-t/\tau_i}). \tag{2.7}$$

According to Eq. (2.6) and Eq. (2.7), it is illustrated that the steady-state mean value ($t \to \infty$) of the junction temperature is dependent on the thermal resistance

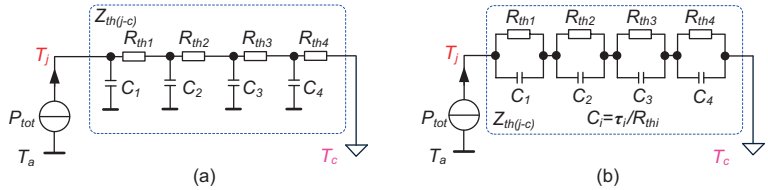

Figure 2.12: *Thermal impedance (Figure 2.11) models: (a) Cauer model and (b) Foster model [87, 88].*

Table 2.2: *The thermal parameters of an IGBT module from a leading manufacturer.*

Impedance		$Z_{th(j-c)}$				$Z_{th(c-h)}$
i		1	2	3	4	-
IGBT	R_{thi} (k/W)	0.074	0.173	0.526	0.527	0.7
	τ_i (s)	0.0005	0.005	0.05	0.2	0
Diode	R_{thi} (k/W)	0.123	0.264	0.594	0.468	0.7
	τ_i (s)	0.0005	0.005	0.05	0.2	0

R_{thi}; while the dynamic behavior of the junction temperature is affected mainly by the thermal capacitance C_i (time constant $\tau_i = C_i R_{thi}$). Moreover, the case temperature (T_c) has a much slower dynamic response than that of junction temperature (T_j) due to much larger time-constants of the thermal impedances ($Z_{th(c-h)}$ and $Z_{th(h-a)}$) [88, 90]. The thermal parameters for the IGBT modules used in this project are listed in Table 2.2, and the PV inverter prototypes are shown in Figures 2.5 and 2.7.

Similarly, due to the power losses on the Equivalent Series Resistor (ESR) of the capacitors in a PV system, failures may occur when the hot-spot temperature of the capacitor goes beyond the limitation during operations. Hence, the decoupling capacitors, shown in Figure 2.13(a), are also very important for a reliable operation of PV systems. Figure 2.13(b) shows both electrical and thermal models of the decoupling capacitors in PV systems. Unlike the multi-layer model of power devices, the thermal model of capacitors is basically simple. Normally, only the thermal resistance, R_{th}, is considered, and it can be found in the data-sheets. In respect to capacitor sizing, it is determined by the following constraints:

$$\Delta V_c \approx \frac{P_o}{2\pi f_0 C V_c}, \text{ and } i_{c,RMS} = \frac{P_o}{\sqrt{2} V_c} \tag{2.8}$$

where P_o is the average power supplied to the grid, f_0 is the fundamental frequency of the grid, ΔV_c is the peak-to-peak ripple of the decoupling capacitor voltage V_c, C is the capacitance of the capacitor, and $i_{c,RMS}$ is the Root-Mean-Square (RMS) current flowing through the capacitor, as it is shown in Figure 2.13(b). It should be pointed out

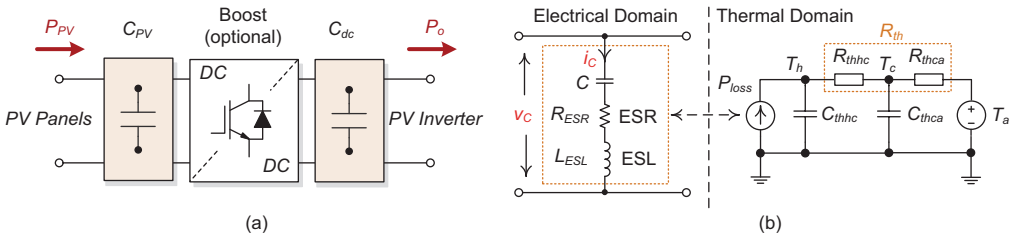

Figure 2.13: *Capacitors in PV systems: (a) decoupling capacitor location and (b) electrolytic capacitor models [91].*

that Eq. (2.8) is not applicable to the filter capacitor (e.g. the capacitor in an *LCL*-filter) design, where for example the reactive power absorbtion and resonant frequency have to be taken into account [43, 82].

2.3 Synchronization in single-phase systems

Synchronization plays an important role in the control of single-phase systems, especially under grid faults where it also acts as grid condition monitoring. A good synchronization system should respond fast and accurately to grid disturbances, e.g. voltage drop, phase jump, and frequency jump, and also good harmonic rejection ability. The reported synchronization techniques in recent literature can be divided into two categories - mathematical analysis methods (e.g. Fourier analysis) and Phase Locked Loop (PLL) based methods, which are nowadays of much attractiveness. A basic PLL structure is presented as Figure 2.14, which consists of a Phase Detector (PD), a Proportional-Integral (PI) based Loop Filter (LF) and a Voltage-Controlled Oscillator (VCO). Thus, the small signal model of this system can be obtained as,

$$\frac{\hat{\Theta}(s)}{\Theta(s)} = \frac{k_p s + k_i}{s^2 + k_p s + k_i} \tag{2.9}$$

where $\hat{\Theta}(s)$, $\Theta(s)$ are the output and input phase respectively, and k_p, k_i are the proportional and integral gains of the loop filter. The details of the PLL modeling can be found in [12]. From Eq. (2.9), the settling time can be given by $t_s = 9.2/k_p$, which is adopted to evaluate the performance of different PLLs.

Among various reported single-phase PLL methods, the main difference is the configuration of the PD, intuitively, being a simple sinusoidal multiplier [92,93]. However, this process will produce a double-frequency term in a single-phase system, as it is shown in Figure 2.15. Applying the *Park* transform to an Orthogonal Signal Generation (OSG) system is another way to extract the phase error of PLL systems. Hence, the task will

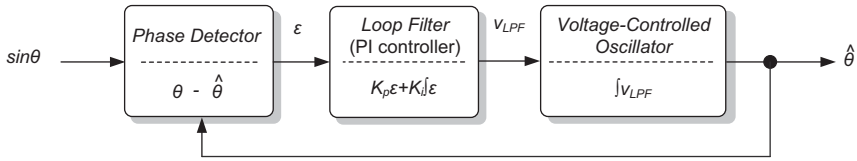

Figure 2.14: *Basic structure of a phase locked loop system.*

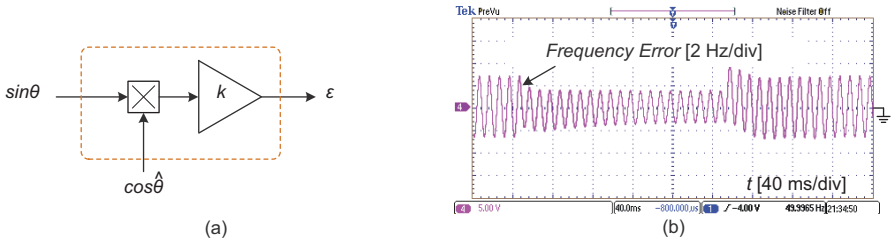

Figure 2.15: *Performance of a basic PLL system: (a) sinusoidal multiplier PD and (b) PLL output frequency error in the case of a voltage sag (45 %).*

be shifted to establish the OSG system. For example, the $T/4$ Delay PLL [12,15] introduces a phase shift of $\pi/2$ rad with respect to the fundamental frequency of the input voltage, v_g. One other possibility is to use Adaptive Filters (AF), which can self-adjust the output according to an error feedback loop. Two popular PLLs - the Enhanced PLL (EPLL) [92, 94] and the Second Order Generalized Integrator based PLL (SOGI-OSG) [12, 15, 95, 96], are based on the combinations of adaptive filters with a sinusoidal multiplier and an OSG system, respectively. The mechanisms of the above mentioned PLL systems are shown in Figure 2.16 , where "ˆ" denotes the corresponding estimated value of the input voltage, $v_g = V_m \sin(\theta)$ with $\theta = \omega t + \varphi$ being the phase of the input voltage, and T is the fundamental period of the voltage.

As it is shown in Figure 2.16, an important feature of the EPLL is that the output signal $\hat{v}_g$ is locked both in phase and in amplitude compared to the other PLL methods, where the amplitude of the grid voltage can be calculated as: $\hat{V}_m = \sqrt{v_\alpha^2 + v_\beta^2}$. The $T/4$ Delay PLL is the simplest one among the other two, while the SOGI-OSG PLL actually adopts two-weight AFs, and thus it will present a better harmonic rejection performance. In order to find the most suitable solution for the single-phase grid-connected PV system in different operation modes, the above synchronization methods are compared when the grid suffers from the disturbances, e.g. a voltage sag and a phase change, and the control structure of the system is given in Appendix A.1. The benchmarking results are shown in Table 2.3 and Figure 2.17.

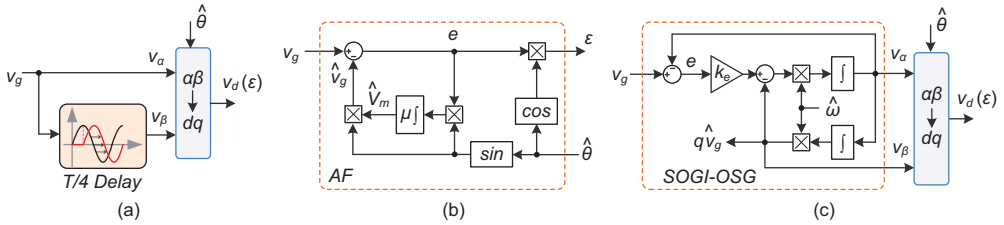

Figure 2.16: *PD structures of three PLL systems: (a) T/4 Delay PLL, (b) EPLL, and (c) SOGI-OSG PLL.*

Table 2.3: *Benchmarking of the selected PLL techniques.*

PLL technique		*T/4* Delay PLL	EPLL	SOGI-OSG PLL
Voltage sag (0.45 p.u.)	settling time (ms)	4.7	7.8	8
	frequency error (Hz)	0.26	0.91	0.62
Phase jump (+90 °)	settling time (ms)	75	120	72
	frequency error (Hz)	16.1	16	19.1
Freq. jump (+1 Hz)	settling time (ms)	Oscillate	186	111
	frequency error (Hz)	(-1.2, 1.2)	8.4	10.4
Harmonic immunity		NO	★★	★★★
OSG mechanism (easy for power calculation)		YES	NO	YES
Implementation complexity		★	★★	★★★

Notes: the more ★, the better the harmonic rejection ability or the more complicated the PLL is.

As it can be observed in the benchmarking results, the performances of these PLL methods are not satisfactory during the voltage sag. The $T/4$ Delay method can follow the amplitude change quickly (a quarter of the grid nominal period approximately), while it cannot be a good synchronization technique when the grid is subjected to frequency variations. The EPLL method presents a slow dynamic variation as shown in Figure 2.17. In respect to the power control of the single-phase systems, the EPLL method is not suitable for calculating the active power and the reactive power because, but it can be used to control the instantaneous power [94]. The SOGI-OSG PLL can track the input voltage with better performance, especially when the grid presents a frequency variation/jump as shown in Table 2.3. It can be concluded that, together with a fast detection unit, the SOGI-OSG PLL is the most promising candidate for single-phase applications in different operation modes.

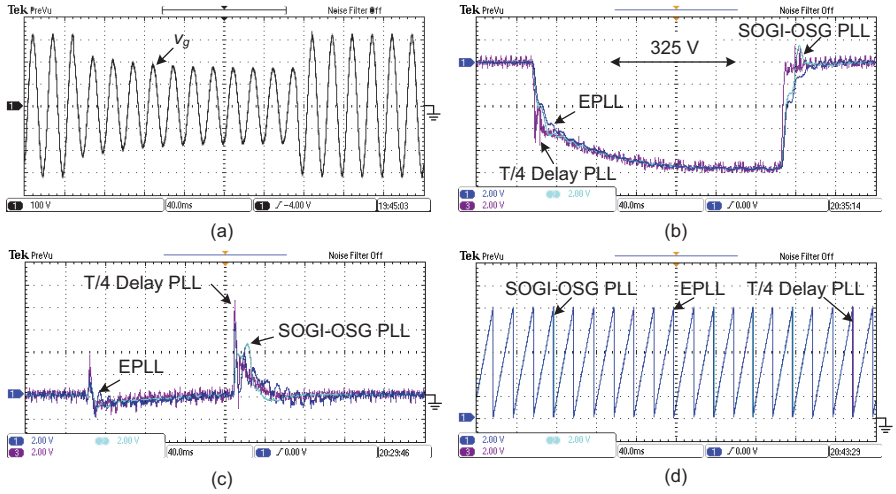

Figure 2.17: *Performance of the three selected PLLs under a grid voltage sag (0.45 p.u.): (a) grid voltage profile v_g [100 V/div], (b) grid voltage amplitude from PLLs [30 V/div], (c) PLL output frequency error [2 Hz/div], and (d) locked phase [2π rad/(5 divs)], time [40 ms/div].*

2.4 Summary

This chapter presented the modelling of single-phase PV systems, from a PV cell to a PV panel, to transformerless inverters, and to the interfaced filters. As for the control of grid-connected PV systems, MPPT algorithms and synchronization methods have been addressed as well. For the reliability assessment of PV systems, the thermal models of power devices and capacitors have also been discussed. Those models are used in the following chapters.

In order to overcome the poor performance of P&O MPPT algorithm under rapid environmental changes, a modified P&O MPPT method has been introduced in this chapter. It adopts two perturbing step-sizes, which are determined by the power tracking error, and thus can reach the MPP faster and more efficiently. Regarding the synchronization, different methods have been compared in the case of grid disturbances. The comparison demonstrates that the SOGI-OSG PLL technique is the promising candidate for single-phase systems under grid faults. The benchmarking results also provide a possibility to select the appropriate synchronization techniques for different applications.

3 Evaluation of Single-Phase PV Inverters

In this chapter, three transformerless inverters discussed in § 2.2 (Full-Bridge with a bipolar modulation scheme (FB-Bipolar), H6 inverter, and the HERIC inverter) are evaluated in terms of efficiency (power losses), leakage currents rejection capability, and also somehow reliability. A mission-profile based multi-disciplinary analysis approach is proposed firstly in this chapter for those evaluations.

3.1 Mission profile based analysis approach

As discussed in previous chapters, efficiency and also reliability are becoming of exceeding interest in order to reduce energy losses, lower maintenance cost, and extend the service time, and thus to achieve a reduced cost of energy [20, 21, 50]. Conventional efficiency analysis is focused on the calculation of power losses on the system under a certain constant condition, e.g. constant DC-link voltage, $v_{dc} = 400$ V, without considering the impact of mission profiles (e.g. solar irradiance level, PV system location, and ambient temperature). Moreover, the extra power devices in transformerless inverters will contribute to a redistribution of the power losses as discussed previously. As a consequence, the energy production will be affected. In regards to reliability of PV systems, currently, too much reliance has been put on the outdated handbooks, e.g. MIL-HDBK 21, or the calculated results of Mean-Time-Between-Failures (MTBF) or Mean-Time-To-Failure (MTTF) [50, 97–100]. It is difficult to find the root causes of failures from the results of the reliability analysis, and thus it makes less contributions to the design and control of PV systems. Prediction of the lifetime of power devices and an entire PV system requires the knowledge of failure mechanism at the device physical level, e.g. involving analysis of the mission profiles [50].

3.1.1 Analysis procedure of the proposed approach

With accumulative real-field experience and the introduction of more and more real-time monitoring systems, better mission profile data is available in various kinds of power electronic systems (e.g. PV inverters) [89]. This offers the possibilities to predictably analyze the lifetime of a certain inverter more accurately and provides a possible estimation of energy production from PV power systems in certain applications. As mentioned above, the solar irradiance together with the ambient temperature is various in different sites and in different seasons, where the efficiency changes will occur in the PV systems even with a high performance transformerless technology. Hence, it is necessary to investigate the transformerless inverters not only in a short-term (e.g. constant condition) but also in a long-term duration (mission profile based investigation) in such a way to predict the PV energy production and the inverter lifetime. In light of those considerations, a multi-disciplinary evaluation method considering mission profiles (i.e.

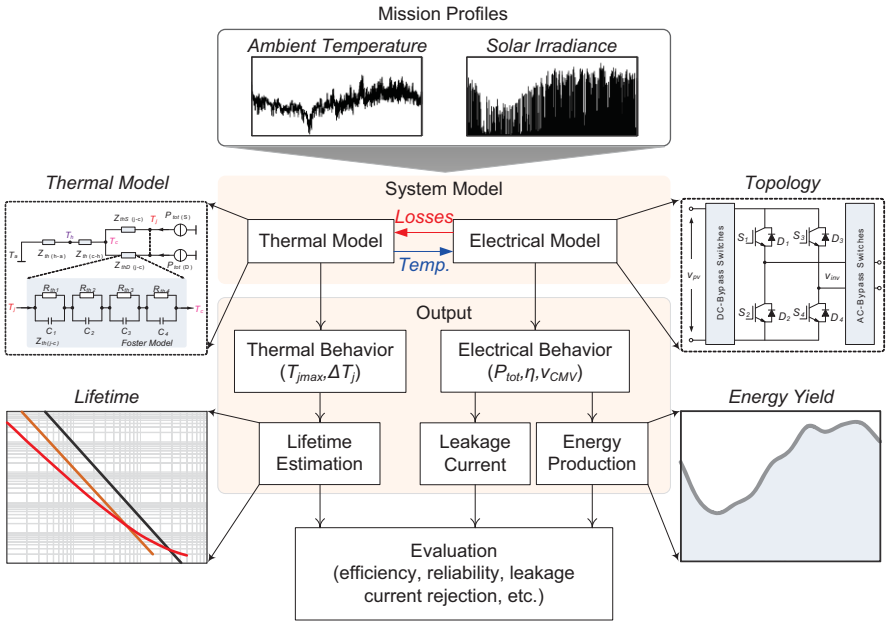

Figure 3.1: *Mission profile based multi-disciplinary analysis method for single-phase transformerless PV inverters.*

solar irradiation and ambient temperature) for single-phase transformerless PV systems is proposed. The analysis procedure of this method is represented in Figure 3.1.

As it is observed in Figure 3.1, the mission profiles (e.g. yearly data, monthly data and/or daily data) are taken as input variables of the proposed evaluation method. The selected different transformerless inverter topologies are simulated in PLECS based on their thermal models, which have been presented in details in § 2.2.3 in Chapter 2. In this way, the mission profile is translated to device loading, including power losses and temperature profiles. According to the proposed analysis procedure in Figure 3.1, the Common Mode Voltage (v_{CMV}), the loss distribution in the power devices and the junction temperature loading of the power modules, including mean/max junction temperature (T_{jm}/T_{jmax}) and temperature cycling (ΔT_j), can be obtained as the outputs of this proposed analysis method. As a result, the energy production can be calculated, the leakage current can be evaluated according to Eq. (2.2) under constant conditions, and the lifetime of a certain transformerless power device/inverter under this mission profile can be obtained by applying appropriate stress interpretation to a dedicated lifetime model. Then, a benchmarking of the topologies could be done in terms of efficiency, energy production, leakage current rejection ability, and reliability.

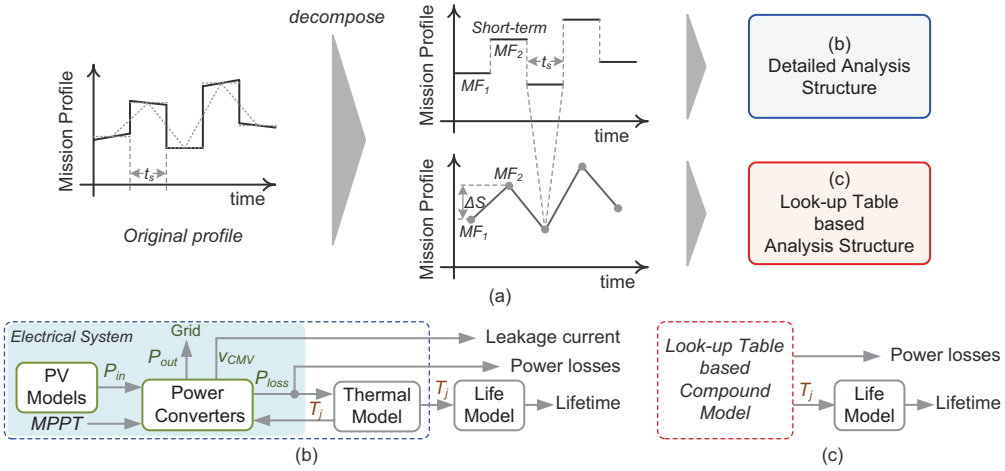

Figure 3.2: *Mission profile decomposition for the proposed multi-disciplinary analysis approach: (a) decomposition procedure, (b) detailed structure for short-term mission profiles, and (c) look-up table based structure for long-term mission profiles.*

3.1.2 Implementation of the analysis method

The mission profile based analysis approach can be adopted for analysis of mission profiles at different time scales, e.g. a yearly mission profile or an hourly mission profile. As for short-term mission profiles (milliseconds to several seconds), both power losses profile and temperature loading profile can directly be obtained from the simulations with a physical-electrical system model. However, for a long-term mission profile (normally longer than few minutes due to ambient or operating condition changes), especially with a high data-sampling rate (e.g. 200 ms), it will be a time-consuming process, or even impossible, to capture the full loading profile under this mission profile. As a consequence, look-up tables are adopted to accelerate the evaluation process [51, 64], which requires appropriately decomposing the mission profile at different time scales. Figure 3.2 shows the decomposing procedure for a long-term mission profile.

It is seen in the decomposition procedure that the original mission profile is decomposed with a period of t_s under the assumption that in this short period the mission profile is constant and so that the system can go into steady state within this period t_s. As a consequence, in each time interval of t_s, the mission profile (e.g. MF_1 and MF_2) can be treated as a short-term mission profile, where the analysis approach shown in Figure 3.2(b) is applicable. Notably, under the decomposed short-term mission profile, the power losses and thermal cycles are mainly at the fundamental frequency with identical cycle period, t'_{on}. However, as it is shown in Figure 3.2(a), there is stress difference (e.g. the stress difference ΔS between MF_1 and MF_2) among those short-term

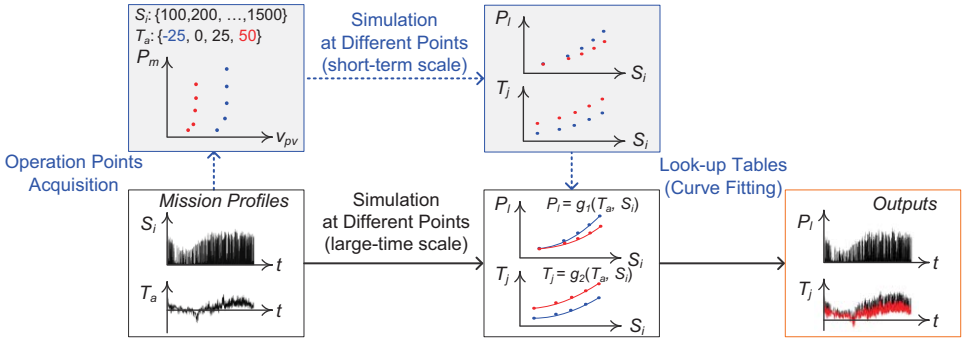

Figure 3.3: *Simulation block diagram using look-up tables (curve-fitting) for the mission profile based analysis approach.*

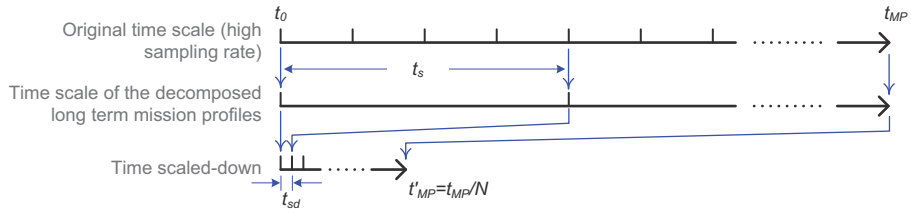

Figure 3.4: *The "time scaling-down" method for accelerating the simulations.*

mission profiles, and this will also introduce stresses on the power devices. Therefore, a long-term mission profile is reconstructed using the average stress from short-term mission profiles (e.g. MF_1 and MF_2). Finally, the look-up table based approach shown in Figure 3.2(c) can be applied to extract long-term loading profiles.

Actually, look-up table based analysis method has been widely used in the power electronics simulations [51, 64, 101]. However, the accuracy of the proposed analysis method is dependent on the decomposition period, t_s, and the curve-fitting algorithm. If t_s is too large, the accuracy is degraded due to the loss of short-term mission profile effects; while too small, it will become a time-consuming process with increased accuracy. The value of the decomposition period is determined by this consideration and the system time-constants. For example, t_s= 1 minute is appropriate for most power electronics systems normally with a response of milliseconds, during which the junction temperature of the power devices can reach the steady-state as well. Figure 3.3 shows an example of the implementation of the analysis approach to acquire the loading profiles by simulations. In addition, for a long-term mission profile (e.g. a year), the resultant decomposed mission profiles are still of a large period (e.g. 365×24×60 mins = 525600 mins), contributing to a time-consuming process. An effective solution adopted in this

proposed approach is called "*time scaling-down*", which squeezes the real-world time, as it is shown in Figure 3.4, where t_{sd} is the scaled-down period of the decomposed long-term mission profiles with a period of t_s, and t_{MP} and t'_{MP} are the original period and the squeezed period of the whole given mission profile (e.g. one day, one month, or one year), respectively. A scaling ratio is defined as $N = t_s/t_{sd} \geq 1$.

3.2 Efficiency and leakage current rejection comparisons

3.2.1 Definitions and mission profiles

According to Figures 3.1 and 3.2, only considering the power losses on the switching devices, the instantaneous conversion efficiency can be calculated as,

$$\eta(t) = \frac{P_{in}(t) - P_{loss}(t)}{P_{in}(t)} \cdot 100\% \tag{3.1}$$

and thus the energy production through the mission profile is obtained as,

$$E = \int_0^{t_{MP}} P_{out}(t)dt = \int_0^{Nt'_{MP}} [P_{in}(t) - P_{loss}(t)]dt = \int_0^{Nt'_{MP}} [P_{in}(t)\eta(t)]dt \tag{3.2}$$

where $P_{in}(t)$ is the PV output power with MPPT control, $P_{loss}(t)$ is the total power losses on the inverter, $P_{out}(t)$ is the inverter output power, and N, t_{MP}, and t'_{MP} are defined previously.

Regarding the leakage current rejection capability, the CMVs of the selected transformerless inverters are compared since they are responsible for the generation of leakage currents. According to Eq. (2.2) and Figures 2.5 and 2.7, the CMV is given by,

$$v_{CMV} = \frac{v_{AO} + v_{BO}}{2}. \tag{3.3}$$

According to Figure 3.2, the leakage current rejection capability of the three PV inverters is evaluated under constant conditions (i.e. special cases of short-term mission profiles).

As it can be seen in Figure 2.4, the MPPT efficiency is highly affected by the ambient conditions. Since the major objective is to evaluate the performance of PV inverters under a mission profile, for simplicity, the efficiency of MPPT for the PV inverters is assumed constant, being 99%. Correspondingly, the maximum power profile v.s. the output voltage of the PV panels under different ambient temperatures can be obtained as shown in Figure 3.5, where the PV panels consist of 46 BP 365 PV modules [64] (2 strings $\times$ 23 modules of each string), being the rated maximum power of 2990 W and the nominal voltage of 405 V at maximum power point under standard test conditions (25 °C, 1000 W/mm^2). The PV panel parameter is shown in Table 2.1. A real-field yearly mission profile shown in Figure 3.6 is used for the evaluations, and the sampling frequency is 5 Hz.

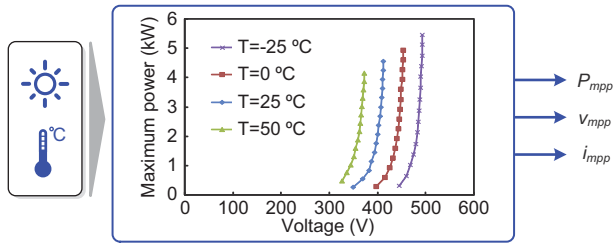

Figure 3.5: *Look-up table based model of PV panels for long-term mission profiles assuming a constant MPPT efficiency.*

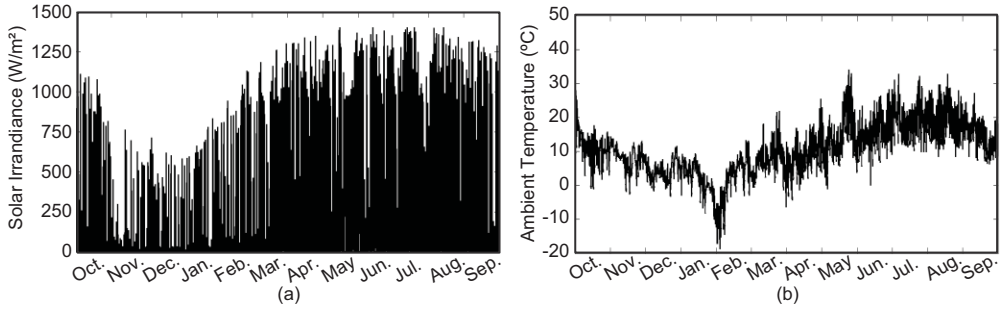

Figure 3.6: *A real-field yearly mission profile from October 2011 to September 2012: (a) solar irradiance and (b) ambient temperature.*

3.2.2 Evaluation results

According to Figures 3.1 and 3.2, the efficiency and leakage current rejection of the three transformerless inverters are firstly evaluated under constant ambient conditions in order to build up the look-up tables. The control structure of the three PV systems and their parameters are provided in Appendix A.1. The evaluation results are shown in Figures 3.7 and 3.8, where the switching frequency is 10 kHz.

Figure 3.7 shows that the loss distributions on the power devices are quite different among these inverters, which illustrates why the efficiency of the transformerless inverters is different. Although the H6 inverter can effectively avoid the generation of a varying CMV, the extra devices (S_5D_5 and S_6D_6) contribute to almost 51.9 % of the total power losses, and thus the efficiency is slightly decreased in contrast to the FB-Bipolar PV system, as it is shown in Figure 3.7. The total power losses of the HERIC inverter are the lowest among three transformerless inverters under a constant input power and constant ambient conditions. It means that the efficiency of the HERIC inverter is the highest, which is proved by the results presented in Figure 3.8.

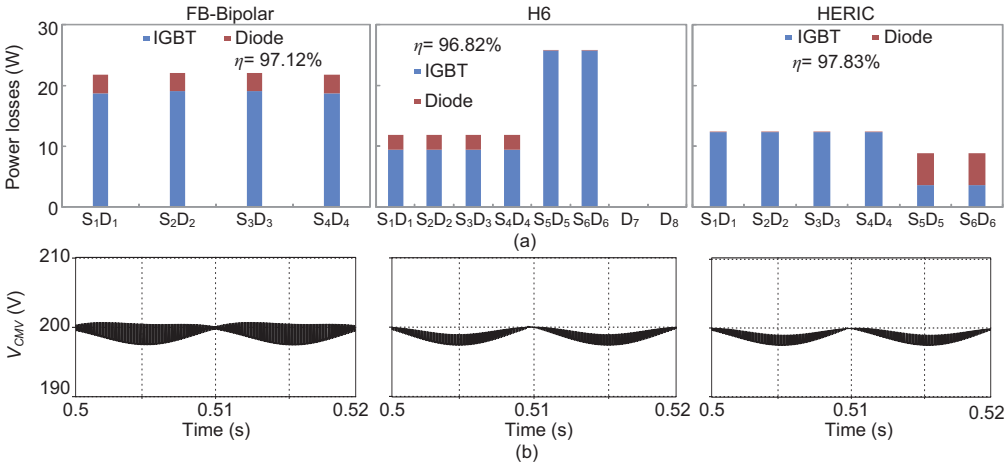

Figure 3.7: *Performance of the selected PV inverters under a constant test condition (v_{mpp} = 405 V, P_{mpp} = 2.99 kW, T = 50 °C): (a) loss distribution and efficiency and (b) common mode voltage, v_{CMV}.*

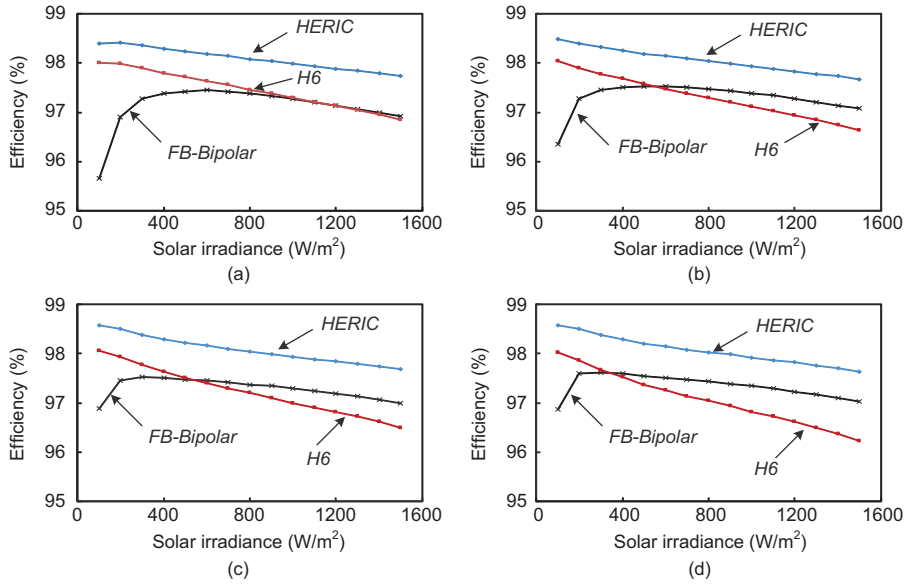

Figure 3.8: *Efficiency of the selected PV inverters under various conditions (constant operating points): (a) T=-25 °C, (b) T=0 °C, (c) T=25 °C, and (d) T=50 °C.*

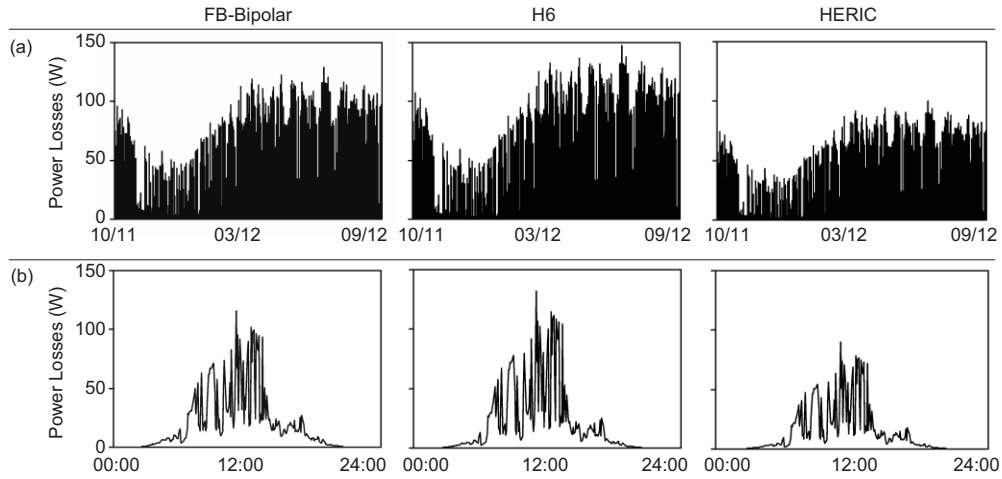

Figure 3.9: *Total power losses on the power devices of three PV inverters under: (a) a yearly mission profile and (b) a daily mission profile (cloudy day).*

Based on the above evaluations, a look-up table was built up, and thus the selected inverters can be assessed under a real-field long-term mission profile shown in Figure 3.6. Notably, here, only the power losses are compared under this mission profile, and the original mission profile is decomposed with a period of $t_s = 5$ mins. The performance of the PV inverters under a yearly mission profile and a daily mission profile is demonstrated in Figure 3.9, which shows that the additional power devices in a transformerless PV inverter will introduce a redistribution of power losses, and thus lead to a redistributed thermal profile. It also shows that the efficiency, and thus the energy production, will be affected by topology modifications and the mission profile.

In order to verify these effects, the annual energy yield of the three PV inverters is roughly calculated according to Eq. (3.2), and the results are shown in Figure 3.10. It can be observed that the PV system with HERIC inverter can produce more energy than the other two through a whole year due to its higher efficiency. Moreover, the annual energy yield from an H6 system is slightly higher than the FB-Bipolar inverter. This is because the average solar irradiance and ambient temperature of the mission profile are approximately 800 W/m^2 and 10 °C as shown in Figure 3.6. Within those ranges, the H6 inverter can achieve a higher efficiency than the FB-Bipolar inverter according to Figure 3.8. Hence, from the total energy production and leakage current rejection points of views, the H6 inverter is better than the FB-Bipolar inverter, and the most promising topology is the HERIC inverter. However, the extra power devices in the H6 and HERIC inverters might be the most stressful components under this mission profile, and thus the inverter reliability is challenged.

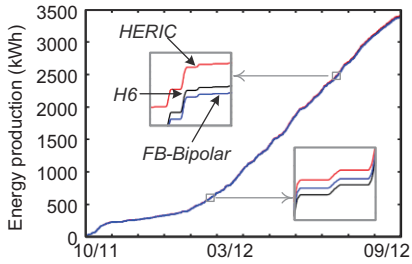

Figure 3.10: *Accumulated energy production of the three PV inverters under the real-field yearly mission profile.*

3.3 Reliability assessment considering mission profiles

3.3.1 Mission profile translation to loading profile

As discussed previously, the mission profiles have a significant impact on the efficiency, power loss distributions, and energy productivity of the system (i.e. PV inverters). According to Eq. (2.6) and Figure 3.1, the redistributed power losses will cause temperature rise due to the thermal impedances. Junction temperature loadings, mainly including mean junction temperature and junction temperature cycle amplitude, have been of clear contributions to power device failures [50, 51]. Besides, failures of capacitors are related to the hot-spot temperature. Hence, it is better to acquire the thermal loading profiles under a mission profile in order to predict the lifetime.

The application of the proposed analysis approach to translate the mission profile into thermal loading profiles of the power devices and capacitors requires look-up tables. Similar to the process done for efficiency and energy production analysis, constant operating conditions are studied first in order to build up the look-up tables. Figure 3.11 shows the thermal behavior of the power devices of the three transformerless PV inverters under a constant test condition, where $v_{mpp} = 405$ V, $P_{mpp} = 2.99$ kW, and $T = 50$ °C, and the system control structure is shown in Appendix A.2. It has been demonstrated in Figure 3.11 that the mean junction temperatures of the power devices of the HERIC transformerless topology are significantly lower than the other two topologies, and thus it offers the most potential to further reduce the current rating and cost of the power devices. Figure 3.11 also shows that the thermal loading of the extra devices (i.e. S_5 and S_6) of the H6 inverter is higher than that of the HERIC and FB-Bipolar topologies. This is in consistence with the power loss distributions.

According to Figures 3.3 and 3.5, a look-up table was built up, which takes the mission profile (solar irradiance is within a range of $0 \sim 1500$ W/m^2, ambient temperature is within a range of -25 $\sim$ 50 °C) as input, and outputs the loading profile on the devices in terms of mean junction temperature T_{jm}, maximum junction temperature T_{jmax}, and

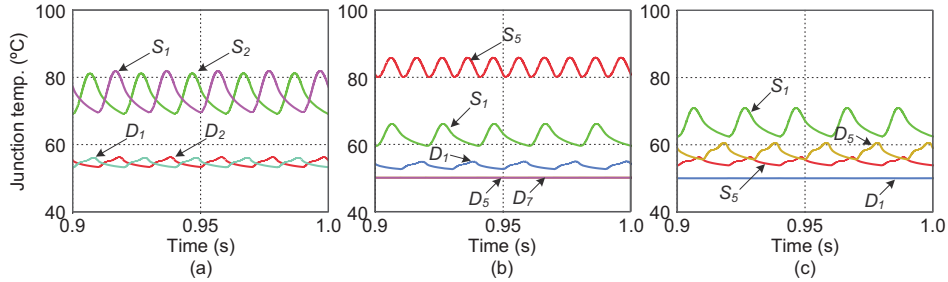

Figure 3.11: *Thermal loading of three PV inverters under a constant condition (v_{mpp} = 405 V, P_{mpp} = 2.99 kW, T = 50 °C): (a) FB-Bipolar, (b) H6, and (c) HERIC.*

junction temperature cycling amplitude ΔT_j. The thermal behaviors of the PV topologies under real-field mission profiles shown in Figure 3.6 are represented in Figure 3.12, where the decoupling period t_s is of 5 mins. It is observed that, although the thermal stress on the four power switches of a H6 transformerless inverter ($S_1 \sim S_4$ in Figure 2.7(a)) are reduced compared to that of the FB-Bipolar topology, the additional devices ($S_5 \sim S_6$ in Figure 2.7(a)) are under much higher thermal loading, similar to the case in Figure 3.11. Thus, in terms of reliability (expected lifetime, e.g. 30 years), the H6 inverter is not very suitable for use. As for the HERIC, it can maintain high efficiency with less thermal stress on the additional devices as shown in Figure 3.12.

Since the DC decoupling capacitors are of importance in single-phase PV systems and serve as energy storage elements to perform functions like power balancing, ripple-voltage limiting, and sufficient energy provision during the hold-up time of the system [102], many efforts have been made to enhance the performance of DC-link capacitors. However, the mission profile effects on the DC-link capacitors have not been covered yet. As the decoupling capacitors can be placed at different locations in single-phase PV systems (see Figure 2.13), the thermal loadings will be affected. In order to find out those effects and thus design reliable decoupling capacitors, referring to Figure 2.13 and the system shown in Appendix A.2, a real-field daily mission profile has been translated to the stresses of the DC-link capacitors, which is shown in Figure 3.13.

As shown in Figure 3.13, the capacitors at the PV side have experienced a wide range of voltage stress (e.g. from 335 V to 415 V) under this daily mission profile, because they are directly "exposed" to the mission profile. Moreover, the PV-side capacitor in a single-stage system are under large voltage variations ($\Delta V \approx 11.5$ V) compared to that in a double-stage system ($\Delta V \approx 4.6$ V) , since it has to maintain the voltage level and also cope with extracted power from the PV panels, as seen from Figure 3.13 (b) and (c). In contrast to those capacitors, the capacitor at the inverter input side (inverter-side) in a double-stage system is of stable voltage stress (i.e. 400 V), but also large ripples (e.g. $\Delta V \approx 6.5$ V) which could be alleviated by tuning inverter control parameters. Thus,

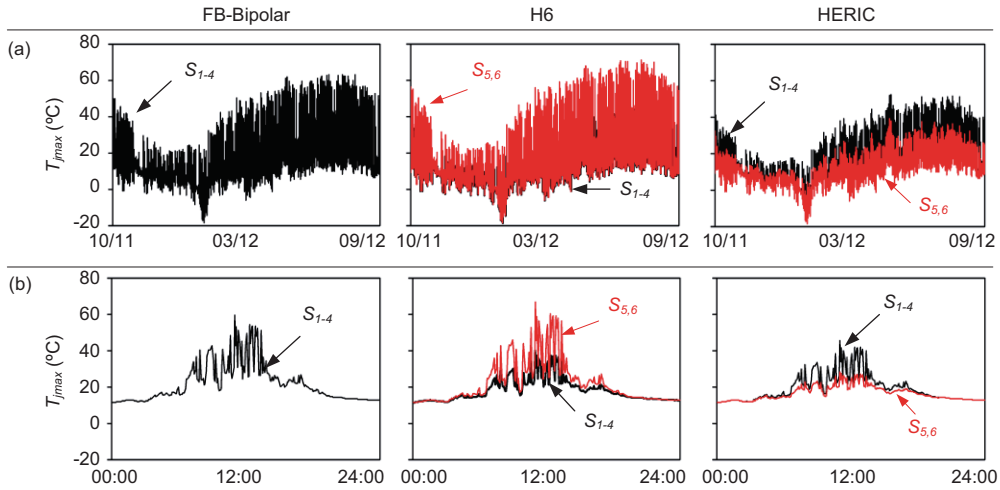

Figure 3.12: *Thermal behaviors of the power devices of three PV inverters under: (a) a yearly mission profile and (b) a daily mission profile (cloudy day).*

from the design point of view, the capacitors at the PV side should have the ability to handle a wide range of voltage stress, and the inverter control parameters should be tuned appropriately to reduce voltage ripples. Those results have demonstrated that the mission profile has a significant impact on the capacitor stresses as well, and this impact should be taken into account in the design phase of a PV system, which has not yet been considered in the past.

3.3.2 Lifetime models

After the translation of the decomposed long-term mission profiles, the temperature loading profiles appearing in the power devices or capacitors should be appropriately extracted according to a specific lifetime model. For example, the Coffin-Manson model (extended Coffin-Manson model) [50, 51, 87, 103–105] can be given by,

$$N_f = A(\Delta T_j)^{-n} e^{E_a/(k_B T_{jm})} \tag{3.4}$$

in which A and n are the model parameters obtained by experimental measurements (e.g. accelerating tests), k_B is the Boltzmann constant, and E_a is the activation energy. This lifetime model indicates that the number of cycles to failure N_f is only dependent on the temperature cycles, including cycle amplitude ΔT_j and mean junction temperature T_{jm}. Those values can easily be obtained under short-term mission profiles, as it is shown in Figures 3.2 and 3.11, while for long-term mission profiles after decomposition, counting algorithms are used to exploit the temperature loading profile. There are many

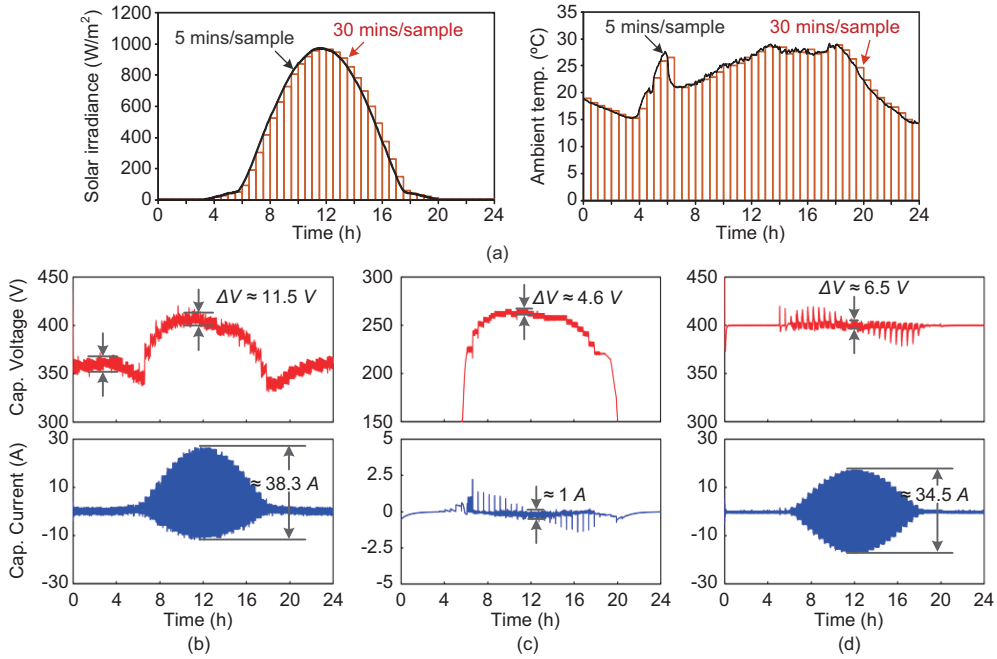

Figure 3.13: *Stresses of the decoupling capacitors in a FB-Bipolar system under a daily mission profile: (a) a daily mission profile (clear day), (b) PV-side capacitor in a single-stage system, (c) PV-side capacitor in a double-stage system, and (d) inverter-side capacitor in a double-stage system.*

cycle counting algorithms reported, e.g. level crossing counting, rain-flow counting, and simple range counting methods [51, 105, 106]. Then, the lifetime can be calculated with the extracted information, as it is illustrated in Figure 3.14.

However, it has been found in other lifetime models that N_f is also affected by the cycle period (t_{on}), bond-wire aspect ratio (ar), and the diode (f_{diode}) [103, 104, 107]. Hence, a detailed lifetime model has been introduced in [107] and it can be given as,

$$N_f = A(\Delta T_j)^{\alpha}(ar)^{\beta_1 \Delta T_j + \beta_0} \left[\frac{C + (t_{ON})^{\gamma}}{C+1}\right] \exp\left(\frac{E_a}{k_B T_{jm}}\right) f_{diode} \tag{3.5}$$

where A, α, β_0, β_1, γ and C are the model parameters that can be obtained by means of curve-fitting using numerical simulation or experimental results. For instance, in [107], a least square curve-fitting method was adopted for parameter extraction of the lifetime model based on the power cycling test results. The extracted parameters of an IGBT module are listed in Table 3.1.

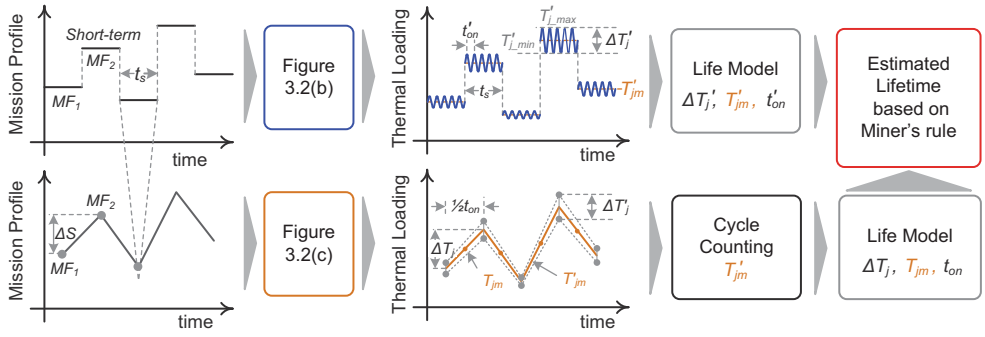

Figure 3.14: *Loading exploitation for lifetime calculation according to Figure 3.2.*

Table 3.1: *Parameters of the lifetime model (Eq. (3.5)) of an IGBT module [107].*

Parameter	Value	Unit	Experimental condition
A	3.4368×10^{14}	-	
α	-4.923	-	$64\ \text{K} \leq \Delta T_j \leq 113\ \text{K}$
β_1	-9.012×10^{-3}	-	$0.19 \leq ar \leq 0.42$
β_0	1.942	-	
C	1.434	-	$0.07\ \text{s} \leq t_{ON} \leq 63\ \text{s}$
γ	-1.208	-	
f_{diode}	0.6204	-	
E_a	0.06606	eV	$32.5\ ^\circ\text{C} \leq T_{jm} \leq 122\ ^\circ\text{C}$
k_B	8.6173324×10^{-5}	eV/K	

According to the Miner's rule [50, 51, 105, 106], the accumulated Life Consumption LC (i.e. damage due to the stress) is linearly dependent on the contributions from different thermal cycles, which can be expressed as,

$$LC = \sum_i \frac{n_i}{N_{fi}} \tag{3.6}$$

in which n_i is the number of cycles at the stress ΔT_{ji}, and N_{fi} is the corresponding number of cycles to fail according to the lifetime model, e.g. Eq. (3.5). As a consequence, the lifetime LF of the power devices can be calculated as,

$$LF = \frac{t_{MP}}{LC} \tag{3.7}$$

where t_{MP} is the mission profile period as defined previously.

In respect to the lifetime models of decoupling capacitors, they are of more simplicity compared to the lifetime models of power devices. The failures of the capacitors are

related to the internal hot-spot temperature, and thus the capacitors will be degraded during operations. Eq. (3.8) presents some lifetime models of capacitors considering those aspects for different applications [91].

$$LF_C = \begin{cases} \left(4.3 - 3.3 \times \dfrac{V_c}{V_n}\right) L_n \times 2^{\dfrac{T_{max} - T_h}{10}}, & \text{Case 1, } L_n = 1000 \text{ hours;} \\ \left(4.3 - 3.3 \times \dfrac{V_c}{V_n}\right) L_n \times 2^{\dfrac{T_{max} - T_h}{10}}, & \text{Case 2, } L_n = 2000 \text{ hours;} \\ L_n \times 2^{\dfrac{T_{max} - T_h}{10}}, & \text{Case 3, } L_n = 24000 \text{ hours.} \end{cases} \tag{3.8}$$

in which V_c and V_n are the operational and rated voltages of the capacitor, respectively, T_{max} is the maximum operating temperature, T_h is the hot-spot temperature, and L_n is the lifetime at maximum operating temperature with maximum allowable ripple current at T_{max} applied.

3.3.3 Reliability evaluation results

With the lifetime models and the extracted temperature information from the thermal loading profile, the lifetime of the power devices and capacitors can be calculated according to the proposed analysis approach shown in Figures 3.2 and 3.14. In this section, firstly, the reliability of the power devices of the selected PV inverters is calculated as a representative demonstration of the proposed method. The yearly thermal loading profiles shown in Figure 3.12 are analyzed. The rain-flow counting results are shown in Figure 3.15.

As it can be seen from Figure 3.15, the number of cycles of both mean junction temperature and junction temperature cycling amplitude are in agreement with the power loss distributions. The additional devices of the H6 inverter ($S_{5,6}$) have a larger number of cycles compared to the other power devices of this topology ($S_{1\sim4}$), which means those devices to realize a rejection of leakage currents are the most critical components of the H6 inverter. Consequently, a choice of more reliable power devices as the extra ones is required when designing a PV system with H6 inverter adopted. In contrast, this is not the same in case that a HERIC inverter is adopted in this PV system, as it is proved in Figure 3.15(c), where the number of cycles of the power devices ($S_{1\sim4}$) is smaller than that of the FB-Bipolar inverter under the same mission profile.

With the counting results, the life consumption and thus the lifetime of the power devices can quantitatively be calculated according to Eqs. (3.5) to (3.7) on condition that the parameters given in Table 3.1 are reliable. However, those parameters are extracted under specific conditions (e.g. $0.07\text{ s} \leq t_{ON} \leq 63\text{ s}$) for a certain power device, and thus they are not suitable to use for a quantitative calculation of the lifetime for the power devices used in this study. Nonetheless, a qualitative comparison can be done

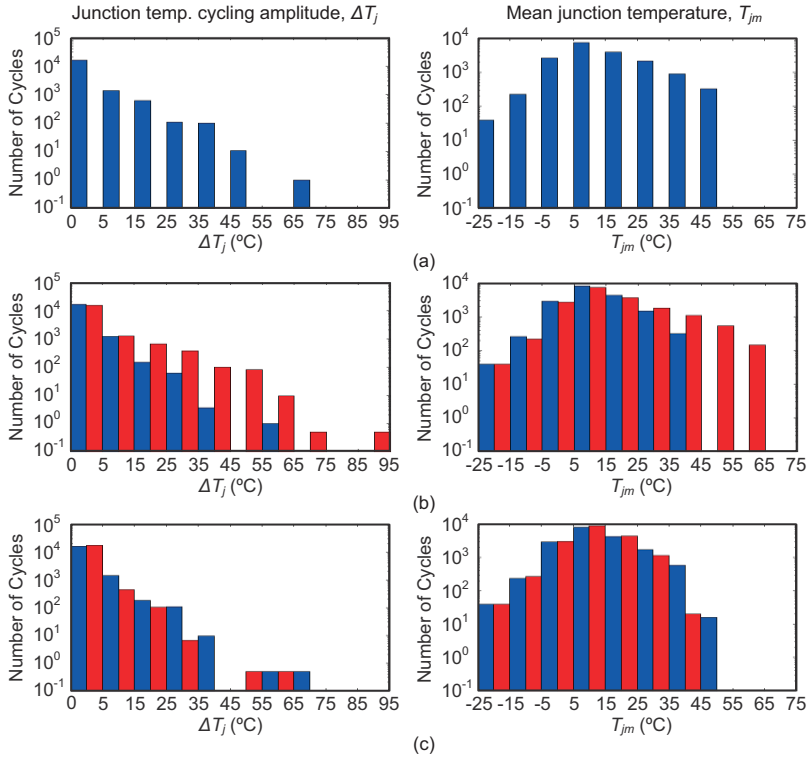

Figure 3.15: *Rain-flow counting results of the thermal loading profiles shown in Figure 3.12(a) (Blue: $S_{1\sim4}$, Red: $S_{5,6}$): (a) FB-Bipolar, (b) H6, and (c) HERIC.*

by normalizing the life consumption so that the parameter dependency is reduced. The normalization of the life consumption can be given as,

$$\overline{LC} = \frac{LC}{LC'} = \frac{\sum_i \frac{n_i}{(\Delta T_{ji})^{\alpha}(ar)^{\beta_1 \Delta T_{ji}}[C + (t_{ONi})^{\gamma}] \exp\left(\frac{E_a}{k_B T_{jmi}}\right)}}{\sum_l \frac{n'_l}{(\Delta T'_{jl})^{\alpha}(ar)^{\beta_1 \Delta T'_{jl}}[C + (t'_{ONl})^{\gamma}] \exp\left(\frac{E_a}{k_B T'_{jml}}\right)}} \tag{3.9}$$

where $\overline{LC}$ is the normalized life consumption, LC' is the base LC for normalization (e.g. life consumption of the power devices of the FB-Bipolar topology), and α, β_1, γ, k_B and E_a are the lifetime model parameters listed in Table 3.1.

According to Eq. (3.9) and the counting results presented in Figure 3.15, the normalized LC of the three PV inverters under the same mission profile is shown in Figure

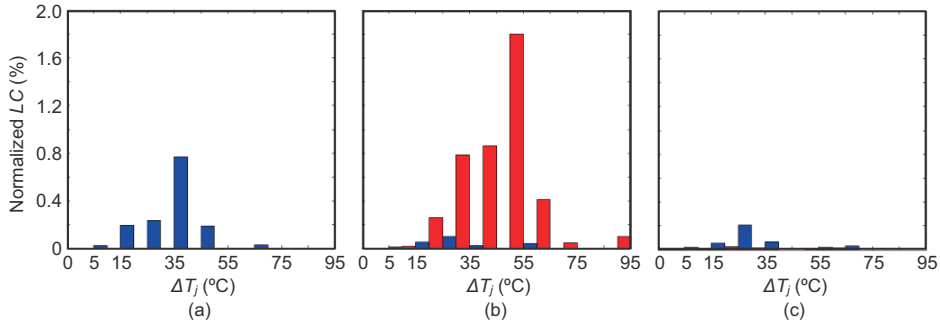

Figure 3.16: *Normalized lifetime consumption (lifetime comparison) of the three inverters under the same mission profile shown in Figure 3.6 (Blue: $S_{1\sim4}$, Red: $S_{5,6}$): (a) FB-Bipoar, (b) H6, and (c) HERIC.*

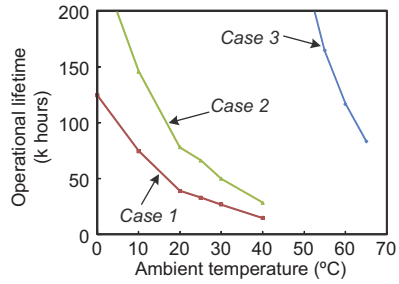

Figure 3.17: *Lifetime prediction of different capacitors in a single-stage single-phase PV system under various ambient temperatures.*

3.16, where the life consumption of power devices of a FB-Bipolar inverter is chosen as the base value for normalization. It can be seen from the results that the extra power devices of a H6 inverter consume much more life of the entire inverter in contrast with those of a HERIC inverter. This comparison further confirmed that the HERIC inverter would be the most promising solution for single-phase PV systems in terms of reliability. Moreover, by comparing the rain-flow counting results with the normalized life consumption shown in Figure 3.16, another interesting conclusion can be drawn is that, although there are a few cycles of large temperature cycling amplitude (e.g. ten cycles of 55 °C $\sim$ 65 °C for the devices $S_{5,6}$ in Figure 3.15(b)), they do contribute much more damage (e.g. 0.4% in Figure 3.16(b)). The large cycling amplitudes are mainly induced by the mission profile. Those results are also in agreement with the loss distributions.

As for the reliability of capacitors, a demonstrative case for 1 kW single-stage single-phase PV system has been studied, where three different types/configurations of ca-

Table 3.2: *Evaluations of the three single-phase transformerless PV inverters.*

Transformerless topology	**FB-Bipolar**	**H6**	**HERIC**
Number of power devices	Four	Six	Six
Efficiency†	97.61%	97.67%	98.29%
Loss distribution (%)‡	$SD_{1\sim4}$: 100%	$SD_{1\sim4}$: 48%	$SD_{1\sim4}$: 27%
	-	$SD_{5\sim6}$: 52%	$SD_{5\sim6}$: 73%
Leakage current (CMV)	Low	Very low	Very low
Device current stresses (p.u.)♯	$S_{1\sim4}$: 1.0	$S_{1\sim4}$: Moderate (0.98)	$S_{1\sim4}$: Low (0.76)
	-	$S_{5\sim6}$: Very high (1.66)	$S_{5\sim6}$: Very low (0.37)
Device switching freq. (f_s)	$S_{1\sim4}$: High f_s	$S_{1\sim4}$: Line freq.	$S_{1\sim4}$: High f_s
	-	$S_{5\sim6}$: High f_s	$S_{5\sim6}$: Line freq.

† Conversion efficiency by only considering the losses on the power devices.
Rated power: 1 kW, DC voltage: 400 V, $T = 25$ °C.

‡ Loss distributions of the power devices in percentage of the total power losses.
Rated power: 3 kW, DC voltage: 405 V.

♯ Base value - device current stresses of the FB-Bipolar.
Rated power: 1 kW, DC voltage: 400 V, $T = 25$ °C.

pacitors with their lifetime models given by Eq. (3.8) are used. It can be seen in the results (Figure 3.17) that the mission profile has significant impacts on the capacitor lifetime. The capacitor of "Case 3" shows a satisfactory reliability performance within a wide ambient temperature range compared to the other two capacitors. In the case of an adoption of those two capacitors, derating operations have to be enabled in order to meet a minimum lifetime requirement, as it is discussed in [91]. Similar to the reliability analysis of the power devices, the long-term mission profile effect on capacitor reliability can also be analyzed using the proposed approach.

3.4 Summary

This chapter has proposed a mission profile based multi-disciplinary analysis approach, and an evaluation of three transformerless PV systems in terms of efficiency, energy production, leakage current rejection capability, and the emerging reliability, has been carried out using the proposed method. A summary of those comparisons has been given in Table 3.2. It can be observed from the results that, although the elimination or reduction of leakage currents can be achieved by those inverters with a satisfactory efficiency, some of the extra-devices that are used for disconnection of the PV panels or the PV inverters might be exposed to higher temperature loading. The thermal loading will further introduce failures of the power devices, and thus challenge the system reliability. Therefore, much attention has to be put on the thermal design of those critical components in a PV inverter in order to reduce the cost of energy. It can be concluded from the comparison that, in terms of efficiency and reliability, the HERIC inverter is the most promising topology for next-generation PV systems.

Besides the power electronic devices, the DC-link capacitors also play an essential role in PV systems. A comparison of the stresses of the capacitors adopted at different locations in single-phase full-bridge PV system has been discussed in this chapter as well. It can be concluded from the comparison that the DC capacitor at the PV panel side is under much more stress during a daily operation compared to the capacitor at the inverter input. This is because that the output current of the PV panels is of ambient condition dependency. Therefore, the design of both decoupling capacitors and power devices/inverters should take the effects from mission profiles into account, and many trade-offs, which have not yet been considered in the past, have to be taken care of in next-generation PV systems in the future. At the end of this chapter, a lifetime prediction example of capacitors has been presented.

Part III

Advanced Control Strategies for Single-Phase PV Systems

In the third part of the Ph.D. thesis, advanced control strategies for single-phase PV systems have been presented. This part includes three chapters. ***Chapter 4****. Control of PV Systems in Different Operations discusses the basic control as well as the advanced control strategies of single-phase grid-connected PV systems both in MPPT operation mode and under grid faults. Reactive power injection strategies and a novel power calculation method are also proposed in this chapter.* ***Chapter 5****. Constant Power Generation Control Concept introduces a new hybrid power control strategy - constant power generation control method for single-phase PV systems considering the distributed grid capacity. Other benefits of this control concept are also discussed in this chapter.* ***Chapter 6****. Thermal Optimized Control Strategy presents an advanced control method to flexibly control the junction temperature of the power devices, and thus to further improve the reliability.*

4 Control of PV Systems in Different Operations

This chapter addresses the basic control as well as the advanced control strategies for single-phase grid-connected PV systems in different operation modes. Firstly, grid-integration standards/requirements are reviewed, and thus suggestions on grid standard modifications are proposed in order to accept more PV systems in the grid. Then, a benchmarking of the most commonly used current controllers is presented, followed by the advanced control of PV systems under grid faults, including reactive power injection strategies. In order to enhance the performance of single-phase PV systems in different operation modes, a new power calculation method has been proposed in this chapter.

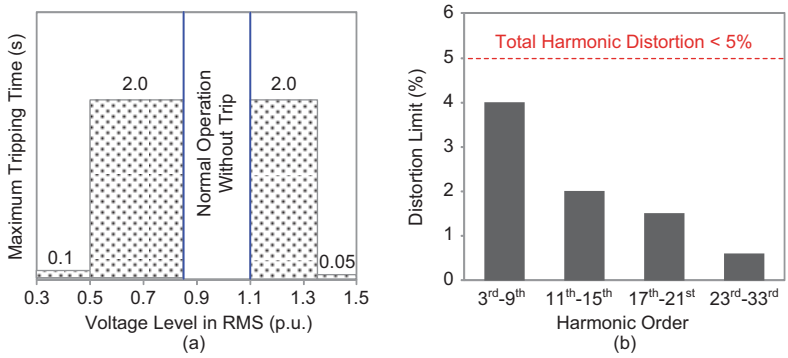

Figure 4.1: *Basic grid requirements: (a) response to abnormal grid voltage conditions and (b) current harmonics requirements defined in IEC 61727 for PV power systems with rated power lower than 10 kW considering a low penetration level [24].*

4.1 Grid-interconnection standards

4.1.1 Evolution of PV grid-integration codes/standards

Grid-integration requirements are the essential guidelines for the design, control and operation of grid-connected PV systems. The grid standards originally addressed elementary demands, as shown in Figure 1.2. For example, most of the grid-connected PV systems should cease to energize the local loads in the case of grid transient disturbances, e.g. voltage sags [20, 21, 24, 108] by means of islanding detection. In normal operation, the PV systems are required to produce as much energy as possible with satisfactory quality of the injected grid currents, which is shown in Figure 4.1 - an example of IEC 61727 [24]. Those grid requirements are introduced to ensure the safety of utility maintenance personnel, to protect the equipment, and also to guarantee the utility stability, on the basis of a low penetration level of PV systems [16, 19, 45], which are different from conventional power plants or large wind power farms.

The influence from a low penetration level of PV systems on the grid has been proven to be negligible. However, in the case of a wide-scale penetration of single-phase PV systems in the distributed grid, the disconnection under grid faults can contribute to: a) voltage flickers, b) power outages, and c) system instability. This is caused by two aspects: the intermittent nature of solar PV sources [109] and the disconnection of aggregated PV systems in response to abnormal grid conditions. In light of the above issues, the present active grid requirements are expected to be revised considering a combination of standardized features and customer demands. In fact, previous research have demonstrated the potential of PV systems to have an active role in the regulation of distributed grids like what conventional power plants do today [18, 19, 21, 110–116].

Moreover, PV systems can provide ancillary services to effectively mitigate the challenges related to mission profiles [109].

Grid codes for medium- or high-voltage systems have already been modified in some countries, and a few countries have also published similar demands for low-voltage applications. For instance, in Germany, the systems connected to the medium- or high-voltage networks should be capable of riding through voltage sag and at the same time to provide reactive current [25], and an power limitation requirement (to achieve constant power production) has been imposed on any pre-designed or new PV systems. In the Italian grid code, similar requirements have been applied to the generation units with the nominal power exceeding 6 kW [26]. Recently, a study done in Japan also presented LVRT requirements on PV systems connected to single-phase low-voltage grids [22, 33]. Obviously, the challenges from the high penetration of PV systems are being forecasted. The Distributed System Operators (DSO) have given priority to find solutions in order to guarantee reliable and stable operation of distributed power systems. As a consequence, current active grid requirements need to be modified in order to enable a wide-scale adoption of PV systems.

4.1.2 Suggestions on grid requirement modifications

The tendency for the next generation multi-functional PV systems features LVRT capability, grid support functionality, flexible power controllability, and intelligent ancillary services. In order to fulfill those advanced features for the future high penetration scenario, the existing active PV grid standards and/or requirements need to be reexamined and updated accordingly based on the following main considerations:

- ✓ Active power control (power curtailment);
- ✓ Reactive power control (Volt-VAR control);
- ✓ Frequency control through active power control (Freq.-Watt control);
- ✓ Dynamic grid support (fault ride-through capability);
- ✓ High reliability and high efficiency.

A. Active power control (power curtailment)

Due to the reverse power flow towards upstream voltage levels [9, 110, 111], and the power difference between PV systems and load demands, voltage rise on distributed feeders has been observed as one of the major issues brought with highly PV-penetrated systems. One possibility to solve this is to directly curtail the active power when the grid voltage hits the upper voltage limitation, e.g. 1.06 p.u. in Japan and 1.03 p.u. in Germany [4]. It implies that the PV systems should be capable to operate with a controllable power generation (e.g. power ramp control, absolute power control, and delta power control). Consequently, a remote active power control function for low-voltage PV systems may be incorporated into the future grid codes.

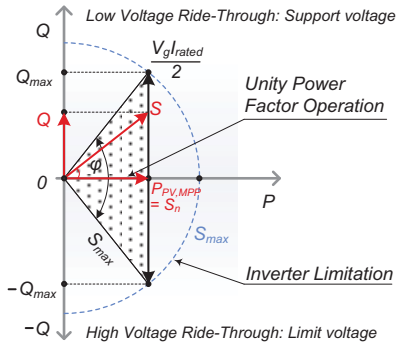

Figure 4.2: *PQ - diagram for a single-phase PV inverter.*

In addition, power curtailment control is a kind of "smart" de-rating operation for PV inverters, which may contribute to improved system reliability and thus reduced cost of energy during lifetime. Notably, the absolute power control has already been introduced to wind turbine systems in Denmark, while the implementation of such a function in the next-generation PV systems shows much more benefits for the entire grid in terms of unloading the distributed network and extended lifetime. It should be noted that all enhancements of a flexible active power control of PV system further call for more advanced system monitoring and communication.

B. Reactive power control (Volt-VAR control)

Another solution for voltage rise mitigation is to allow reactive power injection into the grid. Since PV systems are usually designed with reasonable margins and operate under partial loading conditions, there is a room for reactive power injection, especially during nights when there is no sunshine. However, the amount of the reactive power that a PV inverter can deliver to the grid depends on the inverter apparent power (rated current value, I_{rated}), which is illustrated in Figure 4.2. In MPPT operation mode, the maximum available reactive power Q_{max} of a single-phase PV inverter is calculated as: $Q_{max} = \sqrt{S_{max}^2 - P_{PV,MPP}^2}$, where S_{max} is the inverter maximum apparent power and $P_{PV,MPP}$ is the maximum active power with MPPT control.

In fact, there have been some grid requirements for a very high penetration level of PV systems to activate reactive power control to support the grid [4, 110, 111]. For example, all PV systems in Germany connected to either low- or medium-voltage grids are required to provide reactive power [4], but at the same time, the minimum power factor should be satisfied. In the future, similar requirements are expected to be enhanced on low-voltage PV systems in order to host more PV capacity in the line, since they are able to participate in the reactive power management, and thereby voltage control [117, 118]. As for single-phase low power PV systems, being the typical configurations, the voltage

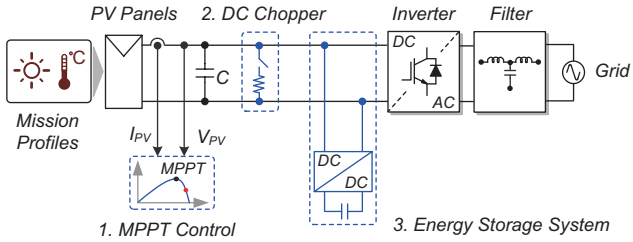

Figure 4.3: *Possible hardware solutions for single-phase grid-connected PV systems with low voltage ride-through capability: 1. modify MPPT, 2. use DC "breaking"-chopper, and 3. use energy storage systems.*

support by controlling reactive power can be achieved at the substation side or integrated in advanced PV inverters, which require more investigations from an operational and economical point of view.

C. Frequency control through active power control (Freq.-Watt control)

As aforementioned, owing to anti-islanding protection, the disconnection of a considerable amount of PV systems unintentionally would further introduce instability problems, e.g. power outage [110, 112–116]. Hence, the suggested modifications of PV grid standards include a provision of frequency control functionality to ensure the grid stability. The frequency control can be realized through active power control, like what has been defined in the German grid codes. For example, it is stated that the reduction of active power has to be activated with a gradient of 40 % generated active power P per Hz, when the grid frequency is within the frequency range of 50.2 Hz to 51.5 Hz [110].

In the meantime, due to the intermittency (i.e. mission profile effects), the output power of a PV system will vary with the environmental conditions, when it is fed into the grid. Consequently, a large amount of fluctuating power will contribute to frequency variations or even instability of the power grid. As the capacity of a single PV system is continuously growing, and also the penetration level, the frequency fluctuation owing to intermittency will become even severe. Therefore, it calls for enhanced frequency control requirement for future PV systems.

D. Dynamic grid support (fault ride-through capability)

Dynamic grid support capability is focused on LVRT and reactive current injection during fault transients [19,22,25,26,39]. The objectives of this function are: a) to prevent the inverter from over-current shutdown and b) to support the grid voltage recovery. The low-voltage PV systems serving single-phase networks have lower physical inertia as the energy storage is currently limited compared to wind turbine systems. However, without appropriate power dispatch, the power devices might also be overheated when the system goes into LVRT operation. As shown in Figure 4.3, the active power dispatch

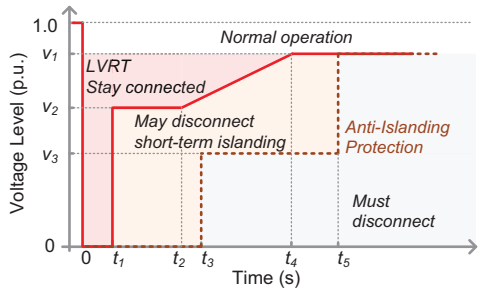

Figure 4.4: *Compatible implementation of low voltage (and zero voltage) ride-through and anti-islanding requirements for PV systems.*

can be done by: a) modifying MPPT control, b) using a DC chopper like the case in wind turbine systems and c) managing the power exchange between PV systems and energy storage systems. The three alternatives can be adopted for single-phase PV systems under grid faults seen from a hardware point of view. Notably, the enhancement of LVRT performance can be achieved by means of advanced grid fault detection (i.e. the monitoring system), synchronization and control technologies.

Additionally, integrating the LVRT function into next-generation PV inverters is a key way to further increase the PV hosting capacity [4, 6, 39]. Hence, it is recommended that the grid codes should focus more on the LVRT capability for PV systems. Nonetheless, the implementation of LVRT is against the anti-islanding requirements [23]. It means that the anti-islanding requirement should be extended in order to incorporate the fault ride-through capability. A compatible implementation of both functions is demonstrated in Figure 4.4.

E. High reliability and high efficiency

To further reduce the cost of energy and extend service time, next-generation PV systems have to be of higher efficiency and higher reliability. Advancement of the transformerless technology will be strengthened, but it also introduces side effects, such as lack of galvanic isolation and the abilities of fault ride-through and reactive power injection, which may further age the power converter technology [47]. Besides, those effects may impose new challenges for the reliability of the entire PV inverter due to the redistributed loss distributions, which again are topology-dependent. Moreover, a better knowledge of the operating conditions together with mission profiles can contribute to better reliability-oriented design and operation of the PV system. Hence, monitoring technologies will be a key to this achievement. These aspects should be considered in the design and also field operation phases of future PV systems.

In addition, the next generation PV systems should be flexibly and appropriately integrated with other systems, e.g. electrical vehicle systems, energy storage systems,

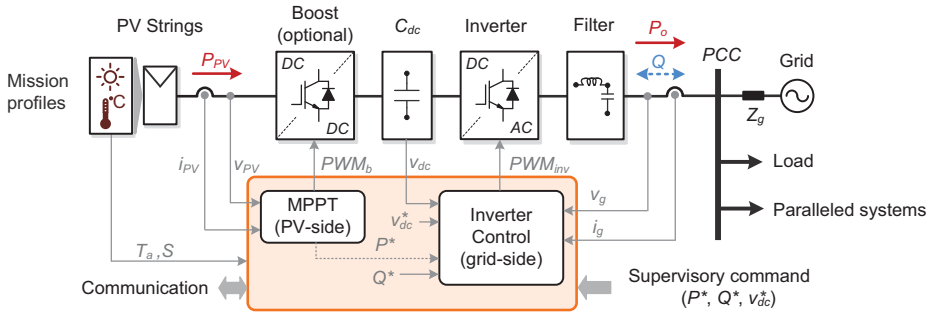

Figure 4.5: *Typical configurations and control structures of single-phase grid-connected PV systems for residential applications.*

smart grids and micro-grid systems. Proper deployment of those systems into PV systems has brought significant benefits to the grid [21, 112–115, 119, 120]. They also have to be able to switch into short-term islanding operation mode smoothly in order to secure the power supply, as it is shown in Figure 4.4, and reconnect after fault clearance. In that case, the future PV systems can provide reactive power compensation and harmonic suppression through intelligent power electronics systems and also more advanced control methods [121, 122]. Those advanced grid-integration features are summarized in Table 4.1.

4.2 Basic control of PV systems in normal operation

4.2.1 Control objectives

Control of single-phase PV systems should be designed in consideration of grid requirements, as the example shown in Figure 4.1. Despite the system configurations, the control objectives of single-phase PV systems can be achieved:

1) at the PV-side to extract the maximum power from the input source considering mission profiles. In general, when a boost converter is adopted, the protection of the DC/DC converter should also be taken into account in this control part.
2) at the grid-side to fulfill the basic requirements shown in Figure 1.2, e.g. control of active and reactive powers, synchronization, and anti-islanding protection.

Typical control strategies for single-phase grid-connected systems are shown in Figure 4.5, including two cascaded loops according to those objectives [14, 15]: a) an inner control loop for current shaping, which has the responsibilities to generate a sinusoidal current (almost ripple-free) and to perform current protection of the inverter and b) an outer control loop (voltage or power control) for current reference generation, where the DC-link voltage or the power is controlled.

Table 4.1: *Summary of grid-integration features for advanced PV systems connected to low voltage grids* †.

Integration features	Current PV systems (MV / LV)	Next-gen. PV systems	Remarks (grid code revision considerations)
A. Active power control (power regulation)	✔✔ / ✔	✔✔	Remote set-point for power regulation should be extended to low voltage systems. Even more stringent, e.g. constant power production and power ramp limit.
B. Reactive power control (Volt-VAR control)	✔✔ / ✔	✔✔	Settings by DSOs are dependent on the power capacity of the PV systems. More reactive power provision strategies, e.g., constant PF.
C. Frequency control (Freq.-Watt control)	✔✔ / ✔	✔✔	Frequency support through active power droop control (e.g. 40% power reduction) is active in some countries. Focuses should be paid to solve intermittency issue.
D. Dynamic grid support (fault ride-through)	✔✔ / ✗	✔✔	PV systems have the ability to support the grid dynamically associated with reactive power injection. This should be enhanced for a wide application range to secure power supply. Zero-voltage ride-through and recurring fault ride-through capabilities are also emerging features for PV systems.
Anti-islanding‡	✔✔	✔	It should be compatible with fault ride-through.
E. Reliability and efficiency	✔ / ✗	✔	Adoption of advanced power devices. Reliability should also be improved to reduce the downtime and thus cost of energy. Fault-tolerant capability is suggested.
Energy storage♯	✔	✔✔	More decentralized grid requires an enhancement of energy reserve, which can be performed by PV systems. It is also a way to produce power more locally.
System monitoring and communication♮	✔	✔✔	Have to be even strengthened to realize the above features.

† ✗-no such ability/requirement, ✔-with the ability, more means higher requirement.

‡ Fault ride-through function may be against the anti-islanding protection requirement. Those two have to be compatible with each other in the future grid integration requirements.

♯ Energy storage systems can also be integrated into the next-generation PV systems to enhance the power controllability, e.g. LVRT.

♮ Monitoring and communication are very important to realize the features for future PV systems of intelligence and flexibility.

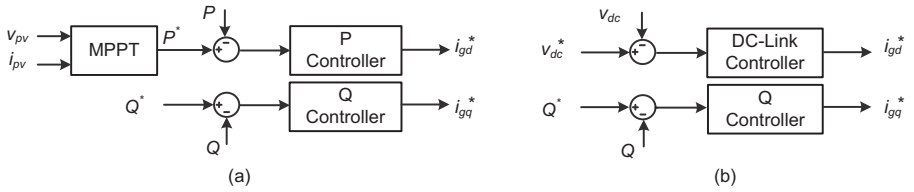

Figure 4.6: *Outer control loop for single-phase systems in the dq−reference frame: (a) single-stage and (b) double stage with boost converter.*

4.2.2 Voltage or power control loop

The voltage or power control loop also provides the system operation conditions (e.g. the grid voltage amplitude and the grid frequency), and then it generates a current reference, which is used in the inner control loop. For example, according to the single-phase PQ theory [47, 79, 94, 123–125], the current reference can be produced by regulating the averaged active power P and reactive power Q, as it is shown in Figures 4.5 and 4.6. This power control method is intuitive with less complexity, since the averaged active power and the averaged reactive power references (P^* and Q^*) can directly be set by the operators or in the control unit, when the MPPT control is activated.

However, the implementation of the outer control loop requires Orthogonal Signal Generation (OSG) systems to create quadrature components ($v_{g\alpha}$, $v_{g\beta}$ and $i_{g\alpha}$, $i_{g\beta}$) corresponding to the real grid voltage v_g and grid current i_g (also used for power calculation). Those components are then transformed into $dq-$components (v_{gd}, v_{gq} and i_{gd}, i_{gq}) using *Park* transformation ($\alpha\beta \rightarrow dq$), resulting in the possibility of Proportional Integral (PI) controllers to regulate the injected current, as shown in Figure 4.7(a), but the current control output has also to be inversely transformed ($dq \rightarrow \alpha\beta$) for the PWM unit. Alternatively, the current control can be done in the $\alpha\beta-$reference frame as shown in Figure 4.7(b), where the inverse *Park* transformation is still required. In fact, according to the single-phase PQ theory, the current reference can also be calculated in the $\alpha\beta-$reference frame, which simplifies the overall control. If PI controllers are used for power regulations, the current references can be expressed as,

$$\begin{bmatrix} i_{g\alpha}^* \\ i_{g\beta}^* \end{bmatrix} = \frac{1}{v_{g\alpha}^2 + v_{g\beta}^2} \begin{bmatrix} v_{g\alpha} & v_{g\beta} \\ v_{g\beta} & -v_{g\alpha} \end{bmatrix} \begin{bmatrix} G_p(s)(P - P^*) \\ G_q(s)(Q - Q^*) \end{bmatrix} \tag{4.1}$$

where "*" denotes the reference signal, $G_p(s)$ and $G_q(s)$ are the PI controllers for active power and reactive power respectively. The control structure is represented in Figure 4.7(c), which shows that there is no need for *Park* or inverse *Park* transformations. Besides, intuitiveness of this power control offers much possibility to implement advanced control strategies by setting the active power and the reactive power references (Q^* and P^*), which will be discussed in more details in the following parts of this thesis.

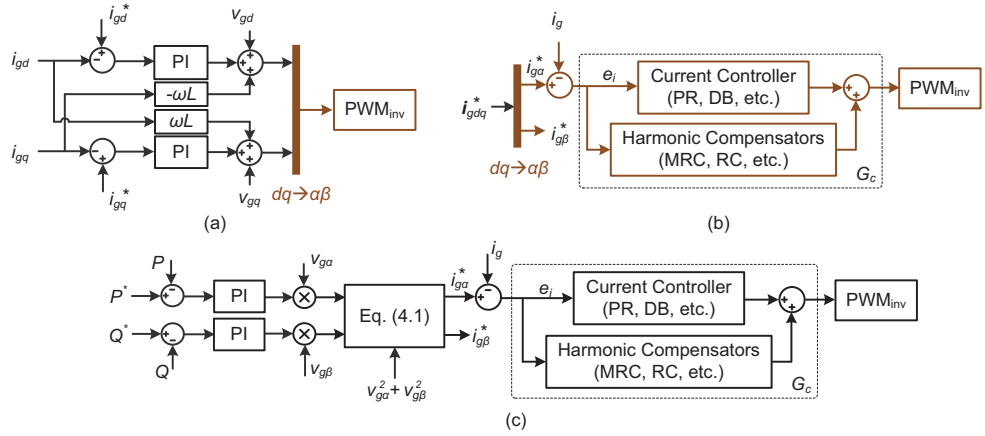

Figure 4.7: *Control structures for single-phase systems in different reference frames: (a) current control loop in dq-reference frame, (b) current control loop in αβ-reference frame, and (c) dual-loop control structure based on the single-phase PQ theory.*

4.2.3 Current controllers considering harmonics injection

The current controller is responsible for the power quality, which is a very important issue for complying with the standards. This can be achieved by means of a robust design of the current controller and a proper selection of the grid-interfaced filters, which have been discussed in § 2.2.2. Besides, by introducing Harmonic Compensators (HC) [12,15] for the controller and adding appropriate damping for the filter [83,85], the current controller tracking performance and thus the power quality can be improved.

Figure 4.7 demonstrates the possible implementation of current controllers in the $dq-$ or $\alpha\beta-$reference frames. As aforementioned, the complexity of a PI-based current control in the $dq-$reference frame is increased, since this implementation requires *Park* and inverse *Park* transformations as well as $dq-$current decoupling (ωL). Moreover, the complexity is also increased when harmonic compensations are required in the current controller. In contrast to PI controllers, Proportional Resonant (PR), Repetitive Control (RC), Multi-Resonant Control (MRC), and also digital Dead-Beat (DB) controllers can be implemented in the $\alpha\beta-$reference frame in Figure 4.7(b) and Figure 4.7(c), because those controllers are capable to track sinusoidal signals without steady-state errors, which is preferable from a power quality point of view.

For the convenience of designing a robust current controller, the harmonic injection mechanism of single-phase PV systems in different operation modes has been introduced in [41]. It has been revealed that the injected current distortion varies with the current level (thus dependent on the mission profile), the power factor, and also the grid voltage level (e.g. voltage sag during fault ride-through). This calls for advanced current control

Table 4.2: *Current controllers in the $\alpha\beta-$reference frame for single-phase systems.*

Controllers	**Transfer functions,** G_c	**Remarks**
DB	$G_{DB}(z) = \dfrac{1}{G_f(z)(z-1)}$	Simple and very fast response (approximately one sampling period). High model-dependency (i.e. poor robustness).
PR	$G_{PR}(s) = k_p + \dfrac{k_i s}{s^2+\omega_0^2}$	Fundamental frequency controller. Harmonic compensators (e.g. MRC) are required for the power quality concern.
PR+MRC	$G_{PR}(s) + \sum \dfrac{k_{ih} s}{s^2+(h\omega_0)^2}$	Fast response. Good harmonic rejection capability at the resonant frequencies. Heavy parallel computation burden, when higher-order harmonics (e.g. 11^{th}, 13^{th}, 15^{th}, and 17^{th}) should be compensated. Also increased complexity.
PR+RC	$G_{PR}(s) + \dfrac{k_{rc} e^{-s\cdot 2\pi/\omega_0} Q(s)}{1-e^{-s\cdot 2\pi/\omega_0} Q(s)} e^{sT_f}$	Easy implementation, which can compensate all harmonics, but only one control gain k_{rc} for the harmonic control is adjustable. Moderate response speed compared to PR+MRC due to its compact recursion property.
DB+RC	$G_{DB}(z) + \dfrac{k_{rc} z^{-N} Q(z)}{1-z^{-N} Q(z)} z^m$	Takes advantage of the strengths of both DB and RC. Simple implementation, good harmonic rejection capability, and less computational burden.

Notes: $G_f(z)$ is the the transfer function of the grid-interfaced filter;
k_p and k_i are the proportional gain and resonant gain of the PR controller, respectively, k_{ih} is the resonant gain with h=3,5,7,...being the harmonic order, w_0 is the grid angular frequency;
k_{rc} is the RC control gain with $0<k_{rc}<2$ [41], $Q(s)$ and $Q(z)$ are low pass filters, T_f is the phase phase lead compensator time and m is the phase lead compensator number.

strategies. Although the PR, RC, MRC, and DB controllers can be adopted in single-phase systems, they may have big differences in terms of transient response and harmonic rejection capability (i.e. lower current THD). The combinations of those controllers have been proved to be an effective way to harmonic rejections, as it can seen in Table 4.2 and Figure 4.8. It is confirmed that, the RC controller together with PR or DB controllers effectively can act on all harmonics (including odd- and even-order harmonics) below the *Nyquist* frequency (half of the sampling frequency, 5 kHz in Figure 4.8), while due to the identical control gain k_{rc}, the low-frequency harmonic attenuation ability is not as good as that in the case of using MRC. To solve this issue, a generic RC control structure has been proposed in [126], which offers the possibility to efficiently eliminate the harmonics of $(nk \pm m)$-order, since the harmonics are classified into several groups and each group has an individual control gain.

In order to find the optimal controller, the mentioned current controllers have been tested experimentally. The test system and its parameters are given in Appendix A and B (Figure A.4,Tables A.1 and A.3, and Figure B.1). The results are presented in Figure 4.9, and the harmonic distributions of the injected current are compared as shown in Figure 4.10. It can be observed from Figure 4.9 that all the "compound" current controllers (PR+MRC, PR+RC and DB+RC) can easily fulfil the THD requirement

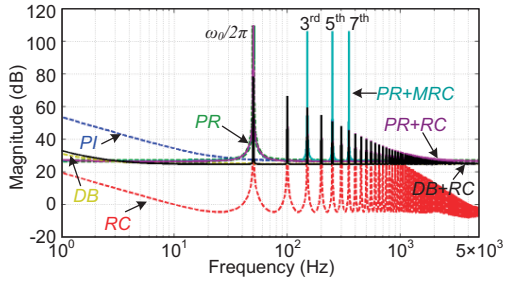

Figure 4.8: *Magnitude response of selected different current controllers in Table 4.2.*

(e.g. THD $<$ 5% in IEC 61727 [24]). However, some of those controllers can not compensate high-order distortions, especially even-order harmonics, which may exceed the limits. For example, when the PR+MRC current controller is adopted, the resultant 10^{th}-order harmonic will exceed the limitation (0.5%) as it is shown in Figure 4.10. In that case, the control gains have to be further tuned or the grid-interfaced filter has to be redesigned. Additionally, those results have confirmed that the RC and RSC controllers provide the most effective solutions for the current harmonic compensation.

4.3 Fault ride-through operation of PV systems

Advanced PV inverters are expected to incorporate a full range of functionalities like what the conventional power plants have, by means of providing ancillary services, e.g. frequency control through active power regulation and dynamic grid support with reactive power injection during fault transients, as suggested in § 4.1.2. Requirements regarding fault ride-through and reactive power injection have been implemented for medium- and high-voltage applications. Those features are undergoing an extension to a wide range of PV applications, from PV modules to utility-scale PV systems [19, 22, 32, 34, 36, 39], so as to cater for an even wider scale adoption of PV systems. Figure 4.11(a) shows an example of stay-online durations versus voltage profiles for different applications, and a requirement for reactive current injection in response to voltage sags is exemplified in Figure 4.11(b) for medium- and high-voltage systems [25, 28, 34].

It should be noted that violation of anti-islanding protection by enabling LVRT capability for single-phase PV systems should be avoided. If achieved, single-phase PV systems should be able smoothly to change to LVRT operation mode from MPPT control at unity power factor, when triggered by the monitored grid voltage. In such a case, monitoring, synchronization, and also communication are of importance to ensure a smooth transition. Thus, a fast voltage fault detection and an accurate synchronization system may contribute to the dynamic performance and the stability margin of the whole PV system under grid faults.

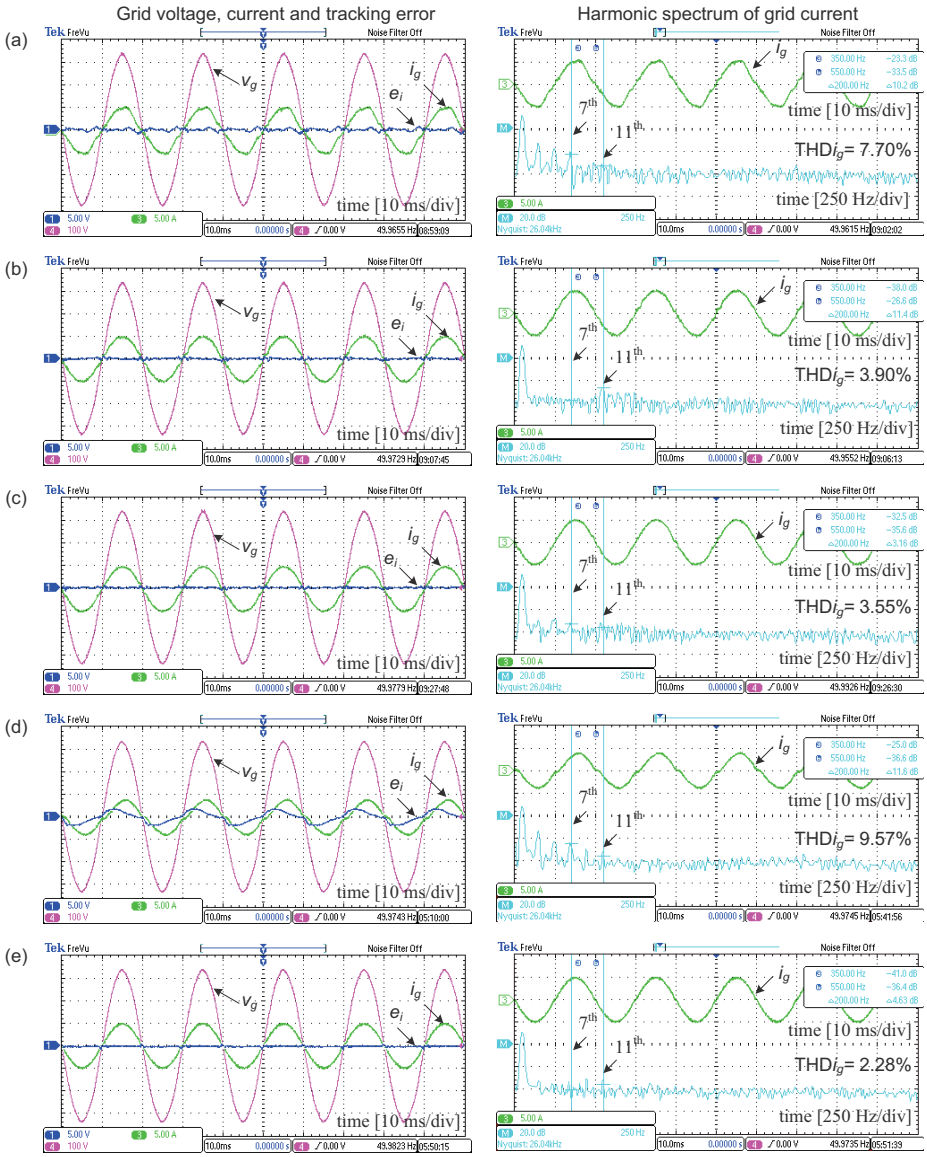

Figure 4.9: *Performance of different current controllers in normal operation mode (grid voltage: v_g [100 V/div], grid current: i_g [5 A/div], tracking error: $e_i = i^*_{g\alpha} - i_g$ [5 A/div]): (a) PR controller, (b) PR+MRC controller, (c) PR+RC controller, (d) DB controller, and (e) DB+RC controller.*

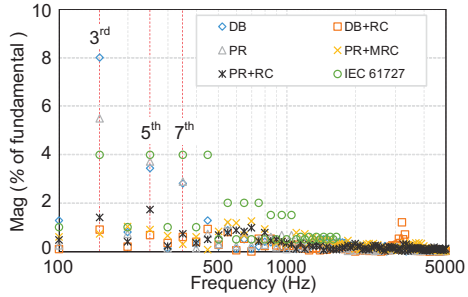

Figure 4.10: *Harmonic distributions of the grid current using different current controllers given in Table 4.2.*

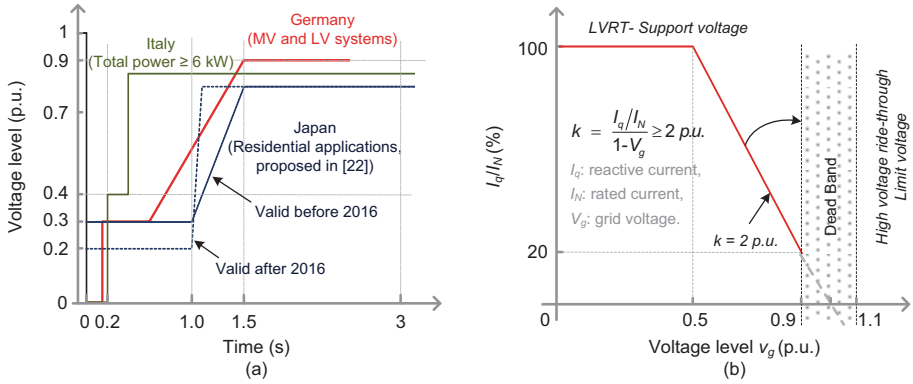

Figure 4.11: *Active grid requirements in respect to voltage disturbances: (a) low voltage ride-through requirement and (b) reactive current injection to support voltage recovery during LVRT for medium- and high-voltage applications [25].*

In regards to the control of single-phase systems under grid faults, which is normally associated with reactive power injection, one possibility is based on the droop concept [127, 128]. This control strategy is effective only when the single-phase line has a large X/R ratio, which is against the situation in real-application cases. Hence, it is not suitable for single-phase system control under grid faults. Another possibility is enabled by the utilization of an adaptive filtering technique, which leads to a direct control of the single-phase instantaneous power. It requires a satisfactory synthesis of the power references as discussed in [94]. Apart from those solutions, according to Figure 4.6 and Eq. (4.1), a simple but effective implementation of the LVRT control for single-phase systems is developed in the $\alpha\beta-$reference frame, as shown in Figure 4.12, where the grid condition monitoring system and the power calculation unit are also included.

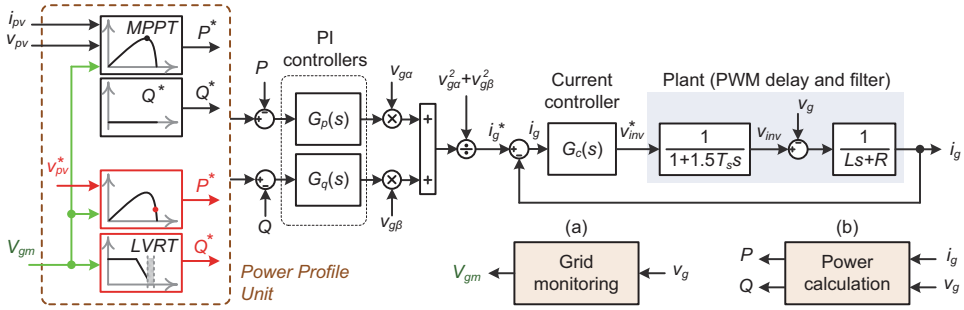

Figure 4.12: *Closed-loop control system of single-phase systems with LVRT capability based on single-phase PQ theory, where it includes (a) grid monitoring system and (b) power calculation unit.*

As shown in Figure 4.12, the "Power Profile" unit is responsible for an appropriate generation of the average active power and reactive power references according to the grid conditions. In the normal operation mode, the average active power reference P^* is the output of MPPT control, and the system is operating at unity power factor as required (i.e., $Q^* = 0$ Var). When the grid fault event is confirmed by the monitoring system, the power reference generation unit (i.e. "Power Profile" unit) will act accordingly, and set the proper references. Take the E.ON grid code [25] for example, the required reactive current under different voltage levels can be given by,

$$I_q = \begin{cases} 0, & 0.9 \text{ p.u.} \leq v_g < 1.1 \text{ p.u.}; \\ k(1-v_g)I_N, & 0.5 \text{ p.u.} \leq v_g < 0.9 \text{ p.u.}; \\ I_N, & v_g < 0.5 \text{ p.u.}. \end{cases} \tag{4.2}$$

in which v_g is the grid voltage in p.u. and I_N is the rated grid current. Then, according to the single-phase PQ theory, the power references can be expressed as,

$$\begin{cases} P^* = \frac{1}{2}V_{gm}I_d \\ Q^* = \frac{1}{2}V_{gm}I_q \end{cases}, \qquad \text{and } I_d^2 + I_q^2 = I_N^2, \tag{4.3}$$

where V_{gm} is the grid amplitude, and I_d is the active current. Notably, the rated current I_N is limited by the inverter maximum allowable current I_{max}, i.e. $I_N \leq I_{max}$, as it is illustrated in Figure 4.2. Considering a predesigned PV inverter, a severe voltage sag (e.g. 0.45 p.u) may trigger the inverter over-current protection. Thus, the active power during fault ride-through have to be dispatched using the solutions shown in Figure 4.3.

Figure 4.13 demonstrates the performance of a 1 kW single-stage single-phase PV system with LVRT control, where the active power is reduced by modifying the MPPT control. The system parameters are given in Appendix A.1. As shown in Figure 4.13,

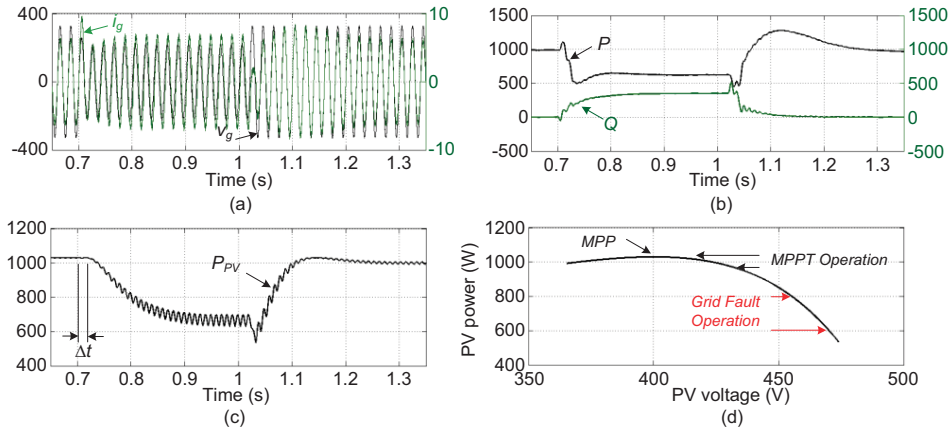

Figure 4.13: *Performance of a single-phase PV system under grid faults (0.35 p.u. voltage sag): (a) grid voltage v_g [V] and current i_g [A], (b) active power P [W] and reactive power Q [Var], (c) PV power P_{PV} [W], and (d) PV power versus PV voltage.*

once the grid fault is detected, the MPPT unit is disabled and the control system is switched to grid fault operation mode. Soon after, the system starts to inject reactive current and limit the active power output. After the fault is cleared (voltage rises to 0.9 p.u.), the system goes back to its normal operation, and again, MPPT control is achieved. Moreover, both the start of the voltage sag and the end of that present a transient time delay. It is mainly because of the fault detection time delay, but also the power calculation delay. However, the results have confirmed the possibilities and the effectiveness of the control strategy for single-phase systems under grid faults.

4.3.1 Reactive power injection of single-phase systems

Reactive power injection may be required for the PV systems under grid faults in future. For an advanced inverter, reactive power injection may also contribute to improved system stability and reliability. In light of those issues, this section considers the dynamic grid support requirement and the inverter maximum current limitation shown in Figure 4.2, three Reactive Power Injection (RPI) strategies are proposed: a) constant average active power control strategy, b) constant active current control strategy, and c) constant peak current control.

A. Constant average active power control strategy (Const.-P)

The control objective of this RPI control strategy is to maximize the output energy with MPPT control during LVRT operation. Therefore, the average active power is maintained constant in the short-term period. According to the reactive power current

requirements in Figure 4.11(b) and Eq. (4.3), the current in the *dq*-rotating reference frame can be expressed as,

$$\begin{cases} I_d = & \dfrac{k_d}{v_g} I_N \\ I_q = & k(1-v_g) I_N \end{cases} \quad \text{and } I_{gmax} = \sqrt{I_d^2 + I_q^2} \tag{4.4}$$

in which $\left(1-\frac{1}{k}\right)$ p.u $\leq v_g < 0.9$ p.u., I_{gmax} is the injected current amplitude, $k_d = P/P_N$ is the power derating factor with P being the injected active power and P_N being the nominal power, and k is defined in Figure 4.11(b). When $v_g < \left(1-\frac{1}{k}\right)$ p.u., the system is required to fully inject reactive power, while the active power output may be disabled. In that case, the system might still operate at *Const.-P* mode, depending on the inverter current limitation (i.e. $I_d = \frac{k_d}{v_g} I_N$ and $I_q = I_N$).

However, when the required injection of reactive power is fulfilled according to Eq. (4.4), the inverter may experience an over-current, and thus over-heating with this control strategy, which has been mentioned in previous section. To prevent inverter shutdown from over-current during LVRT, the following constraints should be satisfied:

$$\begin{cases} \frac{1}{v_g}\sqrt{k_d^2 + k^2(v_g - v_g^2)^2} \leq \frac{I_{max}}{I_N}, & \text{when } \left(1-\frac{1}{k}\right) \text{ p.u.} \leq v_g < 0.9 \text{ p.u.} \\ \frac{1}{v_g}\sqrt{k_d^2 + v_g^2} \leq \frac{I_{max}}{I_N}, & \text{when } v_g < \left(1-\frac{1}{k}\right) \text{ p.u.} \end{cases} \tag{4.5}$$

in which I_{max} is the inverter current limitation. Eq. (4.5) gives a design criterion for the component selection, and it can be further illustrated in Figure 4.14(a).

It has been demonstrated in Figure 4.14(a) that the minimum value of the inverter current limitation (I_{max}) should be $2.24I_N$, when $k = 2$ p.u., so that the RPI strategy can be adopted in the case of a wide range of voltage drop (i.e. the grid voltage is within 0.5 p.u.$\leq v_g < 0.9$ p.u.) without power derating ($k_d = 1$ p.u.). As for a predesigned PV inverter with a robustness margin, the system has to derate the output power in order to inject enough reactive power. For instance, if the allowable maximum current of a PV inverter, $I_{max} = 1.5I_N$ and $k = 2$ p.u., the PV systems should reduce active power output, when the voltage drops below 0.72 p.u., as it is shown in Figure 4.14(a) and (c). Otherwise, the system should change RPI strategy before it is triggered due to over-current (over-heated).

B. Constant active current control strategy (Const.-I_d)

Another RPI control strategy under LVRT operation is to maintain a constant active current (i.e. $I_d = \frac{2P}{V_{gm}} = const.$ with V_{gm} being the grid voltage amplitude). This will result in an automatic reduction of the active power in response to voltage drops, since $P \propto V_{gm}$. In the case of this control strategy ($(1-\frac{1}{k})$ p.u $\leq v_g < 0.9$ p.u.), the current in the $dq-$frame can be expressed as,

$$\begin{cases} I_d = & mI_N \\ I_q = & k(1-v_g) I_N \end{cases} \quad \text{and } I_{gmax} = \sqrt{I_d^2 + I_q^2} \tag{4.6}$$

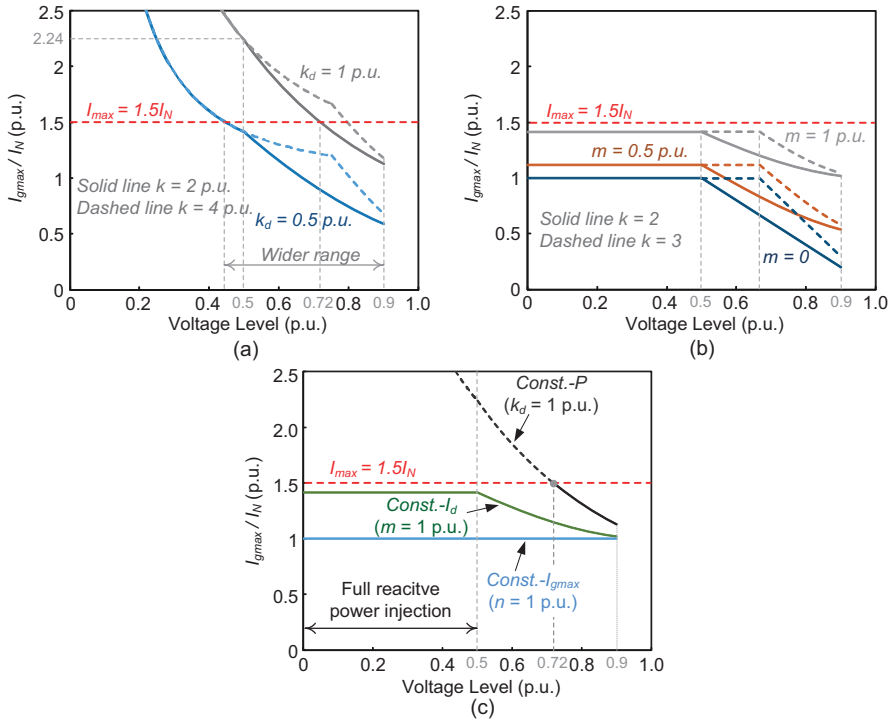

Figure 4.14: *Design constraints of reactive power injection strategies for single-phase systems considering the inverter over-current protection: (a) Const.-P, (b) Const.-I_d, and (c) application conditions when $k = 2$ p.u. and $I_{max} = 1.5I_N$.*

where m is the active current level index corresponding to the nominal current I_N and $0 \leq m \leq 1$. Similar to the case of *Const.-P*, the PV inverter should inject full reactive power (i.e. $I_d = mI_N$, $I_q = I_N$), when a severe voltage fault happens ($v_g < \left(1 - \frac{1}{k}\right)$ p.u.). For simplicity, the active current can be controlled as $I_d = I_N$, i.e. $m = 1$ p.u..

However, adoption of this RPI strategy may also lead to a rise of the current amplitude, which will possibly exceed the inverter current limitation, and thus an inverter trip-off may happen due to over-current. Hence, the following conditions should be fulfilled when it is adopted under grid faults:

$$\begin{cases} \sqrt{m^2 + k^2(1 - v_g)^2} \leq \frac{I_{max}}{I_N}, & \text{when } \left(1 - \frac{1}{k}\right) \text{ p.u.} \leq v_g < 0.9 \text{ p.u.} \\ \sqrt{m^2 + 1} \leq \frac{I_{max}}{I_N}, & \text{when } v_g < \left(1 - \frac{1}{k}\right) \text{ p.u.} \end{cases} \tag{4.7}$$

where m becomes a design parameter. A design guide for this RPI control strategy is shown in Figure 4.14(b). Compared to a PV inverter with *Const.-P* control strategy,

the PV inverter with *Const.-I_d* can be designed with a lower I_{max}/I_N, leading to the possibilities to select power devices with lower current ratings and thus lower cost, as it is shown in Figure 4.14(c). Besides, a derating operation can be achieved by changing m because of the proportional relationship, $P \propto V_{gm}$. Notably, a smaller m will contribute to select power devices of lower ratings.

C. Constant peak current control (Const.-I_{gmax})

The above discussed RPI strategies might pose the PV inverter at a risk of over-current loading during LVRT. However, with constant peak current control strategy, there is no unintentional inverter shutdown, since the peak of the injected grid current is kept constant and lower than the inverter current limitation during LVRT, i.e. $I_{gmax} = const. < I_{max}$. The current under grid faults ($(1 - \frac{1}{k})$ p.u $\leq v_g < 0.9$ p.u.) in this case can be given as,

$$\begin{cases} I_d = & \sqrt{n^2 - k^2(1 - v_g)^2} I_N \\ I_q = & k(1 - v_g) I_N \end{cases} \quad \text{and } I_{gmax} = \sqrt{I_d^2 + I_q^2} \tag{4.8}$$

where n is introduced as the peak current index corresponding to the nominal current I_N, and $I_{gmax} = nI_N$. It is the same as the other strategies that, when $v_g < \left(1 - \frac{1}{k}\right)$ p.u., the full reactive power has to be injected, i.e. $I_d = \sqrt{n^2 - 1} I_N$, $I_q = I_N$.

Notably, n has a maximum value of $\frac{I_{max}}{I_N}$ p.u., when considering the inverter current protection. For instance, when $I_{max} = 2I_N$ for a PV inverter, the maximum n should be 2 p.u. to ensure a stable RPI without tripping-off the inverter during LVRT. Therefore, if $n \leq \frac{I_{max}}{I_N}$, the riding-through operation of the PV inverter will not give an amplitude rise to the injected current. Meanwhile, according to Eqs. (4.3) and (4.8), the active power will be reduced in order to inject sufficient reactive power during LVRT.

During the design and the operation of the PV inverters, those constraints should be considered for different applications. Figure 4.14(c) shows an comparison of the RPI strategies for a PV inverter with $I_{max} = 1.5I_N$ when $k = 2$ p.u.. It can be observed in Figure 4.14(c) that the *Const.-I_{gmax}* can be adopted in a wide range of voltage levels (i.e. $0 \leq v_g < 0.9$ p.u.) even with different values of k. This is also the same case when the *Const.-I_d* is used. However, the *Const.-P* is only effective when the grid voltage is within a certain range, if without power derating operations ($k_d = 1$ p.u.). Nevertheless, based on the above discussions and also Figure 4.14, the corresponding active and reactive power references under voltage sags for the proposed RPI control strategies can be obtained. As a result, the required reactive power complying with grid codes can be injected when the control structure shown in Figure 4.12 is adopted. A summary of the proposed RPI strategies is given in Table 4.3, which shows the advantages and design constraints/considerations of each RPI control strategy.

Referring to Figure 4.12, experimental tests of a single-phase full-bridge inverter were carried out to verify the effectiveness of the proposed RPI strategies. The test system is given in Appendix B.1, and the results are shown in Figure 4.15. It is demonstrated

Table 4.3: *Summary of the proposed reactive power injection strategies.*

RPI Strategy	Advantages	Design Constraints
Const.-P	Maximized energy yield (with MPPT control)	Over-current trip-off; derating operation is necessary under severe faults; large design margin for a wide voltage range.
Const.-I_d	Reduced power operation ($P \propto V_{gm}$)	Over-current issues; it also requires power derating operation; small design margin for a wide voltage range.
Const.-I_{gmax}	No over-current problems; Applicable for all inverters	–

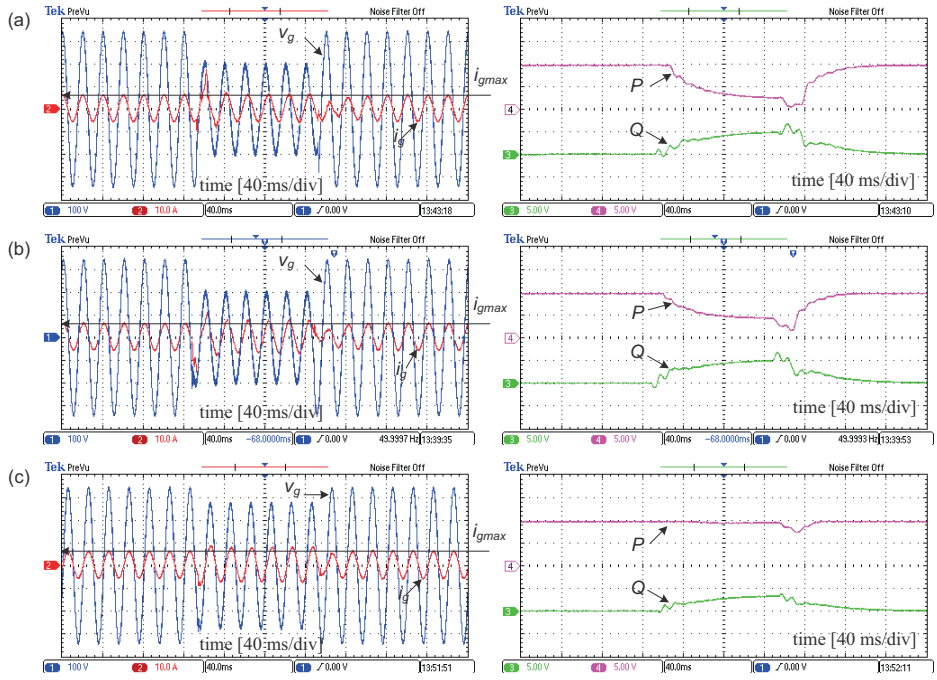

Figure 4.15: *Experimental results of a single-phase system with: (a) Const.-I_{gmax} (voltage sag: 0.45 p.u., $n = 1$ p.u.), (b) Const.-I_d (voltage sag: 0.45 p.u., $m = 1$ p.u.), and (c) Const.-P (voltage sag: 0.2 p.u., $k_d = 1$ p.u.): grid voltage v_g [100 V/div], grid current i_g [5 A/div], active power P [500 W/div], and reactive power Q [500 Var/div], when $k = 2$ p.u..*

that those RPI strategies can fulfil the grid requirements, but by using different control objectives. The *Const.-I_{gmax}* control strategy can contribute to a constant amplitude of the injected current, while the active current is kept constant in the *Const.-I_{gmax}* control

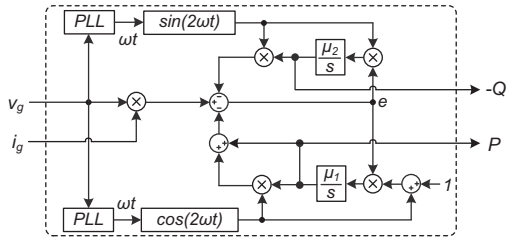

Figure 4.16: *Proposed active and reactive power calculation method for single-phase systems: grid voltage:* $v_g = V_{gm}\cos(\omega t)$*, grid current:* $i_g = I_{gmax}\cos(\omega t + \phi)$.

strategy, and at the same time, both strategies can inject sufficient reactive current during a severe voltage sag (0.45 p.u.). In contrast, the *Const.-P* control strategy has been tested when the grid voltage presents a 0.2 p.u. voltage sag as shown in Figure 4.15(c), since the severe voltage fault will make the inverter shutdown due to over-current [129]. In that case, the system has to derate the active power in order to ride-through the short-term voltage disturbance.

4.3.2 A new single-phase power calculation method

In case that the power control based single-phase PQ theory is adopted for control, it is inevitable to calculate the average active power and reactive power fast and accurately in order to enhance the LVRT capability for single-phase PV systems. The use of low-pass filters and Discrete Fourier Transform (DFT) may introduce delays which are not desirable in LVRT cases. Derived from single-phase PQ theory, the power calculation can also be done when an advanced OSG technique is available. However, the OSG based methods make the transient behavior of the power calculation units highly dependent on the performances of the OSG systems.

Driven by the Enhanced PLL concept proposed in [94], a novel average power calculation method is proposed in the following for single-phase grid-connected photovoltaic systems controlled by the single-phase PQ theory. This power calculation is based on an adaptive filtering technique. Figure 4.16 represents the structure of the proposed power calculation method. As it is shown in Figure 4.16, the calculation requires a dedicated PLL system for synchronization. Then, the following is valid according to Figure 4.16:

$$\begin{cases} \dfrac{\hat{P}(s)}{P(s)} = \dfrac{1.5\mu_1}{s+1.5\mu_1} = \dfrac{1}{\tau_1 s+1} \\ \dfrac{\hat{Q}(s)}{Q(s)} = \dfrac{0.5\mu_2}{s+0.5\mu_2} = \dfrac{1}{\tau_2 s+1} \end{cases} \tag{4.9}$$

where τ_1, τ_2 are the time constants and "$\hat{}$" denotes the desirable/reference power. The detailed derivation of this transfer function can be found in [130].

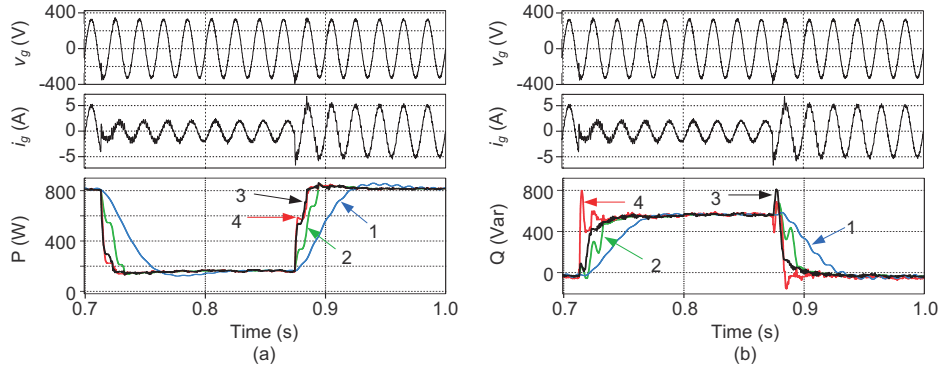

Figure 4.17: *Simulation results of a single-phase grid-connected system in different operation modes (unity power factor and non-unity power factor): (a) active power and (b) reactive power (1. power calculation based on LPF, 2. power calculation based on DFT, 3. SOGI based power calculator, 4. the proposed method with $\tau_{1,2} = 5$ ms).*

It is indicated in Eq. (4.9) that the calculated average power (P and Q) is controlled by μ_1 and μ_1 respectively. A large value of $\mu_{1,2}$ will make the estimated active power or reactive power coming to steady-state quickly, but it will have a high overshoot if it is too large. The settling time can approximately be calculated as: $4\tau_{1,2}$. However, considering the performance of the PLL system, the settling-time for the proposed method may be longer than $4\tau_{1,2}$, which has been verified by the simulation results presented in Figure 4.17. This constraint should be taken into account to tune the parameters. Nevertheless, the proposed power calculation method can also be adopted into other single-phase applications, such as droop-controlled micro grids and also vehicle-to-grid systems [127, 131].

4.3.3 Transformerless PV inverters under grid faults

In Chapter 3, the benchmarking results have shown that the performances of single-phase transformerless inverters are highly dependent on the mission profiles. In terms of reliability and also efficiency, the HERIC inverter has been proved to be the most promising solution for next-generation PV systems in order to achieve a reduction in cost of energy. However, in response to the grid voltage disturbances, some of those inverters might not be able to meet the relevant requirements, e.g. leakage current rejection and reactive power injection capability.

Figures 4.18 and 4.19 show the performance of three transformerless PV inverters under voltage sags, where the *Const.-I_{gmax}* RPI control strategy is adopted and the system parameters are given in Appendix A.1. According to Figures 4.11 and 4.12, once the grid fault is confirmed, the system enters into LVRT operation mode, where

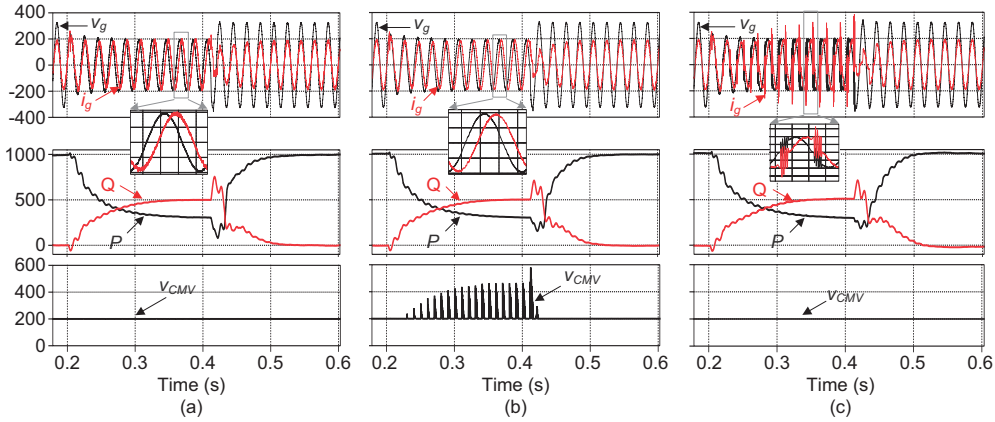

Figure 4.18: *Performance of the three grid-connected transformerless PV systems in low voltage ride through operation (0.43 p.u. voltage sag, grid voltage v_g [V], grid current i_g [30×A], active power P [W], reactive power Q [Var], and common mode voltage v_{CMV} [V]): (a) FB-Bipolar inverter, (b) H6 inverter, and (c) HERIC inverter.*

reactive power should be injected appropriately. As it is shown in those test results, in a wide range of grid voltage levels, the FB-Bipolar inverter can provide the required reactive power during LVRT operation. The H6 inverter is also capable of riding through the voltage sag within a voltage range of 0.5 p.u. to 0.9 p.u.. However, it also presents a high leakage current under grid faults as shown in Figure 4.18(b). Moreover, the current stresses on the extra devices of H6 are significantly higher than the four devices of a FB inverter, as it is shown in Figure 4.19, which also confirmed the discussion in Chapter 3. Since the HERIC inverter is disconnected from the grid when the transformerless inverter is also short-circuited in order to avoid leakage currents, the inverter can only operate at unity power factor (i.e. no reactive power injection capability). In other words, the HERIC is not suitable for use in single-phase PV applications in terms of fault ride-through capability.

4.4 Summary

This chapter has discussed the issues regarding low voltage ride-through operation of single-phase PV systems. Since such an advanced function is against the anti-islanding requirements, grid code/requirement modifications have been suggested to increase the compatibility of low voltage ride-through capability and anti-islanding protection in order to enable more PV installations with secured grid stability. Moreover, suggestions on other advanced features for the next generation PV systems have also been proposed for the future grid requirement revisions after a review of current grid codes. Those fea-

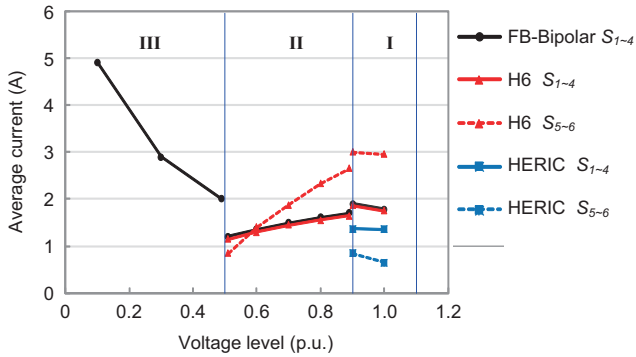

Figure 4.19: *Average current stresses of IGBT devices in the three transformerless PV inverters with different voltage levels: I- normal operation (0.9 p.u.* $\leq v_g <$ *1.1 p.u.), II- LVRT with* Const.-I_{gmax} *(0.5 p.u.* $\leq v_g <$ *0.9 p.u.), and III- full reactive power injection (*$v_g <$ *0.5 p.u.).*

tures are the key to the realization of a wide-scale adoption of single-phase PV systems, where the energy is transferred efficiently and reliably to the grid.

In respect to the control of single-phase PV systems in different operation modes, this chapter has presented a comparison of various current controllers in terms of harmonic rejection capability, as well as a benchmarking of grid faulty mode control. Since reactive power injection is normally required to support the grid voltage, three different strategies have been proposed. Experimental results have demonstrated the effectiveness of the proposed reactive power injection strategies for single-phase systems under grid faults. It has also been verified that the power control based on single-phase *PQ* theory is an effective solution for single-phase systems both in normal operation mode and under grid faults. However, the performance of this control is dependent on the power calculation unit and also the grid monitoring technique. Hence, a new single-phase power calculation method has been introduced to enhance the performance.

At the end of this chapter, different transformerless PV inverters have been evaluated under grid faults in terms of reactive power injection capability and leakage current rejection ability. Together with the benchmarking presented in Chapter 3, it has been found that although the HERIC can achieve the highest efficiency, it is not a good candidate for single-phase PV applications due to its poor reactive power injection capability.

5 Constant Power Generation Control Concept

In this chapter, a constant power generation control concept for PV systems has been introduced to unload the distributed grid capacity when a wide-scale adoption of PV systems is reached. At the beginning of this chapter, the viability of this advanced control strategy is addressed, followed by the implementations of constant power generation control in association with the case studies. In addition, due to the redistributed thermal loading of the power devices in constant power generation mode, the entire system reliability is also affected. Hence, this chapter also gives a discussion on the possibility of reliability improvement of single-phase PV inverters by limiting the maximum feed-in power to the grid.

5.1 Feasibility of constant power generation control

5.1.1 Limitations of increasing renewable energy adoption

With more environmental-condition-dependent renewable energy systems (e.g. PV systems, wind turbine systems, and fuel-cell systems) connected to the grid, aging distributed/transmission lines and local substations have to cope with the increased amount of fluctuating power, which are affected by the mission profiles (e.g. solar irradiation). This spectacular growth of renewable energy systems makes the grid highly decentralized and vulnerable. Further increase of the penetration level of renewable energy systems is required by most countries as discussed in Chapter 1. Consequently, the networks, including substations, may experience severe over-loading [132–134], which may further introduce stability problems and thus maintenance tasks, if the grid remains at its current capacity.

Therefore, it calls for advanced grid reinforcement measures (e.g. replacement of old transformers) for some countries, e.g. Germany. This is of importance, and alternatively, the DSOs have to reduce the renewable energy installations. However, potential costs brought by power grid infrastructure expansion, where the existing systems have to be retrofitted, have become the main obstacles. For instance, studies conducted by the Fraunhofer Institute for Wind Energy and Energy System Technology IWES and Ecofys have demonstrated that, a huge amount of money (approximately 1.1 billion euros) is required for grid expansion alone when the installed PV capacity reaches 70 GW by 2020 in Germany [134]. Thus, seen from a total cost point of view, the grid extension approach is not the optimal solution in order to increase renewable energy utilizations, like the single-phase PV systems.

5.1.2 Constant (absolute) power generation viability

In addition to the above consideration, as discussed in Chapter 1, catering for a vast amount of PV hosting capacity magnifies the influences from PV systems on the grid,

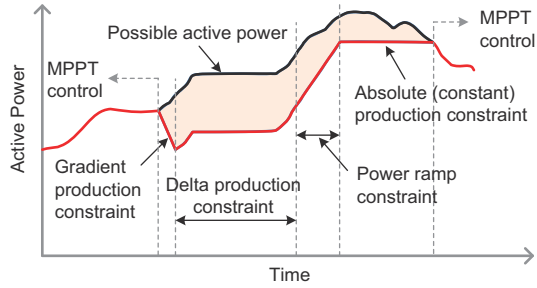

Figure 5.1: *Active power control functions for wind turbine power systems defined in the Danish grid code [142].*

and thus the grid integration policies may change in the future [20, 34, 134, 135], which again may require a flexible power control of PV systems. This lesson is learnt from the application issues of wind turbine systems to solve grid instability problems. For instance, voltage rise on the distributed feeders can be alleviated either by enabling reactive power control or by limiting the active power generation [20, 27, 136–138]. While due to the high R/X ratio of low-voltage grids, reduction of active power shows more effectiveness in voltage regulation than the reactive power control. Curtailing active power output is similar to constant power production when the voltage amplitude reaches the upper level. Moreover, frequency control through active power has been introduced for PV systems as well to stabilize the grid frequency [20, 27, 138–141]. It can be achieved by the droop function of the grid frequency and the active power.

Moreover, in a high penetration degree of PV systems, imbalances in or overloading of the grid may occur due to intermittency and/or reconnection from fault situations as discussed previously. Hence, similar to the requirements for wind power systems in Denmark [142, 143], it is better for PV systems to be equipped with active power control functions, such as active power production constraint, delta production constraint, and power ramp constraint. Those active power control functions are indicated in Figure 5.1. In that case, the PV systems have to provide a wide range of active power controllability, including constant power generation.

Currently, as it has been presented in [113, 119, 120] and [144], integrating energy storage systems into PV systems seems also to be a good solution to desirably control the active power. However, it will introduce additional cost and additional lifetime-limited energy storage components, making it not an optimal approach [140]. Considering the expenses, energy storage systems were mostly installed at the substation side instead of integrated in the PV inverters in order to achieve constant power production. Today, with the advancements of energy storage technology and its still decreasing price, some companies have incorporated battery storage systems into their PV inverters in order to increase the flexibility of the power control or the energy management [145].

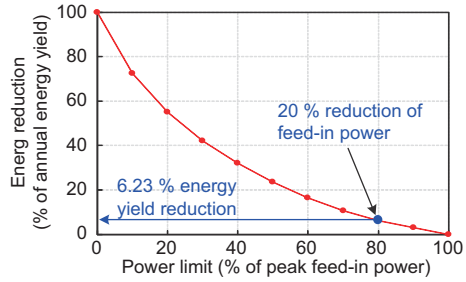

Figure 5.2: *Energy yield reduction due to limiting maximum feed-in power from a 3 kW grid-connected single-phase PV system.*

Actually, the constant (absolute) power production control can also be attained at the PV inverter level. A representative study of a 3 kW single-phase PV system with a yearly mission profile shown in Figure 3.6 has revealed its feasibility. As it is shown in the energy production profile (Figure 5.2), a 20% reduction of the maximum feed-in power from PV systems only leads to a 6.23% reduction of yearly total energy yield. This is because that the PV systems are generally only operating at partial load through a day. Thus, it is viable and reasonable to increase the PV penetration degree without violating the grid capacity and retrofitting the existing systems by limiting the maximum feed-in power from current existing PV systems. At the same time, frequency stability can potentially be improved by enabling absolute power control [140]. Such issues are already being discussed in some countries [133, 135, 144], where the PV systems share a considerable proportion of electricity generation, e.g. Germany [134, 135, 144].

As illustrated, reducing the maximum feed-in power from existing PV systems can contribute to decreased burden of the grid at a high penetration level, and thus allow an even wider-scale adoption of PV systems. When the maximum power is limited, a certain percentage of the energy from the current PV systems is cut off arbitrarily in a long-term operation, which is shown in Figure 5.2, and thus in a short-term operation, the PV systems should be able to operate in constant power generation mode, i.e. absolute production constraint in Figure 5.1, when the output power reaches the power limitation set by the DSOs considering the system demand and supply (e.g. 80% of the nominal maximum power). Possible implementations of Constant Power Generation (CPG) control strategy are detailed in the followings.

5.2 Implementations of constant power generation control

As one of the active power control functions, which are aimed at 1) further increasing the penetration level of renewable energy systems and 2) actively participating in frequency control to ensure grid stability, the CPG control strategy enables more PV systems to

be installed. It can be implemented by means of: a) integrating energy storage systems, b) managing the total power of an aggregated PV system (power balancing), and c) modifying the MPPT control of the PV inverters.

5.2.1 Integrating energy storage systems

Although integration of energy storage systems into highly PV-penetrated grids will increase the total expenses, significant improvements of active power control functions can be achieved [113, 120, 144]. Using energy storage systems, the PV output power can be free of fluctuations and higher than its nominal value by continuously discharging the energy storage systems. Because of the high cost, in the past, energy storage systems were mostly installed at the medium-voltage side (substations), and more suitable for large PV power plant applications. While, the price has dropped today, and also the advancements of this technology make it possible to be integrated in PV inverters [145].

Nonetheless, since this technology has several advantages and gives much flexibility to the active power control by providing an energy "reservoir", and thus smoothing the active power [113, 120], it will be more widely adopted in the next-generation PV systems for a flexible energy management, as discussed in § 4.1.2. In that case, the penalty will only be additional cost and the introduction of lifetime-limited energy storage components into the entire PV system. Besides, due to the significance in the increase of self-consumption abilities and thus reduction of energy bills, many efforts have been made into the integration of PV systems with batteries or mobility energy storage systems (e.g. electric vehicles) [134, 146–148].

5.2.2 Power management/balancing control

Inspired by the active power curtailment control, appropriately managing the power at the secondary control level in an aggregated PV system can contribute to a constant power production. As it is shown in Figure 5.3, when the distributed grid voltage exceeds the limitation due to strong solar insolation in a highly PV-penetrated system, several PV systems have to be cut-off in order to bring the voltage back [138]. Similarly, the total output power can be maintained constant by properly managing the power of each PV unit, as it is shown in Figure 5.4, where the entire system is controlled centrally. The power reference commands for each PV system are determined (managed) by a central control system. The total output power can be expressed as,

$$P_{total} = \begin{cases} \sum_{i=1}^{n} P_i, & \text{when } \sum_{i=1}^{n} P_{maxi} < P_{limit} \\ P_{limit}, & \text{when } \sum_{i=1}^{n} P_{maxi} \geq P_{limit} \end{cases} \tag{5.1}$$

where P_{maxi} is the maximum power of each PV system (unit) achieved by MPPT control and P_{limit} is the total power limitation of the distributed grid.

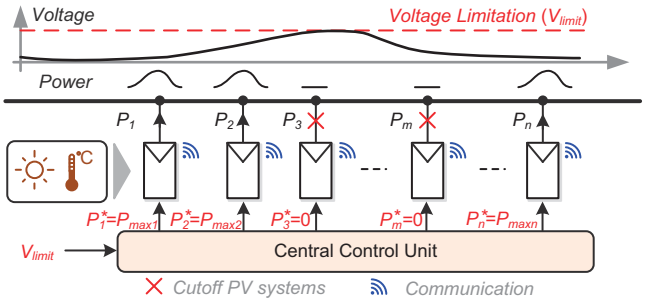

Figure 5.3: *Voltage reduction by cutting off PV systems during peak production period in a highly PV-penetrated system.*

As it is illustrated in Figure 5.4, in this control strategy, some PV units operate in MPPT mode, while some in CPG mode. This means that an individual PV inverter should be able to adjust its output power (e.g. constant power) according to the power set-points from the central control unit. Moreover, this system can also operate in delta power production mode or in a controlled power ramp-rate mode like what has been illustrated in Figure 5.1, only when the power reference for each PV unit is allocated appropriately. Similarly, a constant power production can also be achieved in a hybrid system (e.g. PV system and small wind turbine) as long as it is properly balanced by the central control unit. Notably, the implementation of this control strategy requires the knowledge of the forecasted mission profiles (better monitoring system and forecast algorithms) and an enhanced communication system.

5.2.3 Modifying MPPT control

For an individual PV inverter, the controllability of active power can be achieved by modifying the MPPT algorithm [133]. In contrast to constant power production with energy storage systems, using a modified MPPT control in the CPG operation mode (MPPT-CPG control), there is no need to install extra devices and thus there are no additional expenses in order to increase the penetration degree of PV systems.

The control structure of a two-stage single-phase PV system with CPG control by modifying the MPPT control algorithm can be represented as shown in Figure 5.5, where the MPPT-CPG control is implemented in the control of the DC-DC stage. Hence, the whole system can be divided into two operation modes based on the output power of the PV panels - the MPPT control mode and the constant power production mode. Hence, the actual power production can be expressed as,

$$P_o = \begin{cases} P_{PV}(t), & \text{MPPT, when } P_{PV}(t) < P_{limit} \\ P_{limit}, & \text{CPG, when } P_{PV}(t) \geq P_{limit} \end{cases} \tag{5.2}$$

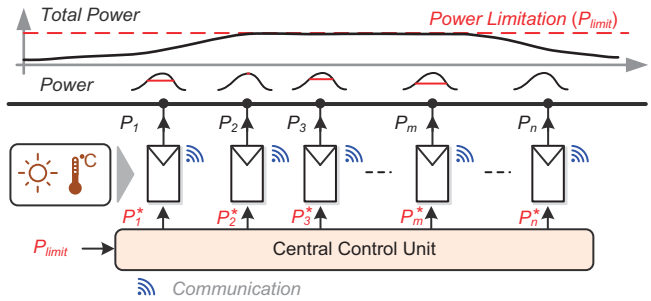

Figure 5.4: *Power management control to achieve a total constant power production in an aggregated PV system.*

in which P_o is the output power, $P_{PV}(t)$ is the instantaneous power of the PV system, and P_{limit} is the power limitation.

During a day, the output power of PV strings is changing with the environmental conditions, which means that the operation modes will also alter with solar insolation and/or ambient temperature, especially in a cloudy day. Figure 5.6 shows an example of different operation regions for a single-phase PV system during a day. Then, the energy production in different operational modes can be calculated as ,

$$\begin{cases} E_{mpp} = \int_{t_0}^{t} P_{PV}(t)dt \\ E_{cpg} = \int_{t_1}^{t_2} P_{limit}dt + \int_{t_3}^{t_4} P_{limit}dt \end{cases} \tag{5.3}$$

where E_{mpp} is the available energy during a day with MPPT control, and E_{cpg} is the energy production in CPG operation mode in regions of II and IV in Figure 5.6. Subsequently, the cut-off energy can be expressed as

$$E_{ess} = \int_{t_1}^{t_2} P_{PV}(t)dt + \int_{t_3}^{t_4} P_{PV}(t)dt - E_{cpg} \tag{5.4}$$

which is the non-used energy, or it could be used to size, e.g. an energy storage system.

According to Figures 5.5, 5.6, and Eq. (5.3), the operation principle of MPPT-CPG control for a PV inverter can be described as follows. When $P_{pv} \geq P_{limit}$, the system enters into CPG operation mode and the MPPT control is deactivated. The PV output power is regulated by a proportional controller (k_{cpg}). The proportional controller is able to maintain the output power constant during the operation. When $P_{pv} < P_{limit}$, the system should deliver as much energy as possible to the grid with an advanced MPPT

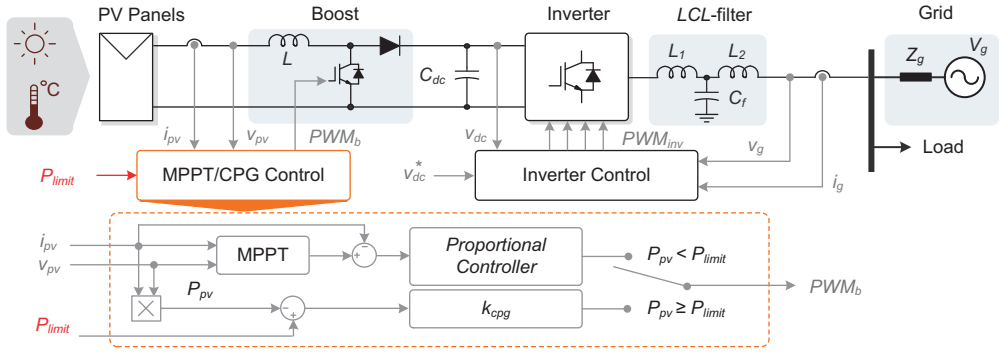

Figure 5.5: *Control diagram of a two-stage single-phase PV system with constant power generation ability by modifying MPPT control.*

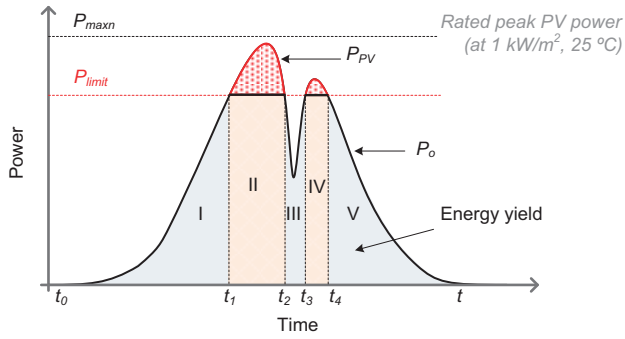

Figure 5.6: *Operation regions (I, III, V - MPPT; II, IV - CPG) for a single-phase PV system during a day with MPPT and CPG operations.*

control algorithm, and thus the CPG control is disabled. In both operation modes, the DC-link voltage (v_{dc}) is regulated via a Proportional Integrator (PI) controller to be constant to ensure the power injection. Current controllers should further be selected in terms of good harmonics rejection.

Besides the above solutions, an alternative way to attain constant power production is to directly modify the MPPT algorithm, as it is presented in [133]. All solutions require a better knowledge of MPPT control algorithms. Typically, the Perturb-and-Observe (P&O) and incremental-conductance MPPT methods can be adopted in a PV system. However, a sudden change of the operation condition (e.g. from MPPT operation to CPG operation mode) may introduce instability [149], being a challenge for those MPPT control systems, which needs more in-depth investigations.

Table 5.1: *Parameters of the 3 kW two-stage single-phase PV system.*

PV panels rated power	$P_n = 3000$ W
Boost converter inductor	$L = 5$ mH
DC-link capacitor	$C_{dc} = 2200$ μF
LCL-filter	$L_1 = 2$ mH, $L_2 = 3$ mH, $C_f = 4.7$ μF
Switching frequencies for boost stage and inverter	$f_{boost} = f_{inv} = 10$ kHz
Grid nominal voltage (RMS)	$V_g = 230$ V
Grid nominal frequency	$\omega_0 = 2\pi \times 50$ rad/s

5.2.4 Operation examples of CPG control

Referring to Figures 4.5 and 5.5, simulations of a two-stage single-phase grid-connected PV system are carried out to verify the effectiveness of the proposed MPPT-CPG control concept. The system parameters are shown in Table 5.1. The control parameters are given in Appendix A.2. The P&O MPPT control method is adopted in the MPPT operation mode [150]. In the CPG operation mode, the control unit receives the power set-point command P_{limit}, and the PV output power is regulated using a simple proportional controller as it is shown in Figure 5.5. The DC-link voltage is maintained as $v_{dc}^* = 400$ V. Firstly, the single-phase PV system with CPG control by modifying MPPT algorithm is tested under constant ambient temperature, but the solar irradiance level has experienced ramp-changes. The results of the PV system under this mission profile are presented in Figure 5.7, which also shows the solar irradiance profile.

It has been shown in the results that, when the maximum power exceeds the limitation (80% of nominal power set by the central control system), the CPG control has been activated and thus a constant output power of the PV strings is achieved effectively. Once the output power goes below the limitation due to lower solar irradiance (or higher ambient temperature), the system returns to the MPPT operation with ensured stability, as it is shown in Figure 5.7(b). Then, the maximum power from the PV strings are fed into the grid.

In order to further test the performance of the PV system with MPPT-CPG control under longer mission profiles, two daily environmental conditions have been applied to the two-stage system shown in Figure 5.5, and the system parameters are listed in Table 5.1. Energy production is also estimated using Eq. (5.3). The effectiveness of the advanced control strategy by modifying MPPT control to limit maximum feed-in power has been demonstrated in the results shown in Figure 5.8. However, the injected power to the grid presents a larger overshoot as shown in Figure 5.8 due to rapid solar irradiance changes of a cloudy day. This means that the robustness of the control system has to be enhanced by optimizing the control parameters. Nonetheless, the CPG concept is able to control the PV systems with a constant power output and limited loss of energy, and thus more PV systems can be installed without upgrading the grid capacity.

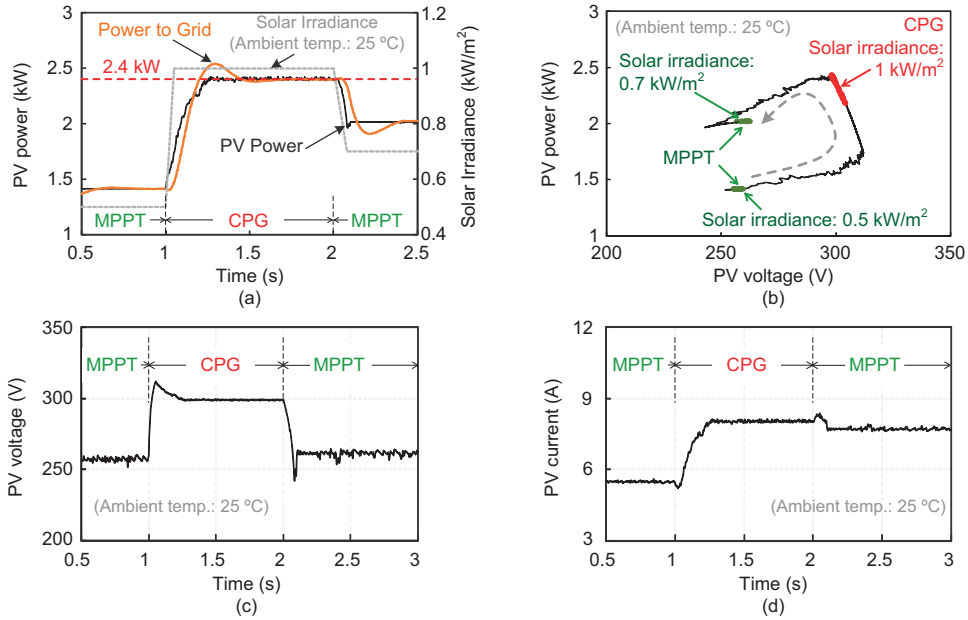

Figure 5.7: *Performance of a 3 kW single-phase PV system with constant power generation control: (a) output power and solar irradiance profile, (b) PV power v.s. PV voltage, (c) PV voltage, and (d) PV current.*

5.3 Reliability analysis of full-bridge PV inverters in constant power generation mode

The effectiveness of MPPT-CPG control strategy for PV systems has been demonstrated above. Due to the reduction of feed-in peak power, overloading issues can at least be alleviated with this control strategy, and thus allowing more installations of PV systems or other renewable energy systems on the same grid, as long as the CPG control is also enabled in the new systems. In addition, according to Figure 3.1, the CPG control attains a possibility to reduce the thermal stress on the power devices, since the power loss profile is changed through a long mission profile, when the PV system enters into CPG mode from MPPT mode and vice versa. As a result, the thermal stresses will affect the reliability of the PV system as it has been discussed in Chapter 3. Although limiting feed-in peak power from PV systems is already required in some countries, e.g. Germany [134], there is still a lack of quantitative and qualitative analysis on the potential reliability improvement by the MPPT-CPG control besides unloading the grid. On the basis of the mission profile based reliability analysis approach proposed in Chapter 3, the following will demonstrate this benefit.

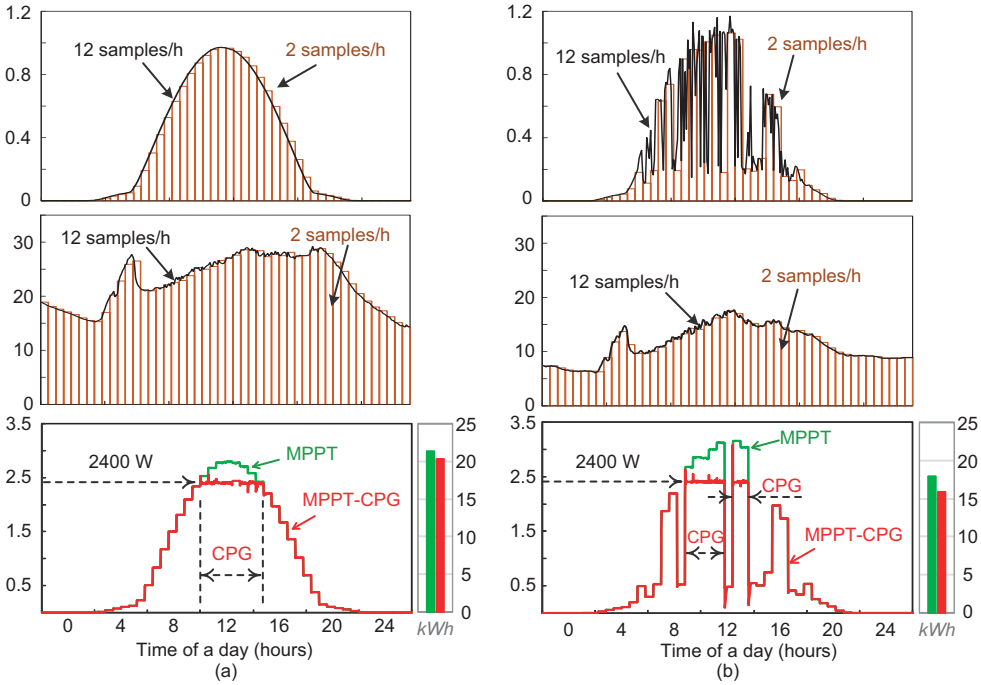

Figure 5.8: *Results of a 3 kW single-phase PV system with constant power generation control (top: solar irradiance [kW/m^2], middle: ambient temperature [°C], bottom: output power [kW]): (a) clear day profile and (b) cloudy day profile.*

5.3.1 Mission profile reconstruction

As it has been presented in § 5.2, there are several possibilities to realize a constant power generation. Considering real-field applications, where limiting feed-in peak power was not initially included, the CPG control based on modifying MPPT algorithm is adopted in a two-stage single-phase PV system for lifetime investigations. Referring to Figures 4.5 and 5.5, the block diagram of a two-stage single-phase PV system with MPPT-CPG control is represented as Figure 5.9, where the decoupling relationship between the power losses and the temperature is also shown. The parameters of this single-phase system are listed in Table 5.1.

It can be observed in Figure 5.9 that the mission profile will contribute to lower power losses and thus lower junction temperatures due to the arbitrary cut-off power in CPG operation mode. The resultant thermal loading profile can then be applied to the mission profile based analysis approach for a quantitative and/or qualitative lifetime estimation, which have been detailed in Chapter 3, as long as it is appropriately

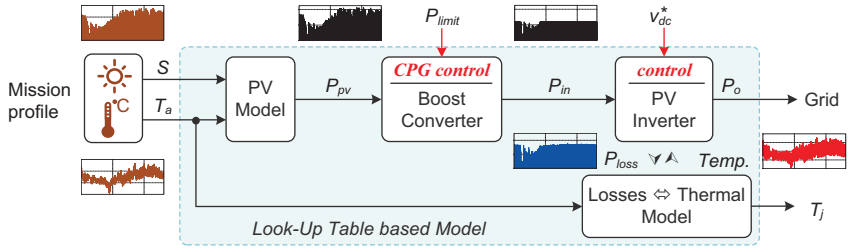

Figure 5.9: *Power flow block diagram of a single-phase two-stage PV system with CPG control referring to Figure 5.5.*

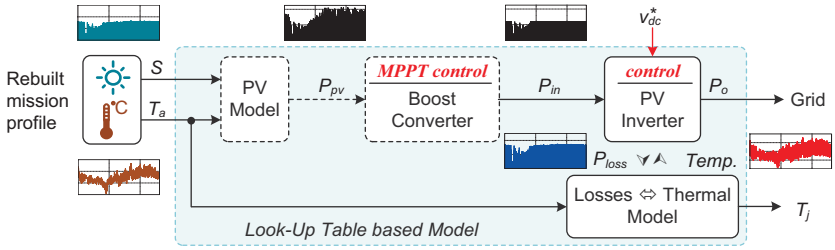

Figure 5.10: *Power flow block diagram of a single-phase two-stage PV system with MPPT control under a reconstructed mission profile to emulate the thermal loading profile when CPG control is applied.*

interpreted to a lifetime model. Besides, the mission profile based analysis approach also requires a compound loss/thermal model based on look-up tables to accelerate the evaluation process, especially under a long term mission profile, e.g. one year.

However, repeating work is also time-consuming to build a look-up table based model for this specific application - single-phase full-bridge PV inverter in MPPT-CPG operation mode, since such a compound model for the system in MPPT operation mode has already been constructed in Chapter 3. That model takes the mission profile as input, and the thermal loading and the power loss profiles of the power devices in the PV inverter are the outputs. As a result, alternatively, a mission profile can be reconstructed or retrofitted in order to obtain the same translated power loss profile of the power devices in this system on an assumption that the MPPT control is of good robustness. The power flow block diagram of a single-phase PV system with MPPT control under the reconstructed mission profile is shown in Figure 5.10.

As seen in Figures 5.9 and 5.10, retrofitting the mission profile to acquire the thermal loading of the same inverter with the MPPT-CPG control is valid, since in a two-stage system, the DC-link voltage v^*_{dc} is controlled to be constant. This means that the power

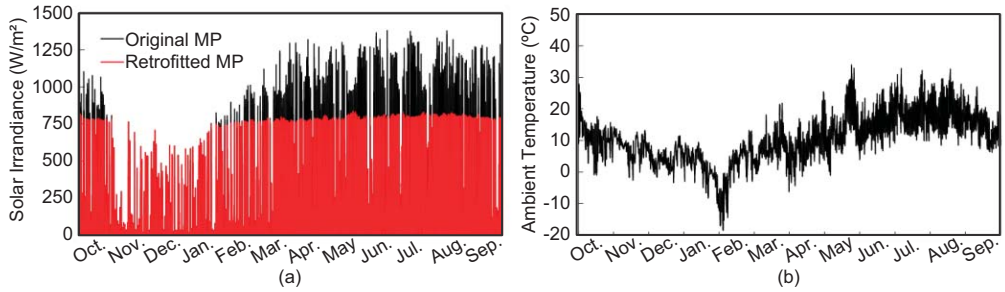

Figure 5.11: *Reconstructed mission profile by 20 % reduction of peak feed-in power.*

loss profile will be a function of the input current (thus, input power P_{in}) if the other conditions (e.g. switching frequency) are the same. Therefore, as long as the mission profile is reconstructed appropriately, the same loading profile as that of the system with the MPPT-CPG control can be obtained. A reconstructed Mission Profile (MP) by 20 % reduction of peak feed-in power has been compared in Figure 5.11 with the original MP for a 3 kW PV system. Notably, due to the thermal model dependency of the ambient temperature, only the solar irradiance level is retrofitted, which ensures that the resultant thermal loading profile under a reconstructed MP with MPPT control will be the same as that under the original MP with the MPPT-CPG control.

5.3.2 Lifetime analysis results

After the reconstruction of a long-term mission profile, e.g. a yearly mission profile shown in Figure 5.11, the lifetime of the power devices in a certain PV inverter in both MPPT and MPPT-CPG modes can be compared quantitatively under this mission profile. A yearly mission profile of high sampling rate (5 Hz) shown in Figure 5.11 has been used for this case study. According to the mission profile based analysis approach proposed in Chapter 3, both the original and reconstructed mission profile have to be decomposed into different time-scale mission profiles. In this case, the decomposition frequency is 1 Hz ($t_s = 1$ s). According to Figure 3.14, a rain-flow counting algorithm [106] has been applied to the long-term loading profiles to extract the temperature stress of the thermal profiles. The lifetime model (number of cycles to failure, N_f) given in Eq. (3.5) and [107] is adopted for lifetime calculation due to its relative accuracy, and for convenience, it is given again by,

$$N_f = A(\Delta T_j)^{\alpha}(ar)^{\beta_1 \Delta T_j + \beta_0} \left[\frac{C + (t_{ON})^{\gamma}}{C+1}\right] \exp\left(\frac{E_a}{k_B T_{jm}}\right) f_{diode} \tag{5.5}$$

where A, α, β_0, β_1, γ and C are the model parameters listed in Table 3.1, and ΔT_j, T_{jm}, and t_{ON} are the amplitude, mean value, and the period of the temperature cycles

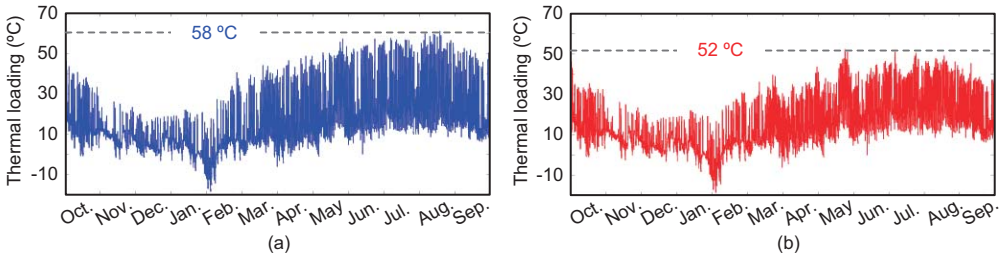

Figure 5.12: *Power device thermal loading in different operation modes: (a) MPPT contol and (b) 80% feed-in of peak power in MPPT-CPG mode.*

extracted from the thermal loading profiles. It should be pointed out that the lifetime model shown in Eq. (5.5) is for a single power device, and hence only one power device of the PV inverter is analyzed in the following.

A comparison of the power device thermal loading of the PV inverter in different operation modes is represented in Figure 5.12, where in MPPT-CPG operation mode, the power limitation is set to be 80 % of the peak power (e.g. 2400 W) under standard test conditions. It is clearly shown in Figure 5.12 that the maximum junction temperature of the power devices is reduced by 6 °C in MPPT-CPG operation mode, and thus the temperature cycle amplitude is also reduced. According to Eqs. (5.5) and (3.6), even without rain-flow counting, a qualitative result obtained is that the CPG control can contribute to a large number of cycles to failure and thus less lifetime is consumed.

Quantitative results enabled by rain-flowing counting are given in Figure 5.13, which shows that the number of cycles of the temperature cycling amplitudes ΔT_j from 15 °C to 65 °C has been reduced significantly, and the number of cycles of the mean junction temperatures ΔT_{jm} within a range of 35 °C $\sim$ 65 °C are also clearly reduced. Consequently, the Life Consumption LC given by Eq. (3.6) is reduced in comparison with that in MPPT operation mode. According to Eqs. (3.7) and (3.9), the lifetime of the power devices of the PV inverter under this mission profile given by Eq. (5.6) has been improved.

$$LF_{CPG} = \frac{1}{\overline{LC}} LF_{MPPT} \tag{5.6}$$

with LF_{CPG}, LF_{MPPT} being the lifetime of the power devices in MPPT-CPG and MPPT modes respectively, and $\overline{LC}$ being the LC of the power devices in the MPPT-CPG operation mode normalized to that in MPPT mode. This has been illustrated in the calculated LC distributions in Figure 5.14.

It is also seen in Figure 5.14(a) that the temperature cycles within a range of 15 °C $\sim$ 55 °C consumed most of the lifetime under the decomposed mission profile (long-term). Moreover, although the temperature cycles with large amplitudes (e.g. 45 °C $<$ ΔT_j $<$ 55 °C) account for a small number, they have contributed to much loading. One

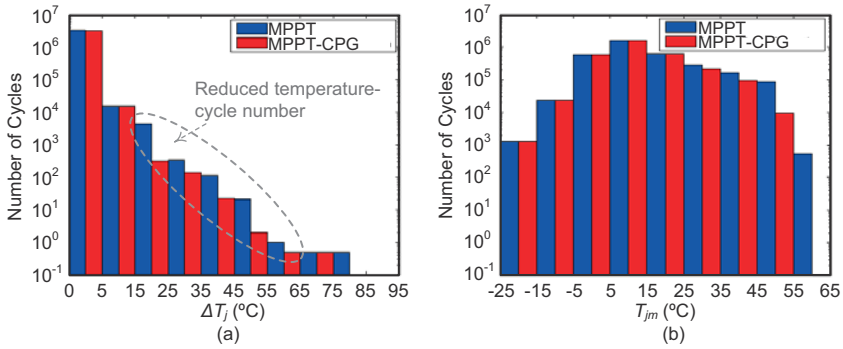

Figure 5.13: *Rain-flow counting results of the power device of a 3 kW single-phase PV inverter considering a long-term mission profile in different operation modes (MPPT and MPPT-CPG with 80 % of peak power feed-in): (a) junction temperature cycling amplitude ΔT_j and (b) mean junction temperature T_{jm}.*

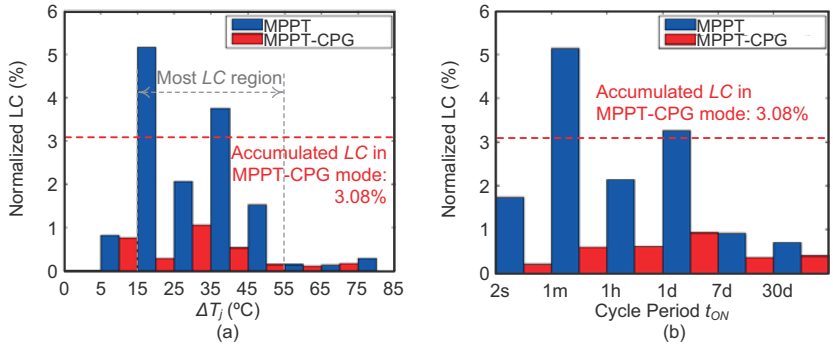

Figure 5.14: *Life consumption (LC) distribution of the power device of a 3 kW single-phase PV inverter considering a long-term mission profile in different operation modes (MPPT and MPPT-CPG with 80 % of peak power feed-in): (a) normalized LC distribution on ΔT_j and (b) normalized LC distribution on the cycle period t_{ON}.*

conclusion drawn from Figure 5.14(b) is that temperature cycles with the periods of 1 min to 1 hour are the main contributors of damage under the decomposed mission profile. In fact, the real-field mission profile used in this study varies at a rate of minutes, which means that the previous assumption for the mission profile decomposition is reasonable, and thus the temperature cycles within this range consume much lifetime. Those results have shown that the MPPT-CPG control can contribute to improved reliability of the power devices in a certain PV inverters with a limited energy loss.

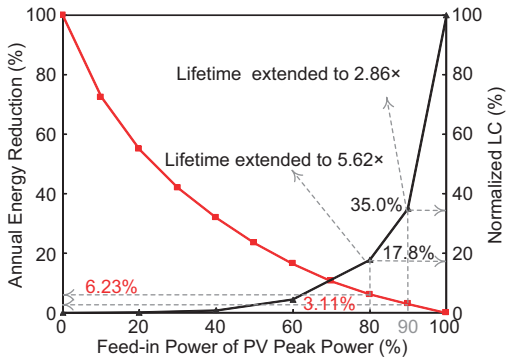

Figure 5.15: *Energy reduction and normalized life consumption due to the limitation of maximum feed-in power considering the mission profile in Figure 5.11.*

To further investigate the benefits of reliability improvement by limiting maximum feed-in power of PV systems at different levels, more evaluations have been carried out. The results are shown in Figure 5.15, the LC is normalized to that of power devices in MPPT operation mode considering both decomposed long-term and short-term mission profiles. It can be seen from Figure 5.15 that, when the maximum power is limited to 90 % and 80 % of the rated one, the corresponding energy yield reductions are of 3.11 % and 6.23 %, respectively, while the accumulated damage under this mission profile has been reduced by 65.0 % and 82.2 %. Thus, the lifetime of the power devices is significantly extended to 2.86 times and 5.62 times according to Eq. (5.6). Those evaluations have verified the effectiveness of reliability improvement by limiting feed-in power. A trade-off between the lifetime extension and the yearly energy generation can be done according to Figure 5.15.

5.4 Summary

This chapter has discussed the feasibility of the constant power generation control strategy for PV systems in order to cater for more PV energy in the line without violating the grid capacity. Possible implementations of this control strategy have also been presented, including a) integration with energy storage systems, b) power management control in an aggregated PV system, and c) modifying MPPT control. Considering real-field applications, where limiting peak power control is not initially included, the CPG control with MPPT modification can still be applied for extending the lifetime of the existing PV inverters by only software algorithm adjustments. Operation examples for two-stage single-phase grid-connected PV systems in constant power generation mode with MPPT modification have been demonstrated to show the effectiveness of this control strategy.

Besides, this chapter has also revealed that improved reliability of the power devices in single-phase PV inverters by the constant power generation control has been achieved. Using the time-efficient mission profile based reliability analysis approach proposed in Chapter 3, the lifetime of power devices by considering the temperature loading profiles is calculated in different operation modes. The results have illustrated that, besides the peak power limiting function considering grid capacity, the MPPT-CPG control can also extend the lifetime of the devices in PV inverters, when the maximum power is limited below the rated level, while the energy yield reduction is quite limited.

This penalty is economically viable since it avoids large investment in expanding the grid capacity and reduces the cost due to PV inverter failures, and thus lowers the cost of energy. The quantitative study performed in this chapter provides a guidance on the trade-off between the lifetime extension and the yearly energy generation for a 3 kW single-phase system. As this control strategy has been in effectiveness in some countries, the same philosophy may also be applied to other renewable energy systems, e.g. fuel-cell systems for further reduction of cost of energy.

6 Thermal Optimized Control Strategy

This chapter deals with the controllability of junction temperatures of the power devices in PV systems through appropriate power allocation, also named as "*Thermal Optimized Control*", in order to propose means to extend lifetime. Firstly, the principle of this control strategy is illustrated. Then, the implementation of this advanced control strategy for PV systems under grid fault is presented in details. Simulation and experimental results are included to verify the effectiveness of this thermal optimized control method of PV systems.

6.1 Thermal optimized control of PV systems

As it is discussed and suggested in § 4.1, the next generation PV inverters are expected to comply with more stringent grid codes, including higher reliability requirements, especially when a high penetration degree of PV systems, in order to further lower the cost of energy. The reliability requirement will be more strict in a highly PV-penetrated system (consists of many PV units), since the PV systems should not cease energizing in the case that some PV units fail to operate; otherwise, the stoppage of all PV units will lead to a power blackout in this system. A PV inverter typically consists of power devices (e.g. IGBT and MOSFET), where various factors can contribute to the failures, e.g. thermal stress, electrical stress, mechanical stress, materials of the part and deviation in product process. Since the temperature stress has been the most commonly observed failure mechanism for power electronics based systems [50,51], proper thermal management/control of the power devices may possibly contribute to an improved reliability of the power devices, and thus extended lifetime of the entire inverter. Moreover, the temperature is coupled with the power losses on the device as indicated in Figure 2.11 and Eq. (2.6), and thus thermal control can be achieved through power control in the PV inverter. In light of this, a thermal optimized control strategy is introduced for the power devices in single-phase PV inverters in order to reduce the junction temperature stress, and thus to achieve improved reliability of a PV inverter. The viability of the proposed thermal optimized control strategy is illustrated in the following.

6.1.1 Feasibility of junction temperature control strategy

To study the viability of the junction temperature control strategy, a 3 kW single-phase system has been built. Figure 6.1 shows the hardware schematic and control diagram of this system with the ability to achieve a controllable (reduced or constant) junction temperature. As it can be observed, a temperature reference (e.g. device maximum allowable junction temperature) is set in the control system. The system can not only perform standard functionalities like a) optimization/maximization of the input power, b) control of the inverter output voltage (i.e. voltage control), and c) synchronization

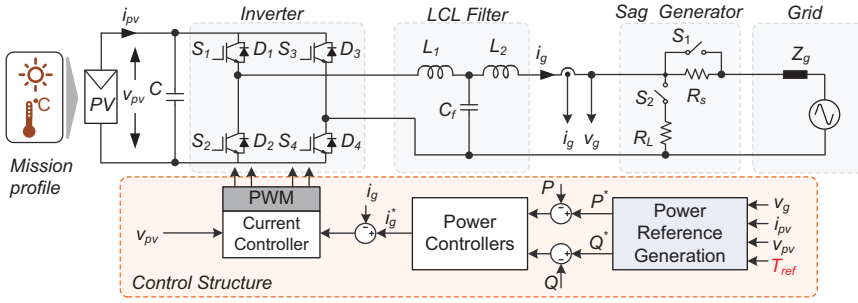

Figure 6.1: *Hardware schematic and control diagram of a single-phase single-stage full-bridge PV system with thermal optimized control.*

with the grid voltage [16, 19, 151], but also advanced control strategies, like LVRT and reactive power injection as discussed in Chapter 4.

When the reactive power injection is enabled under grid faults, the thermal behavior of the power devices will be affected. Besides, in real-field applications, the PV systems are operating in harsh environments, where the solar irradiance level is not constant, and thus the input power of the PV inverters are also varying. This will influence thermal loading conditions of the power devices. As it has been indicated in Figure 6.2, the power loadings on the power devices are different under various solar irradiation levels. Consequently, the junction temperature (e.g. maximum junction temperature T_{gmax} and the junction temperature fluctuation amplitude ΔT_j) will vary with the solar irradiance changes, which will affect the number of cycles to failure as illustrated by Eq. (6.1) [152]. In addition, both a high ambient condition change (e.g. solar irradiance level drop due to running clouds) and a sudden operation mode change (e.g. from MPPT mode to LVRT mode) may cause catastrophic failures of the power devices.

$$N_f = A \cdot (\Delta T_j)^{\beta_1} \cdot \exp(\frac{\beta_2}{T_{jm}}) \cdot (t_{ON})^{\beta_3} \cdot i^{\beta_4} \tag{6.1}$$

in which N_f is the number of cycles to failure, A, $\beta_{1,2,3,4}$ are the model coefficients related to the power device material, t_{ON} is the switching pulse width, and i is the wire current. As illustrated above, there are various factors that will affect the device temperature, e.g. current level i, voltage stress v, ambient temperature T_a, switching frequency f_s, and power losses P_{loss}. The relationship between the device temperature and the failure mechanisms can simply be given as,

$$T_j = f(i, v, T_a, f_s, P_{loss}, ...). \tag{6.2}$$

It is clear that the power losses as well as the current stresses have a strong relationship with the injected power. According to Eqs. (6.1) and (6.2), the resultant power

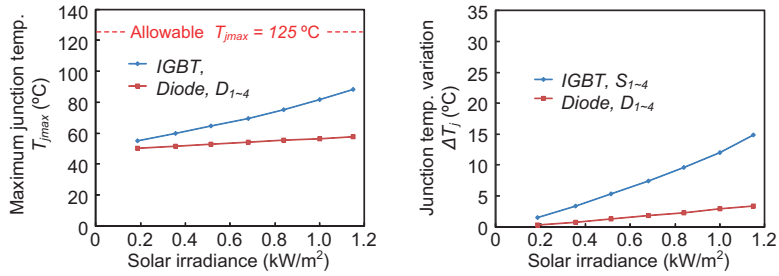

Figure 6.2: *Thermal loading of the power devices of the full-bridge PV inverter shown in Figure 6.1 under different solar irradiance levels: (a) maximum junction temperature and (b) junction temperature variation.*

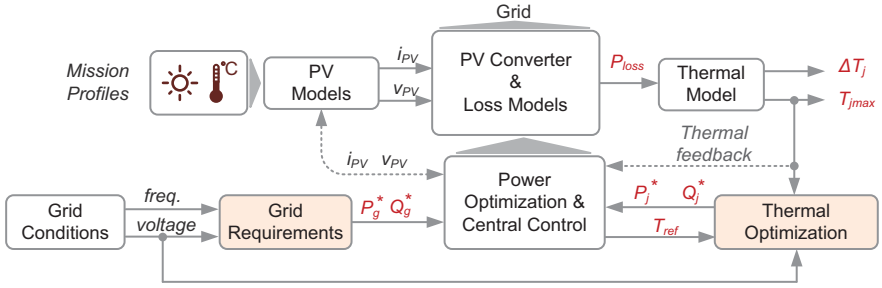

Figure 6.3: *Implementation of thermal optimized control strategy for PV systems.*

loss profile will lead to a redistribution of the thermal stresses on the power devices, and then affect the lifetime. Therefore, it is reasonable that the junction temperature of the power devices can be manipulated indirectly through an appropriate allocation/control of the injected active power and reactive power.

6.1.2 Implementation of thermal optimized control

The philosophy of the proposed thermal optimized control method has been illustrated in § 6.1.1. A detailed implementation of this control strategy is represented in Figure 6.3. By optimizing the power references (P^* and Q^*) as shown in Figure 6.1 according to the system operation conditions (e.g. fault ride-through operation mode), an allocation of the active power and reactive power can be done, and thus the goals of a controllable junction temperature can be achieved.

As it is shown in Figure 6.3, with the advanced thermal optimized control strategy, the next-generation PV systems can not only meet the basic and specific grid integration requirements (e.g. power quality issues and LVRT in response to grid faults), but

can also enhance the reliability performance by means of controlling the power device junction temperature through active and reactive powers exchanging with the grid. The key of the implementation of this control method is to find the optimum power references, which are dependent on the system operating conditions, by means of look-up tables or mathematical derivations.

6.2 Operation examples with thermal optimized control

In order to demonstrate the proposed control strategy, a 3 kW single-phase PV system is tested under grid faults, where reactive power injection is also required. The thermal models of the power devices and the thermal parameters are given in Figure 2.12(b) and Table 2.2. The other parameters are given in Appendix A (Figure A.2 and Table A.1). As proposed in § 4.3.1, there are three reactive power injection strategies for single-phase PV systems in LVRT operation mode. Here, the constant peak current control (*Const.-*I_{gmax}) and the constant active power control (*Const.-P*) are selected to illustrate the principle of the proposed control strategy.

6.2.1 Case study description

In case that *Const.-P* has been adopted for this single-phase system under grid faults, the active power will be maintained constant during the short-term operations. According to Eq. (4.4), the power factor can be expressed as,

$$\cos\varphi = \frac{P_n}{S} = \frac{P_n}{\sqrt{P_n^2+Q^2}} = \begin{cases} \dfrac{1}{\sqrt{1+k^2\cdot(v_g-v_g^2)^2}}, & \left(1-\frac{1}{k}\right)\ \text{p.u.} \le v_g < 0.9\ \text{p.u.} \\ 0, & 0 \le v_g < \left(1-\frac{1}{k}\right)\ \text{p.u.} \end{cases} \tag{6.3}$$

where k is defined in Figure 4.11(b), P_n is the active power before fault, Q is the required reactive power depending grid voltage level v_g, and S is the instantaneous apparent power. When the *Const.-*I_{gmax} is adopted, the injected grid current amplitude I_{gmax} is kept to be the inverter rated current I_N, i.e. $I_{gmax} = I_N$. According to Eq. (4.8), the corresponding power factor in LVRT operation mode can be given by,

$$\cos\varphi = \frac{P}{S} = \frac{P}{\sqrt{P^2+Q^2}} = \begin{cases} \sqrt{1-k^2\cdot(1-v_g)^2}, & \left(1-\frac{1}{k}\right)\ \text{p.u.} \le v_g < 0.9\ \text{p.u.} \\ 0, & 0 \le v_g < \left(1-\frac{1}{k}\right)\ \text{p.u.} \end{cases} \tag{6.4}$$

in which P is the active power, k, Q, and S have been defined previously.

As aforementioned, the thermal performance of a PV inverter is affected by the power losses, which are dependent on the power allocations in the devices. Under these two reactive power injection strategies, the ratio between the active power and the required reactive power is varied, and thus the power factor. Therefore, the junction temperature is affected. According to Eqs. (6.3) and (6.4), the control areas for these two strategies

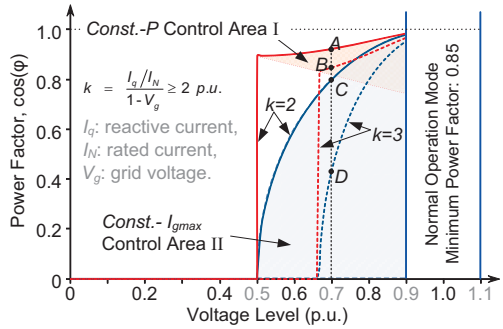

Figure 6.4: *Power factor curves vs. voltage levels for different control strategies according to Figure 4.11(b): solid lines: $k = 2$ p.u. and dashed lines: $k = 3$ p.u..*

under grid faults can be plotted in Figure 6.4. The upper borders (solid lines) of the control areas (*I* and *II*) are the maximum power factor ($k = 2$) that is required under grid faults according to Figure 4.11(b). Thus, in these control areas (*I* and *II*), the active power and reactive power can be allocated properly and intentionally, and varied by adjusting the slope k or by changing the control strategies.

For instance, when a voltage sag (0.3 p.u.) occurs, the *Const.-*I_{gmax} control strategy is firstly activated. In this case, the required power factor should be approximately 0.8 with $k = 2$ p.u.. By adjusting k to 3 p.u. or changing the mode of control to *Const.-P* control strategy, the operation points will change from ***C*** to ***D*** or from ***C*** to ***A***. Thus, the injected active power and reactive power are controlled, allowing the control of the junction temperature by varying k or changing the control strategies.

6.2.2 Power references

Regarding the implementation of the thermal optimized control strategy, the power references should be acquired firstly either using look-up tables or mathematical derivations. The latter requires a better knowledge of the power device materials, the topologies, the switch schemes, and etc.. Meanwhile, the coupled relationship between power losses and the junction temperature further increases the derivation complexity. A look-up table based method is simple, and can easily be implemented. Thus, a look-up table based implementation method is chosen for this case based on pre-calculated values.

In order to create a satisfied look-up table and thus to find the optimum power references for the proposed method, different cases (varying allocations of reactive power and active power) are simulated when a low-voltage fault occurs. The results are presented in Figure 6.5, which shows that the maximum junction temperature (T_{jmax}) of the power devices will exceed the allowable value (e.g. 125 °C) under very low voltage conditions (e.g. 0.4 p.u.). It also reveals that the maximum junction temperature will

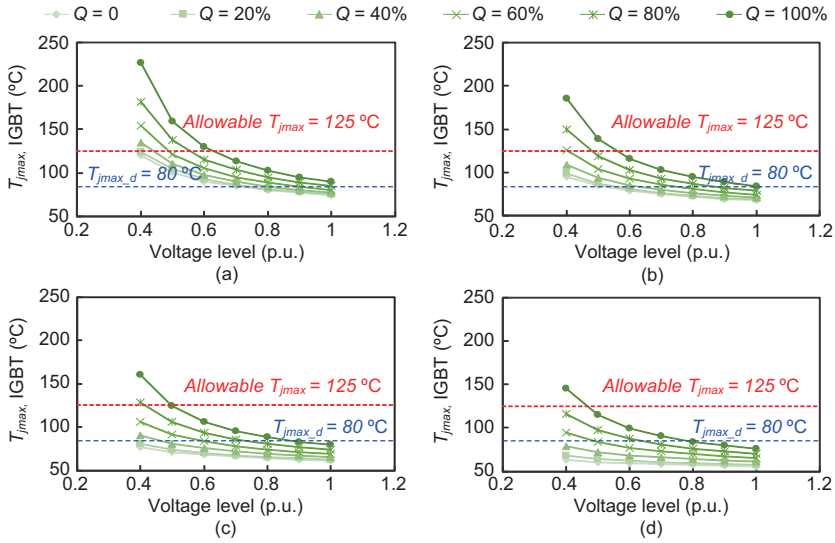

Figure 6.5: *Maximum junction temperature (T_{jmax}) of a full-bridge inverter (rated power P_n = 3 kW) with different injected powers: (a) P = 80% P_n, (b) P = 60% P_n, (c) P = 40% P_n, and (d) P = 20% P_n.*

increase with injecting required reactive power in *Const.-P* control mode. By decreasing the active power output and limiting the reactive power injection, the maximum junction temperature could be controlled below a desirable value (e.g. T_{jmax_d}= 80 °C), and consequently the maximum/mean junction temperature can be kept almost constant during ride-through operation. Notably, the desirable temperature T_{jmax_d} may be higher than 80 °C in other applications of higher power ratings (e.g. 6 kW).

Considering the required reactive power injection in Figure 4.11(b), the active power and reactive power references can be obtained as shown in Figure 6.6(a) under different voltage sag levels. While for a constant junction temperature of 80 °C, based on Figure 6.5, the power references can be obtained and shown in Figure 6.6(b). Consequently, the reference generation zones (*I* and *II*) can be implemented as the "*Power Reference Generation*" unit in Figure 6.1. In the detailed control structure of the proposed method in Figure 6.3, the power references for grid (LVRT) requirements (Figure 6.6(a)) and constant junction temperature (Figure 6.6(b)) can be implemented as the "*Grid Requirements*" and "*Thermal Optimization*" units, respectively.

The use of the power references can be illustrated as follows. When the grid sag e.g. is 0.6 p.u., there are at least two sets of power references available in Figure 6.6(b) to achieve a constant junction temperature - 1) P^*_{J1} = 0.2 p.u., Q^*_{J1} = 0.68 p.u. and 2) P^*_{J2} = 0 p.u., Q^*_{J2} = 1 p.u.. For the first case, if the *Const.-I_{gmax}* is adopted, the active

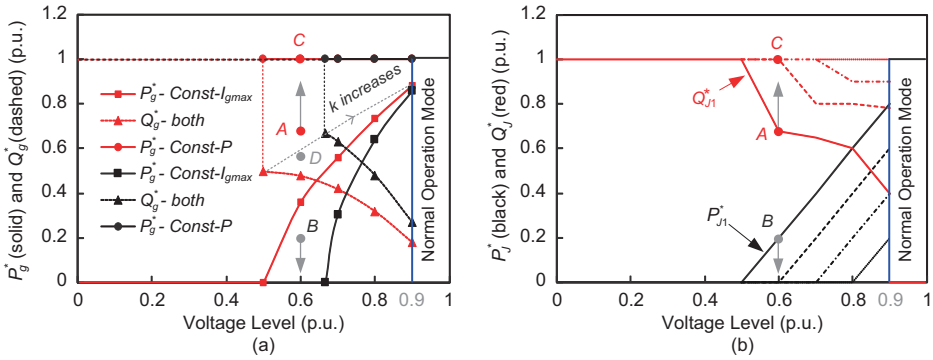

Figure 6.6: *Reactive power and active power references for a PV inverter: (a) to comply with the grid requirement of reactive power injection during LVRT, "g" - Grid, k=2 p.u. (red) and k=3 p.u. (black) in respect to Figure 4.11(b) and (b) to achieve a constant junction temperature (T_{jmax_d} = 80 °C), "J" –Junction.*

power should be 0.2 p.u. (Point ***B*** in Figure 6.6(a)). One way to generate this active power is to change the slope k, being 2.36 p.u., while the corresponding reactive power Q_g^*= 0.57 p.u. (Point ***D*** in Figure 6.6(a)). This reactive power is insufficient to keep the junction temperature constant as shown in Figure 6.6(b) (Point ***A***), and thus, the maximum junction will be lower than the desired value T_{jmax_d}. Once the appropriate reactive power ($Q^* = Q_g^* = Q_J^*$ = 0.68 p.u. optimized by the "*Power Optimization and Central Control* " unit) is injected to the grid, the peak value of the injected current will not be constant during LVRT, but the maximum junction temperature will be kept constant. Then, both LVRT and thermal optimized control goals are achieved. Another way to achieve a constant junction temperature is to further decrease the active power generation either by increasing k or changing the reactive power injection strategies (from ***D*** to ***C***), as it is shown in Figure 6.6(a).

According to Figure 6.5, the junction temperature of the power devices is proportional to the injected reactive power and the generated active power (power losses). Thus, in order to achieve a constant or reduced junction temperature and considering the grid requirements under grid faults, there might be several sets of power references as long as the power losses are kept constant or reduced as it is illustrated in Figure 6.7. If the power optimization objectives given by Eq. (6.5) is implemented in the "*Power Optimization and Central Control* " unit in Figure 6.3, a reduced junction temperature control will be achieved and the LVRT requirement will also be fulfilled.

$$\begin{cases} P^* = \min\left\{P_g^*, P_J^*\right\} \\ Q^* = \min\left\{Q_g^*, Q_J^*\right\} \end{cases} \tag{6.5}$$

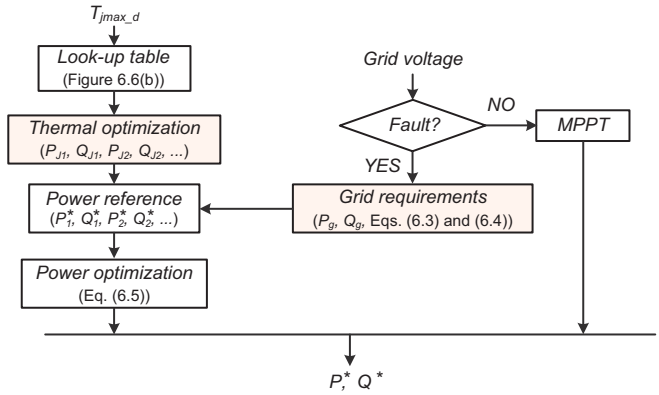

Figure 6.7: *Flowchart of the thermal optimized control strategy.*

Table 6.1: *Power loss distributions of the IGBT modules of a 3 kW single-phase PV inverter in different operation modes (unit: W, voltage sag: 0.4 p.u.).*

Device No. in Figure 6.1	S_1	D_1	S_2	D_2	S_3	D_3	S_4	D_4
MPPT mode	19.2	3.1	18.95	3.1	18.95	3.1	19.2	3.1
Const.-P	38.9	10.6	38.5	10.7	38.9	10.6	38.5	10.7
Const. junction temp. control	18.62	8	18.38	8.1	18.38	8.1	18.62	8
Const.-I_{gmax}	16.4	5.85	16.2	5.9	16.2	5.9	16.4	5.85
Reduced junction temp. control	13.5	5.4	13.3	5.5	13.3	5.5	13.5	5.4

6.2.3 Simulation and experimental results

In order to verify the effectiveness of the thermal optimized control strategy to achieve a reduced or even constant junction temperature operation, referring to Figure 6.1, a 3 kW single-phase PV system shown in Appendix A.2 was studied under different operation conditions in simulations. In regards to LVRT operation, the *Const.-P* and *Const.-I_{gmax}* are selected as the reactive power injection strategies for comparison and consistency. The power losses on the devices are firstly presented in Table 6.1. Figures 6.8 and 6.9 show the thermal behaviors of the PV system under grid faults (0.4 p.u. voltage sag level).

With *Const.-P* control strategy, the injected grid current level may exceed the inverter limitation as it has been discussed in § 4.3.1, and normally the current amplitude is higher than that in MPPT operation mode. Large injected currents will lead to more power losses and thus the mean/maximum junction temperature will increase in LVRT operation, which has been verified by the results presented in Table 6.1 and Figure 6.8(a). By applying the thermal optimized control (constant junction temperature con-

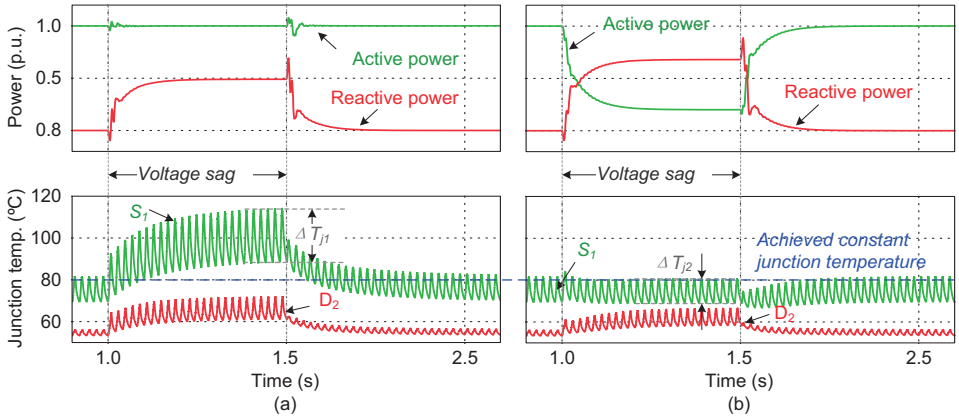

Figure 6.8: *Performance of a single-phase PV system under grid faults (0.4 p.u. voltage sag) with different control strategies: (a) Const.-P control and (b) constant junction temperature control.*

trol), the power losses on the power devices are reduced in LVRT operation mode, as it is shown in Table 6.1. Consequently, the maximum junction temperature is maintained constant, as it is proved in Figure 6.8(b). Moreover, the IGBT temperature cycling amplitude is also reduced to 11.5 °C (ΔT_{j2}) from 27 °C (ΔT_{j1}) with the advanced control strategy, and thus the overall reliability of the PV system is further improved according to Eq. (6.1). In addition, Figure 6.9 shows the results of the same PV system with the proposed control method to achieve a reduced junction temperature during LVRT when the *Const.*– I_{gmax} control strategy is adopted. Since the power references for this control method are optimized according to Eq. (6.5), in comparison with the constant junction temperature control, the reduced junction temperature control method can fulfill the requirement of reactive power injection and also can reduce the maximum junction temperature. Those results show the effectiveness of the proposed thermal optimized control method to achieve a reduced or even a constant junction temperature of the power devices under grid faults, and thus possible catastrophic failures are at least avoided.

Since the lack of open IGBT modules running in grid-connected mode, the illustration of the junction temperature controllability is experimentally demonstrated on a commercial 3-level Neutral-Point-Clamped (NPC) high power PV inverter operating at low power conditions, which is available in the lab. The rated current and voltage of the NPC PV inverter are 30 A and 1200 V respectively, and each leg of the NPC inverter consists of two IGBTs, two clamped diodes and two MOSFETs, as it is shown in Figure B.3(a) in Appendix B. The system parameters are shown in Appendix B (Table B.1). The experimental results are presented in Figure 6.10 and Table 6.2 , which demonstrate

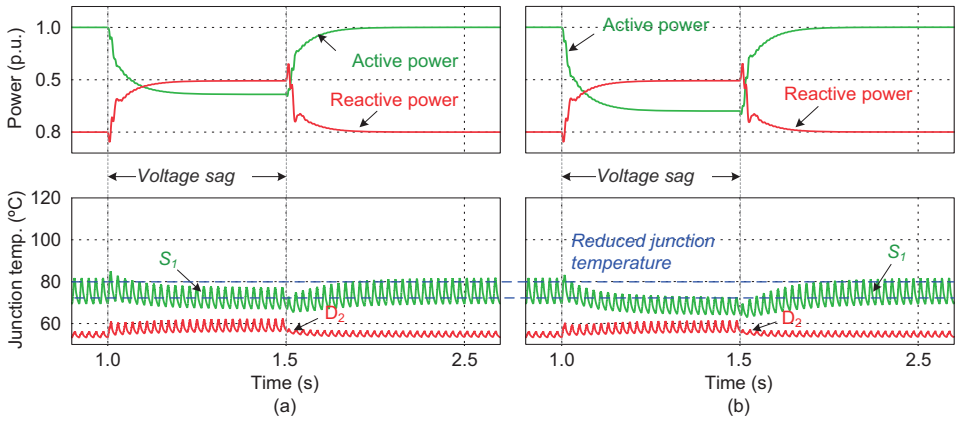

Figure 6.9: *Performance of a single-phase PV system under grid faults (0.4 p.u. voltage sag) with different control strategies: (a) Const.-I_{gmax} control and (b) reduced junction temperature control.*

Table 6.2: *Test results of a single-phase 3-level NPC PV inverter under different power factors.*

Test No.	Power Factor	P (W)	Q (Var)	S (VA)	Hotspot Temperature (°C)		
					Sp1	Sp2	Sp3
1	0.4538	257.4	505.5	567.3	23.7	23.3	22.6
2	0.8955	507.5	252.3	566.8	24.1	24.6	23.6
3	0.9996	564.7	16.8	565	23.7	24.9	23.4

that the junction temperature of the clamped diode (i.e. hotspot *Sp2*) experienced a linear change with the power factor (by changing the resistive-inductive load as shown in Table B.2 of Appendix B). While the junction temperature of the IGBT is kept the same, but the power factors are different (Test No. 1 and No. 3). This verifies the possibility to achieve a constant (or reduced) junction temperature of the power devices through active power and reactive power control, which is the essential idea of this advanced control strategy.

6.3 Summary

In this chapter, a thermal-optimized control strategy for PV systems has been introduced. Applying this advanced control strategy, a reduced or constant junction temperature of the power devices in PV inverters can then be achieved, and thus an improved overall reliability can be ensured. The controllability of junction temperatures through

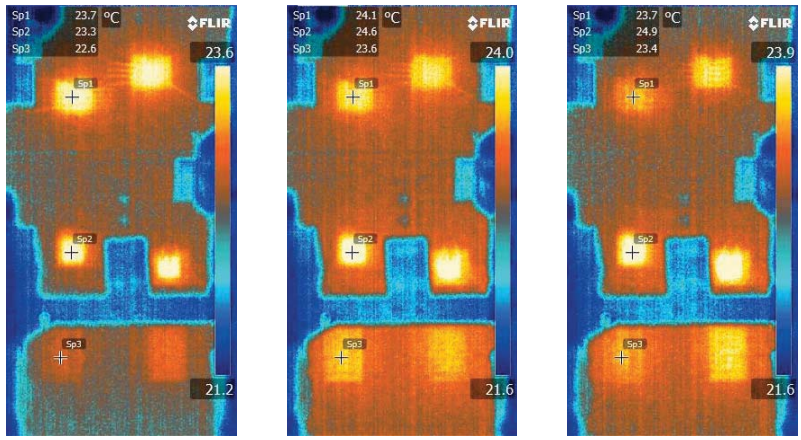

Figure 6.10: *Experimental results (thermal measurements) of a single-phase 3-level NPC PV inverter under different power factors: Sp1 – IGBT, Sp2 – Clamped Diode and Sp3 – MOSFET.*

appropriate allocation of the active power and reactive power has been demonstrated on a single-phase PV system undergoing grid faults in simulations. It has been shown that the introduced control strategy can contribute to an improved robustness of the PV systems in response to abnormal grid conditions. In addition, the effectiveness of this advanced control strategy has also been confirmed by the experiments of a three-level neutral-point-clamped PV inverter.

Although the above verifications were conducted on a single-phase PV system specially in the fault ride-through operation mode, the essence of the thermal optimized control strategy - the controllability of power device junction temperature through the injected power regulations can also be applied to other systems. For example, the thermal optimized control strategy offers the possibility to maintain a controllable junction temperature of the power devices under varying solar irradiance levels only if a wide range of reactive power injection is allowed. By circulating the reactive currents between paralleled inverters, the junction temperature variations are possible to be reduced, as it has been discussed in [153] for wind turbine applications.

Part IV

Conclusions

This part is the conclusion of the Ph.D. thesis, which consists of one chapter - ***Chapter 7****. Summary and Outlook.*

7 Summary and Outlook

The intent of this chapter is to summarize the work, which has been done throughout this Ph.D. project, and to emphasize the main contributions of this project documented in this thesis - *evaluation of transformerless PV inverters, including reliability* and *advanced control strategies for the next generation PV systems*. Then, this chapter ends with an outlook of this topic in order to enrich the future research outcomes.

7.1 Summary

The main subjects of this project are: a) evaluation and benchmarking of single-phase transformerless PV systems and b) advanced control strategies for single-phase PV systems. The first subject has been described in *Chapter 3* using the models detailed in *Chapter 2*. Based on the evaluations, advanced control strategies have been proposed and detailed in *Chapters 4, 5*, and *6*. Moreover, the models in *Chapter 2* have been used to verify the appropriation and effectiveness of the proposed control strategies.

In the *Introduction*, an overview of the grid-connected PV technologies has been presented. Seen from the discussion, the single-phase transformerless PV technology was selected as the candidate for the next-generation advanced PV inverters. Hence, detailed electrical models of mainstream transformerless PV systems have been given in *Chapter 2*, also including modelling of the PV panels and grid interfaced filter (L filter). Since currently the PV systems are required to inject the maximum power to the grid and the injected current should be synchronized with the grid voltage, the MPPT control

algorithms and the modelling of grid synchronization systems have also been discussed in this chapter. After a brief introduction of the most commonly used MPPT methods, *P&O*, and *INC*, a modified *P&O* MPPT control method has been proposed in order to solve the shortcoming of the conventional one - instability under rapid condition changes. Meanwhile, in order to find the best synchronization method for single-phase PV systems under grid faults, a benchmarking of several synchronization approaches has also been done in *Chapter 2*.

With regards to efficiency and reliability, the performance of a single-phase transformerless PV system differs with the inverter topology and the operation conditions (e.g. grid voltage, ambient temperature and solar irradiance level). Hence, a thorough comparison of the selected transformerless PV inverters in terms of conversion efficiency and thermal loading has been conducted in *Chapter 3* considering mission profiles. Firstly, a mission profile based multi-disciplinary analysis method for single-phase transformerless PV inverters has been introduced. The proposed analysis method takes the mission profiles - solar irradiance and ambient temperature (yearly data, monthly data and/or daily data) as the input variables, and based on the models built in *Chapter 2* the power losses and thermal distributions on the power devices can be obtained. Then, estimations of the energy production and reliability of a certain PV topology can be achieved. Although verifications of the proposed method was carried out on three mainstream transformerless inverters, it can also be utilized in the evaluation of other renewable energy systems (e.g. wind turbine system) at different time scales.

In order to accept more PV energy, advanced technologies have to be developed for the next-generation PV inverters, which have to comply with the grid requirements imposed by the system operators. Hence, starting from *Chapter 4*, advanced control strategies have been proposed. At the beginning of *Chapter 4*, the feasibility of current valid grid requirements, when a very high penetration level of PV systems reaches, has been explored. One important conclusion from the exploration is that it would be very desirable for all PV inverter to have advanced functions in order to realize the above goal. As a result, several grid code modification suggestions have been proposed. It is recommended for the development and implementation to consider functions, like a) reactive power control, b) frequency control through active power control, c) fault ride-through capability, and d) high reliability/availability and also high efficiency, to get the maximum energy yield. Besides those stringent grid requirements, the PV systems should also fulfill basic demands, e.g. power quality. Hence, in this chapter, the basic control strategies for single-phase systems were presented. Possible current control methods have been explored in terms of harmonic suppression.

The first advanced control strategy proposed in this project is related to the dynamic grid support capability for the next generation PV systems. This control strategy is mainly focused on LVRT capability and reactive current injection under voltage faults. From the results presented in *Chapter 4*, it can be concluded that there are extensive control possibilities in single-phase grid-connected PV systems, which are ready

and able to meet the upcoming requirements regarding dynamic grid support function. Fortunately, unlike three-phase systems, the reactive power injection for single-phase systems is less complicated. In this chapter, three reactive power injection strategies have been proposed for single-phase systems. A comparison of those reactive power injection strategies was also carried out and shown in this chapter, and it is focused on the ability to fulfill grid requirements and the stresses on the devices during LVRT operation. It should be pointed out that the performance of a single-phase PV system in LVRT operation can be enhanced by an accurate power calculation system and a fast fault detection unit. With this consideration, a new power calculation method has been proposed in this project for single-phase inverters.

Since the loss distribution and the modulation schemes are different in the selected transformerless topologies, fault ride-through operation with reactive power injection may affect the reliability of the inverters. This has been proved by a benchmarking of the selected transformerless inverters in LVRT operation as discussed in *Chapter 4*. Together with the comparative results presented in *Chapter 3*, one important conclusion is that, although the transformerless inverter can achieve a high efficiency, but it may not be special suitable for use in the next generation PV systems with LVRT capability or reactive power injection. Nevertheless, for different applications, the presented benchmarking provides a convenient way to select appropriate devices of those inverters and to further optimize them.

As it has been discussed in *Chapter 1*, the penetration level of PV systems will further increase. A wide-scale adoption of PV systems pushes the system operators to expand the power grid infrastructures. However, the potential cost brought by such extensions and increased maintenances impose new obstacles. To solve those issues, in *Chapter 5*, a constant power generation control strategy has been proposed. It limits the feed-in power of the existing PV systems to a certain level in order to reduce the requirement of grid capacity expansion, and at the same time enables an increase of the PV penetration level. Firstly, the rationality of this advanced control strategy was explored. Then, implementations of the constant power generation control strategy have been presented. Finally, the test results verified the effectiveness of this control strategy in terms of unloading of distribution grids and also the potential of improved reliability. This issue has been discussed in some countries, e.g. in Germany, and it will be included in the future grid demands at a very high penetration level. The same philosophy may be imposed on other renewables.

At last, in *Chapter 6*, a thermal optimized control strategy has been proposed in order to increase the overall reliability. The proposed advanced control strategy is able to control the junction temperature, which is the most observed factor that induces failures, by optimizing the injected active and reactive powers. The effectiveness of this control strategy in terms of thermal performance and electrical performance has also been demonstrated by simulations and experiments. The results show that by applying the proposed control strategy, the junction temperature can be maintained at a constant

level or reduced during LVRT. Hence, the overall reliability of the system is improved by reallocating the active power and the reactive power.

7.2 Main contributions

The significance and main contributions of this project from the author's point of view can be summarized as follows:

Comprehensive Comparison of Transformerless Inverters-

A comprehensive comparison of three mainstream transformerless inverters was done in terms of efficiency, leakage current rejection capability, and reliability (thermal loading). Besides, a benchmarking of single-phase synchronization methods under grid faults was also given. Those comparison results offer the possibility to select appropriate devices and synchronization methods, and to further optimize transformerless PV systems. Several current controllers have been compared in terms of harmonic mitigation ability.

Proposed Grid Code Modifications-

One essential basis of the design, control and operation for grid-connected PV inverters is the grid requirements. Thus, based on an overview of the existing PV related grid requirements, suggested grid code modifications were proposed in order to increase the adoption of PV systems and reduce the cost of energy from PV systems. It is recommended to reexamine and update the grid requirements accordingly considering the following features like:

- Reactive power control (Volt-VAR control);
- Frequency control through active power control (Freq.-Watt control);
- Active power control (power curtailment);
- Fault ride-through capability;
- Higher reliability and higher efficiency;
- Intelligent and advanced control for better power quality;
- Advanced monitoring and communication.

New Power Calculation Method-

A new power calculation method has been proposed, since the power calculation has a significant impact on the control of single-phase PV systems under grid faults. The proposed method is based on an adaptive filtering technique, and it has been successfully used in a single-phase PV system. It can also be adopted in other single-phase applications (e.g. droop-controlled systems), where the average active power and the reactive power are required to be controlled.

Proposed Reactive Power Injection Strategies-

In regards to the control of single-phase systems in low voltage ride-through operation, three reactive power injection strategies have been proposed, considering the over-current protection of PV inverters and the reactive current injection requirements under grid faults. The proposed reactive power injection strategies are:

- Constant peak current strategy;
- Constant active current control strategy;
- Constant active power control strategy.

Advanced Control Strategies for Single-Phase PV Systems-

Advanced control strategies have been proposed in this project in order to enable a more wide-scale adoption of single-phase PV systems:

- Dynamic grid support provided by PV systems to ensure the stability of the entire system during low voltage ride-through operation, when a high penetration degree of PV systems reaches.
- Constant power generation control strategy to enable more installations of PV systems without upgrading the grid infrastructure. It is also able to contribute to improved reliability.
- Thermal optimized control strategy to control the junction temperature of power devices through appropriate power allocations. The power device reliability and thus the system lifetime can be enabled by this control strategy.

7.3 Research perspectives

Although many aspects have been documented in this thesis for advanced single-phase PV inverter technologies, there are still a lot of possibilities for technology improvement. Some issues of high interest for future investigations are listed below:

1) The evaluation of the transformerless PV systems under grid voltage faults is only focused on the inverter and the DC-link capacitor. As a whole system, the stability of *LCL*-filter might also be challenged in such cases. Hence, this would be an interesting point to investigate the response of *LCL*-filter, when the advanced PV functionalities are enabled in the future. Moreover, in this thesis, several current control methods have been examined, but a detailed benchmarking of those control methods in different operation modes might also be useful for the inverter design and control.
2) Regarding the reactive power control to stabilize the grid voltage, the power losses might increase, when it is activated. The power loss distribution will affect the thermal behavior, and thus the lifetime of the PV inverter is challenged. It could

be another interesting topic to look into how this effect will be and thus to develop potential solutions.

3) Due to the intermittent property of PV systems, mitigation of power fluctuations and voltage variations might be further enhanced in the grid-connection standards. This initiates some important issues to investigate, e.g. the integration of energy storage systems, electric vehicles, and the modifications of grid codes, especially when a large-scale penetration level of PV systems comes into reality. In Denmark, a delta power generation control for wind turbine systems is already in the grid codes. It might be extended to PV systems in order to alleviate the above impacts on the grid, and thus more benefits from PV systems can be obtained.

4) Moreover, the constant power generation control strategy proposed in this project also stimulate some issues that are worth investigating into. For example, to analyze the reduction of the energy yield due to the advanced control strategy to study its feasibility from an economic point of view, and to benchmark different MPPT methods in the operation mode (thus to develop robust control methods). Those aspects should be well studied in order to efficiently and reliably realize a large-scale adoption of PV systems with reduced cost of energy.

5) In addition, regarding the junction temperature control (thermal optimized control), it calls for an analytical method to calculate how to do a constant junction temperature control for other applications (not the case in this thesis). Long term effect of those methods on the devices or the entire system is also worth to investigate.

Besides those interesting topics, the development and implementation of inverter technical standards are still far from finalization. Hence, the investigation on the feasibility of new grid requirements will be another interesting research direction. Moreover, applying those advanced methods on the future PV inverters based on new power devices (e.g. wide-bandgap devices) is still open, and might be an interesting study.

Bibliography

[1] European Photovoltaic Industrial Association, "Global market outlook for photovoltaics 2013-2017," [Online]. Available: http://www.epia.org/, 2013.

[2] REN 21, "Renewables 2013: Global Status Report (GSR)," [Online]. Available: http://www.ren21.net/, Jun. 2013.

[3] K.O. Kovanen, "Photovoltaics and power distribution," *Renewable Energy Focus*, vol. 14, no. 3, pp. 20–21, May/Jun. 2013.

[4] M. Braun, T. Stetz, R. Brundlinger, C. Mayr, K. Ogimoto, H. Hatta, H. Kobayashi, B. Kroposki, B. Mather, M. Coddington, K. Lynn, G. Graditi, A. Woyte, and I. MacGill, "Is the distribution grid ready to accept large-scale photovoltaic deployment? State of the art, progress, and future prospects," *Progr. Photovolt: Res. Appl.*, vol. 20, no. 6, pp. 681–697, 2012.

[5] A. Izadian, N. Girrens, and P. Khayyer, "Renewable energy policies: A brief review of the latest U.S. and E.U. policies," *IEEE Ind. Electron. Mag.*, vol. 7, no. 3, pp. 21–34, 2013.

[6] Solarpraxis and Sunbeam Communications, "Inverter, storage and pv system technology 2013," [Online]. Available: http://www.pv-system-tech.com/, Jul. 2013.

[7] C. Winneker, "World's solar photovoltaic capacity passes 100-gigawatt landmark after strong year," [Online]. Available: http://www.epia.org/news/, Feb. 2013.

[8] K. Ogimoto, I. Kaizuka, Y. Ueda, and T. Oozeki, "A good fit: Japan's solar power program and prospects for the new power system," *IEEE Power Energy Mag.*, vol. 11, no. 2, pp. 65–74, Mar./Apr. 2013.

[9] J.V. Appen, M. Braun, T. Stetz, K. Diwold, and D. Geibel, "Time in the Sun: the challenge of high PV penetration in the german electric grid," *IEEE Power Energy Mag.*, vol. 11, no. 2, pp. 55–64, Mar./Apr. 2013.

[10] P. Denholm, R. Margolis, T. Mai, G. Brinkman, E. Drury, M. Hand, and M. Mowers, "Bright future: Solar power as a major contributor to the U.S. grid," *IEEE Power Energy Mag.*, vol. 11, no. 2, pp. 22–32, Mar./Apr. 2013.

[11] Greentech Media, Inc. and Solar Energy Industries Association (SEIA), "U.S. solar market insight 2012 year in review," [Online]. Available: http://www.seia.org/cs/research/solarinsight, 2013.

[12] R. Teodorescu, M. Liserre, and P. Rodriguez, *Grid converters for photovoltaic and wind power systems.* Hoboken, NJ, USA: Wiley, 2011.

[13] PV GRID, "European advisory paper: Consultation version," [Online]. Available: http://www.pvgrid.eu/, Jan. 2014.

[14] T. Orłowska-Kowalska, F. Blaabjerg, and J. Rodríguez (eds.), *Advanced and intelligent control in power electronics and drives*. Studies in Computational Intelligence 531, Springer, 2014.

[15] F. Blaabjerg, R. Teodorescu, M. Liserre, and A.V. Timbus, "Overview of control and grid synchronization for distributed power generation systems," *IEEE Trans. Ind. Electron.*, vol. 53, no. 5, pp. 1398–1409, Oct. 2006.

[16] S.B. Kjaer, J.K. Pedersen, and F. Blaabjerg, "A review of single-phase grid-connected inverters for photovoltaic modules," *IEEE Trans. Ind. Appl.*, vol. 41, no. 5, pp. 1292–1306, Sept./Oct. 2005.

[17] F. Blaabjerg, Z. Chen, and S.B. Kjaer, "Power electronics as efficient interface in dispersed power generation systems," *IEEE Trans. Power Electron.*, vol. 19, no. 5, pp. 1184–1194, Sept. 2004.

[18] Y. Xue, K.C. Divya, G. Griepentrog, M. Liviu, S. Suresh, and M. Manjrekar, "Towards next generation photovoltaic inverters," in *Proc. of ECCE*, pp. 2467-2474, 17-22 Sept. 2011.

[19] Y. Yang, F. Blaabjerg, and Z. Zou, "Benchmarking of grid fault modes in single-phase grid-connected photovoltaic systems," *IEEE Trans. Ind. Appl.*, vol. 49, no. 5, pp. 2167–2176, Sept./Oct. 2013.

[20] Y. Yang, P. Enjeti, F. Blaabjerg, and H. Wang, "Grid code modifications to ensure wide-scale adoption of photovoltaic energy in distributed power generation systems," *IEEE Ind. Appl. Mag.*, vol. 99, no. 99, pp. 1–10, in press, Sept.-Oct. 2015.

[21] E. Romero-Cadaval, G. Spagnuolo, L. Garcia Franquelo, C.A. Ramos-Paja, T. Suntio, and W.M. Xiao, "Grid-connected photovoltaic generation plants: Components and operation," *IEEE Ind. Electron. Mag.*, vol. 7, no. 3, pp. 6–20, 2013.

[22] H. Kobayashi, "Fault ride through requirements and measures of distributed PV systems in Japan," in *Proc. of IEEE-PES General Meeting*, pp. 1-6, 22-26 Jul. 2012.

[23] "IEEE Application Guide for IEEE Std 1547, IEEE Standard for Interconnecting Distributed Resources With Electric Power Systems," *IEEE Std 1547.2-2008*, 2009.

[24] International Electrotechnical Commission, "Characteristics of the utility interface for photovoltaic (PV) systems," *IEC 61727*, 2004.

[25] E.ON GmbH, "Grid Code-high and extra high voltage," 2006.

[26] Comitato Elettrotecnico Italiano, "Reference technical rules for connecting users to the active and passive LV distribution companies of electricity," *CEI 0-21*, Dec. 2011.

[27] VDE Verband der Elektrotechnik Elektronik Informationstechnik e.V., "Power generation systems connected to the low-voltage distribution network - Technical minimum requirements for the connection to and parallel operation with low-voltage distribution networks," *VDE-AR-N 4105:2011-08*, Aug. 2011.

[28] Bundesverband der Energie- und Wasserwirtschaft (BDEW), "Technical Guideline: Generating plants connected to the medium-voltage network," Jun. 2008.

[29] F. Iov, A.D. Hansen, P. Sørensen, and N.A. Cutululis, "Mapping of grid faults and grid codes," Risø Nat. Lab., Tech. Univ. Denmark, Roskilde, Denmark, Tech. Rep., 2007.

[30] P. Rodriguez, A. Luna, R.S. Munoz-Aguilar, I. Etxeberria-Otadui, R. Teodorescu, and F. Blaabjerg, "A stationary reference frame grid synchronization system for three-phase grid-connected power converters under adverse grid conditions," *IEEE Trans. Power Electron.*, vol. 27, no. 1, pp. 99–112, Jan. 2012.

[31] A. Marinopoulos, F. Papandrea, M. Reza, S. Norrga, F. Spertino, and R. Napoli, "Grid integration aspects of large solar PV installations: LVRT capability and reactive power/voltage support requirements," in *Proc. of IEEE Trondheim PowerTech*, pp. 1-8, 2011.

[32] M.S. El Moursi, W. Xiao, and J.L. Kirtley, "Fault ride through capability for grid interfacing large scale PV power plants," *IET Gener. Transm. Distrib.*, vol. 7, no. 9, pp. 1027–1035, Sept. 2013.

[33] K. Fujii, N. Kanao, T. Yamada, and Y. Okuma, "Fault ride through capability for solar inverters," in *Proc. of EPE'11*, pp. 1-9, 2011.

[34] Y. Bae, T.-K. Vu, and R.-Y. Kim, "Implemental control strategy for grid stabilization of grid-connected pv system based on german grid code in symmetrical low-to-medium voltage network," *IEEE Trans. Energy Conversion*, vol. 28, no. 3, pp. 619–631, Sept. 2013.

[35] J. Eloy-Garcia Carrasco, J.M. Tena, D. Ugena, J. Alonso-Martinez, D. Santos-Martin, and S. Arnaltes, "Testing low voltage ride through capabilities of solar inverters," *Electric Power Systems Research*, vol. 96, pp. 111–118, Mar. 2013.

[36] C.H. Benz, W.T. Franke, and F.W. Fuchs, "Low voltage ride through capability of a 5 kW grid-tied solar inverter," in *Proc. of EPE/PEMC*, pp. T12-13-T12-20, 2010.

[37] G.M.S. Azevedo, G. Vazquez, A. Luna, D. Aguilar, and A. Rolan, "Photovoltaic inverters with fault ride-through capability," in *Proc. of ISIE'09*, pp. 544-548, 2009.

[38] M. Castilla, J. Miret, J.L. Sosa, J. Matas, and L.G. de Vicuna, "Grid-fault control scheme for three-phase photovoltaic inverters with adjustable power quality characteristics," *IEEE Trans. Power Electron.*, vol. 25, no. 12, pp. 2930–2940, Dec. 2010.

[39] N. Papanikolaou, "Low-voltage ride-through concept in flyback inverter-based alternating current- photovoltaic modules," *IET Power Electron.*, vol. 6, no. 7, pp. 1436–1448, Aug. 2013.

[40] T.S. Sidhu and D. Bejmert, "Short-circuit current contribution from large scale PV power plant in the context of distribution power system protection performance," in *Proc. of IET RPG*, pp. 1-6, Sept. 2011.

[41] Y. Yang, K. Zhou, and F. Blaabjerg, "Harmonics suppression for single-phase grid-connected PV systems in different operation modes," in *Proc. of IEEE APEC'13*, pp. 889-896, Mar. 2013.

[42] M. Liserre, R. Teodorescu, and F. Blaabjerg, "Stability of photovoltaic and wind turbine grid-connected inverters for a large set of grid impedance values," *IEEE Trans. Power Electron.*, vol. 21, no. 1, pp. 263–272, Jan. 2006.

[43] M. Liserre, F. Blaabjerg, and S. Hansen, "Design and control of an *LCL*-filter-based three-phase active rectifier," *IEEE Trans. Ind. Appl.*, vol. 41, no. 5, pp. 1281–1291, Sept.-Oct. 2005.

[44] I. Patrao, E. Figueres, F. González-Espín, and G. Garcerá, "Transformerless topologies for grid-connected single-phase photovoltaic inverters," *Renewable and Sustainable Energy Reviews*, vol. 15, no. 7, pp. 3423 – 3431, 2011.

[45] D. Meneses, F. Blaabjerg, O. Garcia, and J.A. Cobos, "Review and comparison of step-up transformerless topologies for photovoltaic AC-module application," *IEEE Trans. Power Electron.*, vol. 28, no. 6, pp. 2649–2663, 2013.

[46] T. Kerekes, M. Liserre, R. Teodorescu, C. Klumpner, and M. Sumner, "Evaluation of three-phase transformerless photovoltaic inverter topologies," *IEEE Trans. Power Electron.*, vol. 24, no. 9, pp. 2202–2211, Sept. 2009.

[47] Y. Yang, F. Blaabjerg, and H. Wang, "Low voltage ride-through of single-phase transformerless photovoltaic inverters," *IEEE Trans. Ind. Appl.*, vol. 50, no. 3, pp. 1942–1952, May/Jun. 2014.

[48] F. Blaabjerg, F. Iov, T. Terekes, R. Teodorescu, and K. Ma, "Power electronics - key technology for renewable energy systems," in *Proc. of PEDSTC*, pp. 445-466, 2011.

[49] E. Koutroulis and F. Blaabjerg, "Design optimization of transformerless grid-connected PV inverters including reliability," *IEEE Trans. Power Electron.*, vol. 28, no. 1, pp. 325–335, 2013.

[50] H. Wang, M. Liserre, and F. Blaabjerg, "Toward reliable power electronics: Challenges, design tools, and opportunities," *IEEE Ind. Electron. Mag.*, vol. 7, no. 2, pp. 17–26, 2013.

[51] H. Huang and P. Mawby, "A lifetime estimation technique for voltage source inverters," *IEEE Trans. Power Electron.*, vol. 28, no. 8, pp. 4113–4119, 2013.

[52] A. Golnas, "PV system reliability: An operator's perspective," *IEEE Journal of Photovoltaics*, vol. 3, no. 1, pp. 416–421, 2013.

[53] Y. Firouz, M.T. Bina, and B. Eskandari, "Efficiency of three-level neutral-point clamped converters: analysis and experimental validation of power losses, thermal modelling and lifetime prediction," *IET Power Electronics*, vol. 7, no. 1, pp. 209–219, Jan. 2014.

[54] S.B. Kjaer, "Design and control of an inverter for photovoltaic applications," Ph.D. Thesis, Department of Energy Technology, Aalborg University, Jan. 2005.

[55] SMA Solar Technology AG, "PV inverters - Basic facts for planning PV systems," [Online]. Available: http://www.sma.de/, Jun. 2010.

[56] SMA Solar Technology AG, "Advisory Guide - String inverters in large-scale plants," [Online]. Available: http://www.sma.de/, Sept. 2010.

[57] R. Gonzalez, J. Lopez, P. Sanchis, and L. Marroyo, "Transformerless inverter for single-phase photovoltaic systems," *IEEE Trans. Power Electron.*, vol. 22, no. 2, pp. 693–697, Mar. 2007.

[58] T. Kerekes, "Analysis and modeling of transformerless photovoltaic inverter systems," Ph.D. Thesis, Department of Energy Technology, Aalborg University, Aug. 2009.

[59] Y. Wang and R. Li, "Novel high-efficiency three-level stacked-neutral-point-clamped grid-tied inverter," *IEEE Trans. Ind. Electron.*, vol. 60, no. 9, pp. 3766–3774, Sept 2013.

[60] L. Zhang, K. Sun, Y. Xing, and M. Xing, "H6 transformerless full-bridge PV grid-tied inverters," *IEEE Trans. Power Electron.*, vol. 29, no. 3, pp. 1229–1238, March 2014.

[61] M.G. Villalva, J.R. Gazoli, and E.R. Filho, "Comprehensive approach to modeling and simulation of photovoltaic arrays," *IEEE Trans. Power Electron.*, vol. 24, no. 5, pp. 1198–1208, May 2009.

[62] D. Sera, "Real-time modelling, diagnostics and optimised MPPT for residental PV systems," Ph.D. Thesis, Department of Energy Technology, Aalborg University, Jan. 2009.

[63] Y. Yang and F. Blaabjerg, "A modified P&O MPPT algorithm for single-phase PV systems based on deadbeat control," in *Proc. of IET PEMD'12*, pp. 1-5, Mar. 2012.

[64] Plexim, "PLECS User Manual: Version 3.5," [Online]. Available: http://www.plexim.com/sites/default/files/plecsmanual.pdf, Feb. 2014.

[65] T. Esram and P.L. Chapman, "Comparison of photovoltaic array maximum power point tracking techniques," *IEEE Trans. Energy Conversion*, vol. 22, no. 2, pp. 439–449, Jun. 2007.

[66] S.K. Kollimalla and M.K. Mishra, "Variable perturbation size adaptive P&O MPPT algorithm for sudden changes in irradiance," *IEEE Trans. Sustain. Energy*, vol. 5, no. 3, pp. 718–728, Jul. 2014.

[67] R. Khanna, Q. Zhang, W.E. Stanchina, G.F. Reed, and Z. Mao, "Maximum power point tracking ssing model reference adaptive control," *IEEE Trans. Power Electron.*, vol. 29, no. 3, pp. 1490–1499, Mar. 2014.

[68] T. Kerekes, R. Teodorescu, P. Rodriguez, G. Vazquez, and E. Aldabas, "A new high-efficiency single-phase transformerless PV inverter topology," *IEEE Trans. Ind. Electron.*, vol. 58, no. 1, pp. 184–191, Jan. 2011.

[69] S.R. Gonzalez, C.J. Coloma, P.L. Marroyo, T.J. Lopez, and G.P. Sanchis, "Single-phase inverter circuit for conditioning and converting dc electrical energy into ac electrical," International Patent Application, Pub. No. WO/2008/015 298, Feb. 7, 2008.

[70] H. Schmidt, S. Christoph, and J. Ketterer, "Current inverter for direct/alternating currents, has direct and alternating connections with an intermediate power store, a bridge circuit, rectifier diodes and a inductive choke," German Patent, DE10 221 592 A1, Dec. 4, 2003.

[71] M. Victor, F. Greizer, S. Bremicker, and U. Hubler, "Method of converting a direct current voltage from a source of direct current voltage, more specifically from a photovoltaic couse of direct current voltage, into a alternating current voltage," US Patent Application, Pub. No. US 2005/0 286 281 A1, Dec. 29, 2005.

[72] L. Zhang, K. Sun, L. Feng, H. Wu, and Y. Xing, "A family of neutral point clamped full-bridge topologies for transformerless photovoltaic grid-tied inverters," *IEEE Trans. Power Electron.*, vol. 28, no. 2, pp. 730–739, Feb 2013.

[73] R. González, E. Gubía, J. López, and L. Marroyo, "Transformerless single-phase multilevel-based photovoltaic inverter," *IEEE Trans. Ind. Electron.*, vol. 55, no. 7, pp. 2694–2702, Jul. 2008.

[74] B. Ji, J. Wang, and J. Zhao, "High-efficiency single-phase transformerless PV H6 inverter with hybrid modulation method," *IEEE Trans. Ind. Electron.*, vol. 60, no. 5, pp. 2104–2115, May 2013.

[75] J. Sun, "Small-signal methods for ac distributed power systems: A review," *IEEE Trans. Power Electron.*, vol. 24, no. 11, pp. 2545–2554, Nov. 2009.

[76] T. Messo, J. Jokipii, J. Puukko, and T. Suntio, "Determining the value of DC-link capacitance to ensure stable operation of a three-phase photovoltaic inverter," *IEEE Trans. Power Electron.*, vol. 29, no. 2, pp. 665–673, Feb. 2014.

[77] J. Sun, "Impedance-based stability criterion for grid-connected inverters," *IEEE Trans. Power Electron.*, vol. 26, no. 11, pp. 3075–3078, Nov. 2011.

[78] M. Fazeli, J.B. Ekanayake, P.M. Holland, and P. Igic, "Exploiting PV inverters to support local voltage – a small-signal model," *IEEE Trans. Energy Convers.*, vol. 29, no. 2, pp. 453–462, Jun. 2014.

[79] C.-H. Chang, Y.-H. Lin, Y.-M. Chen, and Y.-R. Chang, "Simplified reactive power control for single-phase grid-connected photovoltaic inverters," *IEEE Trans. Ind. Electron.*, vol. 61, no. 5, pp. 2286–2296, May 2014.

[80] X. Zhang, J.W. Spencer, and J.M. Guerrero, "Small-signal modeling of digitally controlled grid-connected inverters with LCL filters," *IEEE Trans. Ind. Electron.*, vol. 60, no. 9, pp. 3752–3765, Sept. 2013.

[81] L. Yin, Z. Zhao, T. Lu, S. Yang, and G. Zou, "An improved DC-link voltage fast control scheme for a PWM rectifier-inverter system," *IEEE Trans. Ind. Appl.*, vol. 50, no. 1, pp. 462–473, Jan. 2014.

[82] W. Wu, Y. He, and F. Blaabjerg, "An LLCL power filter for single-phase grid-tied inverter," *IEEE Trans. Power Electron.*, vol. 27, no. 2, pp. 782–789, Feb. 2012.

[83] M. Liserre, A. Aquila, and F. Blaabjerg, "Genetic algorithm-based design of the active damping for an LCL-filter three-phase active rectifier," *IEEE Trans. Power Electron.*, vol. 19, no. 1, pp. 76–86, Jan. 2004.

[84] R. Peña Alzola, M. Liserre, F. Blaabjerg, R. Sebastián, J. Dannehl, and F.W. Fuchs, "Analysis of the passive damping losses in LCL-filter-based grid converters," *IEEE Trans. Power Electron.*, vol. 28, no. 6, pp. 2642–2646, Jun. 2013.

[85] W. Wu, Y. He, T. Tang, and F. Blaabjerg, "A new design method for the passive damped LCL and LLCL filter-based single-phase grid-tied inverter," *IEEE Trans. Ind. Electron.*, vol. 60, no. 10, pp. 4339–4350, Oct. 2013.

[86] L.M. Moore and H.N. Post, "Five years of operating experience at a large, utility-scale photovoltaic generating plant," *Progr. Photovoltaics, Res. Appl.,*, vol. 16, no. 3, pp. 249–259, 2008.

[87] A. Wintrich, U. Nicolai, W. Tursky, and T. Reimann, *Application manual power semiconductors.* ISLE-Verlag, 2011.

[88] ABB, "Application note: Thermal design and temperature ratings of IGBT modules," [Online]. Available: http://www.abb.com/semiconductors, Oct. 2011.

[89] Y. Yang, H. Wang, F. Blaabjerg, and K. Ma, "Mission profile based multi-disciplinary analysis of power modules in single-phase transformerless photovoltaic inverters," in *Proc. of EPE'13 ECCE Europe*, pp. 1-10, 2-6 Sept. 2013.

[90] K. Ma and F. Blaabjerg, "Modulation methods for neutral-point-clamped wind power converter achieving loss and thermal redistribution under low-voltage ride-through," *IEEE Trans. Ind. Electron.*, vol. 61, no. 2, pp. 835–845, Feb. 2014.

[91] H. Wang, Y. Yang, and F. Blaabjerg, "Reliability-oriented design and analysis of input capacitors in single-phase transformerless photovoltaic inverters," in *Proc. of APEC'13*, pp. 2929-2933, Mar. 2013.

[92] R.M. Santos Filho, P.F. Seixas, P.C. Cortizo, L.A.B. Torres, and A.F. Souza, "Comparison of three single-phase PLL algorithms for UPS applications," *IEEE Trans. Ind. Electron.*, vol. 55, no. 8, pp. 2923–2932, Aug. 2008.

[93] S. Golestan, M. Monfared, F.D. Freijedo, and J.M. Guerrero, "Design and tuning of a modified power-based PLL for single-phase grid-connected power conditioning systems," *IEEE Trans. Power Electron.*, vol. 27, no. 8, pp. 3639–3650, 2012.

[94] S.A. Khajehoddin, M. Karimi-Ghartemani, A. Bakhshai, and P. Jain, "A power control method with simple structure and fast dynamic response for single-phase grid-connected DG systems," *IEEE Trans. Power Electron.*, vol. 28, no. 1, pp. 221–233, 2013.

[95] M. Ciobotaru, R. Teodorescu, and F. Blaabjerg, "A new single-phase PLL structure based on second order generalized integrator," in *Proc. of PESC'06*, pp. 1-6, Jun. 2006.

[96] M. Ciobotaru, "Reliable grid condition detection and control of single-phase distributed generation systems," Ph.D. Thesis, Department of Energy Technology, Aalborg University, Jan. 2009.

[97] F. Chan and H. Calleja, "Design strategy to optimize the reliability of grid-connected PV systems," *IEEE Trans. Ind. Electron.*, vol. 56, no. 11, pp. 4465–4472, Nov. 2009.

[98] F. Chan and H. Calleja, "Reliability estimation of three single-phase topologies in grid-connected PV systems," *IEEE Trans. Ind. Electron.*, vol. 58, no. 7, pp. 2683–2689, Jul. 2011.

[99] S. Harb and R.S. Balog, "Reliability of candidate photovoltaic module-integrated-inverter (PV-MII) topologies: A usage model approach," *IEEE Trans. Power Electron.*, vol. 28, no. 6, pp. 3019–3027, Jun. 2013.

[100] S.E. De León-Aldaco, H. Calleja, F. Chan, and H.R. Jiménez-Grajales, "Effect of the mission profile on the reliability of a power converter aimed at photovoltaic applications: A case study," *IEEE Trans. Power Electron.*, vol. 28, no. 6, pp. 2998–3007, Jun. 2013.

[101] The MathWorks, Inc., "MATLAB Documentaion Center: R2013b," [Online]. Available: http://www.mathworks.se/help/, Sept. 2013.

[102] H. Wang, H.S.-H. Chung, and W. Liu, "Use of a series voltage compensator for reduction of the DC-link capacitance in a capacitor-supported system," *IEEE Trans. Power Electron.*, vol. 29, no. 3, pp. 1163–1175, Mar. 2014.

[103] I.F. Kovačević, U. Drofenik, and J.W. Kolar, "New physical model for lifetime estimation of power modules," in *Proc. of IPEC*, pp. 2106-2114, Jun. 2010.

[104] C. Busca, R. Teodorescu, F. Blaabjerg, S. Munk-Nielsen, L. Helle, T. Abeyasekera, and P. Rodriguez, "An overview of the reliability prediction related aspects of high power IGBTs in wind power applications," *Microelectronics Reliability*, vol. 51, no. 9–11, pp. 1903–1907, 2011.

[105] A.T. Bryant, P.A. Mawby, P.R. Palmer, E. Santi, and J.L. Hudgins, "Exploration of power device reliability using compact device models and fast electrothermal simulation," *IEEE Trans. Ind. Appl.*, vol. 44, no. 3, pp. 894–903, May 2008.

[106] M. Musallam and C.M. Johnson, "An efficient implementation of the rainflow counting algorithm for life consumption estimation," *IEEE Trans. Reliability*, vol. 61, no. 4, pp. 978–986, Dec. 2012.

[107] U. Scheuermann, "Pragmatic bond wire model," ECPE Workshop, 3-4 Jun. 2013.

[108] "IEEE recommended practice for utility interface of photovoltaic (PV) systems," *IEEE Std 929-2000*, Jan. 2000.

[109] H. Alatrash, R.A. Amarin, and L. Cheung, "Enabling large-scale PV integration into the grid," in *Proc. of IEEE Green Technologies Conf.*, pp. 1-6, 19-20 Apr. 2012.

[110] M. Marten, J. von Appen, and M. Braun, "German perspectives on future energy system challenges by photovoltaic," [Online]. Available: http://www.twenties-project.eu/, Jan. 2013.

[111] T. Fawzy, D. Premm, B. Bletterie, and A. Gorsek, "Active contribution of PV inverters to voltage control – from a smart grid vision to full-scale implementation," *e & i Elektrotechnik und Informationstechnik*, vol. 128, no. 4, pp. 110–115, 2012.

[112] I. Serban and C. Marinescu, "Enhanced control strategy of three-phase battery energy storage systems for frequency support in microgrids and with uninterrupted supply of local loads," *IEEE Trans. Power Electron.*, vol. 29, no. 9, pp. 5010– 5020, Sept. 2014.

[113] H. Gaztanaga, J. Landaluze, I. Etxeberria-Otadui, A. Padros, I. Berazaluce, and D. Cuesta, "Enhanced experimental PV plant grid-integration with a MW lithium-ion energy storage system," in *Proc. of ECCE*, pp. 1324-1329, Sept. 2013.

[114] V. Cecchi, S. Kamalasadan, J. Enslin, and M. Miller, "Grid impacts and mitigation measures for increased PV penetration levels using advanced PV inverter regulation," in *Proc. of ECCE*, pp. 561-568, Sept. 2013.

[115] M. Datta, T. Senjyu, A. Yona, T. Funabashi, and C.-H. Kim, "A frequency-control approach by photovoltaic generator in a PV-diesel hybrid power system," *IEEE Trans. Energy Convers.*, vol. 26, no. 2, pp. 559–571, Jun. 2011.

[116] H. Xin, Y. Liu, Z. Wang, D. Gan, and T. Yang, "A new frequency regulation strategy for photovoltaic systems without energy storage," *IEEE Trans. Sustainable Energy*, vol. 4, no. 4, pp. 985–993, Oct. 2013.

[117] T. Stetz, F. Marten, and M. Braun, "Improved low voltage grid-integration of photovoltaic systems in Germany," *IEEE Trans. Sustain. Energy*, vol. 4, no. 2, pp. 534–542, Apr. 2013.

[118] E. Dall'Anese, S.V. Dhople, and G.B. Giannakis, "Optimal dispatch of photovoltaic inverters in residential distribution systems," *IEEE Trans. Sustain. Energy*, vol. 5, no. 2, pp. 487–497, Mar. 2014.

[119] H. Beltran, E. Perez, N. Aparicio, and P. Rodriguez, "Daily solar energy estimation for minimizing energy storage requirements in PV power plants," *IEEE Trans. Sustain. Energy*, vol. 4, no. 2, pp. 474–481, Apr. 2013.

[120] H. Beltran, E. Bilbao, E. Belenguer, I. Etxeberria-Otadui, and P. Rodriguez, "Evaluation of storage energy requirements for constant production in PV power plants," *IEEE Trans. Ind. Electron.*, vol. 60, no. 3, pp. 1225–1234, Mar. 2013.

[121] R. Majumder, "Reactive power compensation in single-phase operation of microgrid," *IEEE Trans. Ind. Electron.*, vol. 60, no. 4, pp. 1403–1416, Apr. 2013.

[122] S. Munir and Y.W. Li, "Residential distribution system harmonic compensation using PV interfacing inverter," *IEEE Trans. Smart Grid,*, vol. 4, no. 2, pp. 816–827, Jun. 2013.

[123] M. Saitou and T. Shimizu, "Generalized theory of instantaneous active and reactive powers in single-phase circuits based on Hilbert transform," in *Proc. of PESC'02*, vol. 3, pp. 1419-1424, 2002.

[124] R. Carnieletto, D.I. Brandão, F.A. Farret, M.G. Simões, and S. Suryanarayanan, "Smart grid initiative: A multifunctional single-phase voltage source inverter," *IEEE Ind. Appl. Mag.*, vol. 17, no. 5, pp. 27–35, 2011.

[125] M. Jang, M. Ciobotaru, and V.G. Agelidis, "A single-phase grid-connected fuel cell system based on a boost-inverter," *IEEE Trans. Power Electron.*, vol. 28, no. 1, pp. 279–288, 2013.

[126] W. Lu, K. Zhou, D. Wang, and M. Cheng, "A general parallel structure repetitive control scheme for multiphase DC/AC PWM converters," *IEEE Trans. Power Electron.*, vol. 28, no. 8, pp. 3980–3987, Aug. 2013.

[127] L.P. Sampaio, M.A.G. de Brito, G. de Azevedo e Melo, and C.A. Canesin, "Power flow control in single-phase and three-phase grid-connected inverters using LMI, state-feedback linearization and D-stability," in *Proc. of EPE'13*, pp. 1-10, 2013.

[128] R.A. Mastromauro, M. Liserre, T. Kerekes, and A. Dell'Aquila, "A single-phase voltage-controlled grid-connected photovoltaic system with power quality conditioner functionality," *IEEE Trans. Ind. Electron.*, vol. 56, no. 11, pp. 4436–4444, Nov. 2009.

[129] Y. Yang, H. Wang, and F. Blaabjerg, "Reactive power injection strategies for single-phase photovoltaic systems considering grid requirements," in *Proc. of APEC'14*, pp. 371-378, Mar. 2014.

[130] Y. Yang and F. Blaabjerg, "A new power calculation method for single-phase grid-connected systems," in *Proc. of ISIE*, pp. 1-6, May 2013.

[131] M.C. Kisacikoglu, B. Ozpineci, and L.M. Tolbert, "EV/PHEV bidirectional charger assessment for V2G reactive power operation," *IEEE Trans. Power Electron.*, vol. 28, no. 12, pp. 5717–5727, 2013.

[132] D. Maxwell, "Parts of Northern Ireland's electricity grid overloaded," *BBC News*, [Online]. Available: http://www.bbc.co.uk/, 13 Nov. 2013.

[133] A. Ahmed, L. Ran, S. Moon, and J.-H. Park, "A fast PV power tracking control algorithm with reduced power mode," *IEEE Trans. Energy Conversion*, vol. 28, no. 3, pp. 565–575, 2013.

[134] Fraunhofer ISE, "Recent facts about photovoltaics in Germany," [Online]. Available: http://www.pv-fakten.de/, 10 Apr. 2014.

[135] D. Rosenwirth and K. Strubbe, "Integrating variable renewables as Germany expands its grid," [Online]. Available: http://www.renwableenergyworld.com/, Mar. 2013.

[136] G. Mokhtari, A. Ghosh, G. Nourbakhsh, and G. Ledwich, "Smart robust resources control in LV network to deal with voltage rise issue," *IEEE Trans. Sustain. Energy*, vol. 4, no. 4, pp. 1043–1050, 2013.

[137] R. Caldon, M. Coppo, and R. Turri, "Distributed voltage control strategy for LV networks with inverter-interfaced generators," *Electric Power Systems Research*, vol. 107, pp. 85–92, 2014.

[138] Y. Miyamoto, "Technology for high penetration residential PV systems on a distribution line in Japan," in *Proc. of the fifth Int'l Conf. on Integration of Renewable and Distibuted Energy Resources*, 4-6 Dec. 2012.

[139] G. Kaestle and T.K. Vrana, "Improved requirements for the connection to the low voltage grid," in *Proc. of CIRED*, pp. 1-5, 6-9 Jun. 2011.

[140] A. Hoke and D. Maksimovic, "Active power control of photovoltaic power systems," in *Proc. of SusTech'13*, pp. 70-77, 2013.

[141] F. Blaabjerg and K. Ma, "Future on power electronics for wind turbine systems," *IEEE Journal of Emerging and Selected Topics in Power Electronics*, vol. 1, no. 3, pp. 139–152, 2013.

[142] ENERGINET.DK, "Wind power plants with a power output greater than 11 kW," *Technical Regulation 3.2.5*, Sept. 2010.

[143] J. Cochran, L. Bird, J. Heeter, and D.J. Arent, "Integrating variable renewable energy in electric power markets: Best practices from international experience," National Renewable Energy Laboratory (NREL), Golden, CO, USA, Tech. Rep., Apr. 2012.

[144] T. Thien, R. Alvarez, Z. Cai, P. Awater, M. Leuthold, A. Moser, and D.U. Souer, "Storage- and grid expansion needs in a European electricity-supply-system with a high share of renwable energy," in *Proc. of IRES'12*, pp. 656-663, Nov. 2012.

[145] Energy Magazine, "Smart energy SMA sunny boy inverter and build 'all in one'," [Online]. Available: http://www.energmagazine.it/, 9 May 2014.

[146] G. Hoffmann, "Intelligent PV- Technologies, costs and potential," in *Proc. of IRES'12*, pp. 976-1009, Nov. 2012.

[147] R. Doelling, "Greater economic viability with smaller storage capacities?" [Online]. Available: http://www.solarenergystorage.org/en/, 2013.

[148] J. Traube, F. Lu, D. Maksimovic, J. Mossoba, M. Kromer, P. Faill, S. Katz, B. Borowy, S. Nichols, and L. Casey, "Mitigation of solar irradiance intermittency in photovoltaic power systems with integrated electric-vehicle charging functionality," *IEEE Trans. Power Electron.*, vol. 28, no. 6, pp. 3058–3067, 2013.

[149] L. Nousiainen, J. Puukko, A. Mäki, T. Messo, J. Huusari, J. Jokipii, J. Viinamäki, D.T. Lobera, S. Valkealahti, and T. Suntio, "Photovoltaic generator as an input source for power electronic converters," *IEEE Trans. Power Electron.*, vol. 28, no. 6, pp. 3028–3038, 2013.

[150] D. Sera, L. Mathe, T. Kerekes, S.V. Spataru, and R. Teodorescu, "On the perturb-and-observe and incremental conductance MPPT methods for PV systems," *IEEE Journal of Photovoltaics*, vol. 3, no. 3, pp. 1070–1078, 2013.

[151] E. Malashenko, S. Appert, and W. al-Mukdad, "Advanced inverter technologies report," California Public Utilities Commission, pp. 1-13, 2013.

[152] D. Wagenitz, A. Hambrecht, and S. Dieckerhoff, "Lifetime evaluation of IGBT power modules applying a nonlinear saturation voltage observer," in *Proc. of CIPS 2012*, pp. 1-5, Mar. 2012.

[153] K. Ma, M. Liserre, and F. Blaabjerg, "Reactive power influence on the thermal cycling of multi-MW wind power inverter," *IEEE Trans. Ind. Appl.*, vol. 49, no. 2, pp. 922–930, Mar. 2013.

Appendix A

Control Structure and System Parameters

1. Control of a single-stage single-phase system

This control structure for a single-phase full-bridge system have been used to test the PLL systems and the LVRT performance [19, 47], as it is shown in Figure A.1. The PV panels have been replaced with a DC source on the assumption that the MPPT control is robust, except for the cases which are specified (e.g. Figure 4.13, where the BP 365 PV panels [64] are used). The system parameters are shown in Table A.1. In the normal operation mode, the power references are $P^* = P_n$ (or P_{MPP}) and $Q^* = 0$ Var. In the LVRT operation mode, the power references are generated according to the voltage sag depth (the grid voltage amplitude is monitored).

The control of the selected transformerless inverter systems is similar to the control of a full-bridge system, and the differences are the modulation schemes. As it is shown in Figure A.2, an LCL-filter is adopted with $L_2 = 708$ μH. The power rating is 2.99 kW and the DC-link voltage is 405 V for the efficiency and thermal loading comparison in long term mission profiles shown in Chapter 3. This system has also been used to test the thermal optimized control strategy, where the power rating is 3 kW and the initial temperature is 50 °C. For the LVRT and leakage currents under grid faults shown in § 4.3.3, the power rating is 1 kW and the DC-link voltage is 400 V. The other parameters are the same as listed in Table A.1.

2. Control of a double-stage single-phase full-bridge system

Figure A.3 shows the hardware schematic and control structure of a two-stage single-phase PV system, which has been used to test the performance of the DC-link capacitors under long term mission profiles (Figure 3.13) and the effectiveness of the CPG control strategy (Chapter 5). The system parameters have been given in Table A.2.

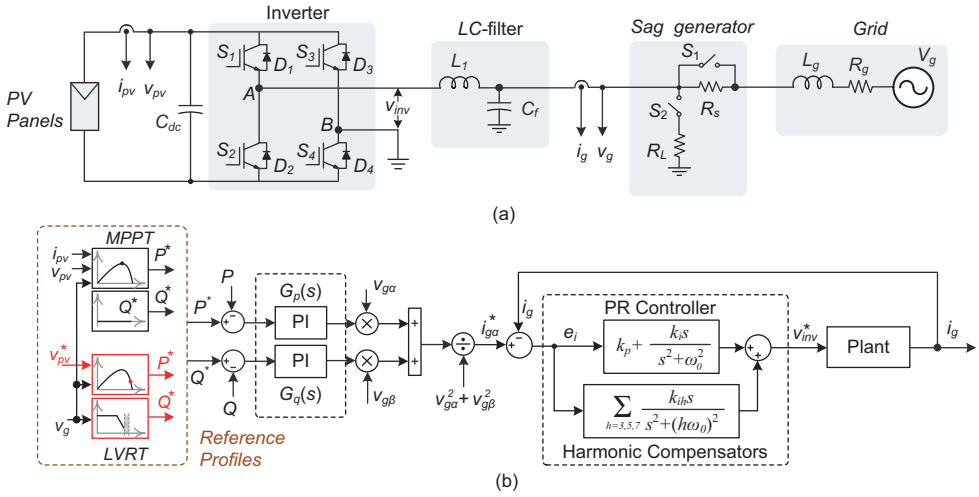

Figure A.1: *Hardware schematic and control structure of a single-phase full-bridge PV system: (a) system configuration and (b) control block diagram.*

Table A.1: *System parameters of a single-phase PV system*

Parameter	Symbol	Value	Unit
Nominal power	P_n	1000	W
Grid voltage (RMS)	v_g	230	V
Grid frequency	ω_0	$2\pi\times50$	rad/s
DC-link capacitor	C_{dc}	1100	μF
DC-link voltage	v_{dc}/v_{pv}	400±5	V
Grid impedance	L_g	4	mH
	R_g	0.02	Ω
LC-filter	L_1	3.6	mH
	C_f	2.35	μF
Sampling & switching frequency	f_s, f_{sw}	10	kHz
Sag generator	R_S	19.3	Ω
	R_L	20	Ω
Active power controller ($G_p(s) = K_{pp} + K_{pi}/s$)	K_{pp}	1.5	-
	K_{pi}	52	-
Reactive power controller ($G_q(s) = K_{qp} + K_{qi}/s$)	K_{qp}	1	-
	K_{qi}	50	-
PR controller	k_p	22	-
	k_i	2000	-
Harmonic compensator (MRC controller)	k_{ih}	5000	-

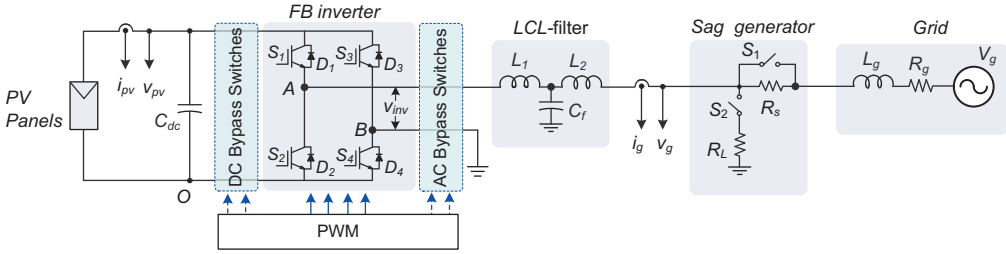

Figure A.2: *Hardware schematic of the selected transformerless PV inverters.*

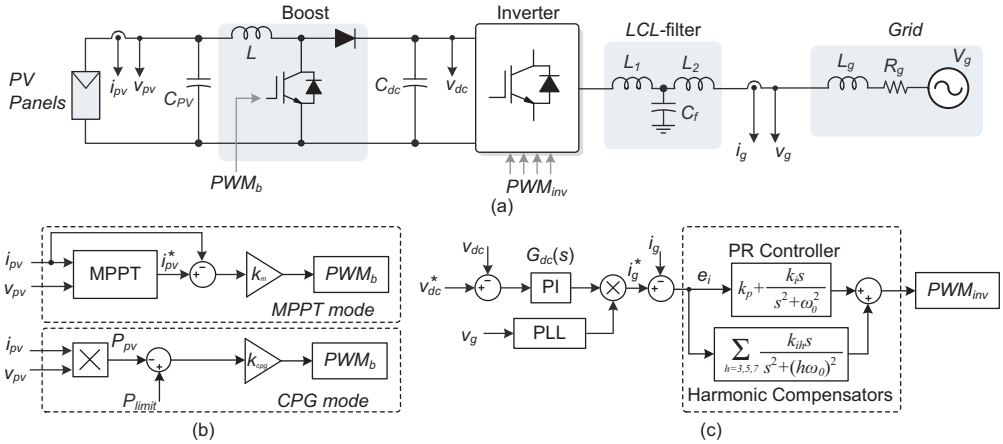

Figure A.3: *Hardware schematic and control structure of a double-stage single-phase full-bridge system: (a) system configuration, (b) boost converter control block diagram (MPPT mode and CPG mode), and (c) inverter control block diagram.*

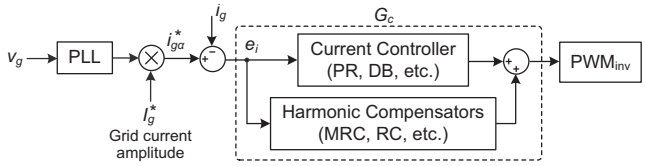

Figure A.4: *Single-loop current control structure of a single-phase full-bridge system.*

Table A.2: *System parameters of a double-stage single-phase full-bridge PV system*

Parameter	Symbol	Value	Unit
Nominal power	P_n	3000	W
Grid voltage (RMS)	v_g	230	V
Grid frequency	ω_0	$2\pi\times50$	rad/s
DC-link voltage	v_{dc}^*	400	V
PV-side capacitor	C_{PV}	2200	μF
DC-link capacitor	C_{dc}	2200	μF
Boost converter inductor	L	5	mH
Grid impedance	L_g	2	mH
	R_g	0.02	Ω
LCL-filter	L_1	2	mH
	C_f	4.7	μF
	L_2	3	mH
Sampling & switching frequency for boost and the inverter	$f_s,\ f_{sw}$	10	kHz
MPPT mode controller	k_m	23.8	-
CPG mode controller	k_{cpg}	0.1	-
DC-link controller (PI) $(G_{dc}(s) = k_{p0} + k_{p0}/s)$	k_{p0}	0.1	-
	k_{i0}	1.25	-
PR controller	k_p	20	-
	k_i	2000	-
Harmonic compensator (MRC controller)	k_{ih}	5000	-

3. Current controllers for single-phase single-stage systems

Referring to Figure A.1, a single-loop current control structure of a single-phase PV system is shown in Figure A.4 in order to test the current performance in terms of harmonic suppression ability (§ 4.2.3). The system parameters have been given in Table A.1, where the grid current amplitude reference I_g^* has been set to be 5 A. The control parameters of the current controllers compared in Table 4.2 and Figure 4.9 are given in Table A.1, except for the RC controller, whose control parameters have been shown in Table A.3.

Table A.3: *Control parameters of the RC controller (Table 4.2 and Figure 4.9).*

Parameter	Symbol	Value
RC control gain	k_{rc}	1.8
Phase-lead compensator step	m	3
Low pass filter $(Q(z) = \alpha_1 z^{-1} + (1 - 2\alpha_1) + \alpha_1 z)$	α_1	0.05

Appendix B

Experimental Setup and System Parameters

1. Single-stage single-phase grid-connected full-bridge system

Figure B.1 shows the experimental setups of a single-phase grid-connected system in different operation mode. In the case of fault ride-though operation, Setup 1 uses a resistor based fault generator (Figures A.1 and A.2) to generate a voltage sag; while in the Setup 2, a programme AC power source is used, which can produce different types of voltage disturbances. The parameters of those test setups are shown in Table A.1, where the transformer leakage inductor is taken as the grid impedance shown in Figures A.1 and A.2. All the control strategies are developed in MATLAB/Simulink, and they have been implemented in the dSAPCE DS1103 control system, which also provides an user-friendly interface (Control Desk) to monitor and control the entire system, as it is shown in Figure B.1. Figure B.2 shows the photos of those two setups.

2. Single-phase three-level NPC PV inverter system

The thermal optimized control strategy (Chapter 6) is verified on a three-level three-phase NPC converter. The PV inverter is controlled by a dSPACE DS1006 system, as it is shown in the control diagram in Figure B.3(a). A photo of this test setup is shown in Figure B.3. The system parameters are given in Table B.1. In order to verify the effectiveness of the junction temperature control through power control, the system has been tested under different power factors by changing the variable inductor load L and resistor load R. The corresponding load parameters are shown in Table B.2 in accordance to Table 6.2 and Figure 6.10.

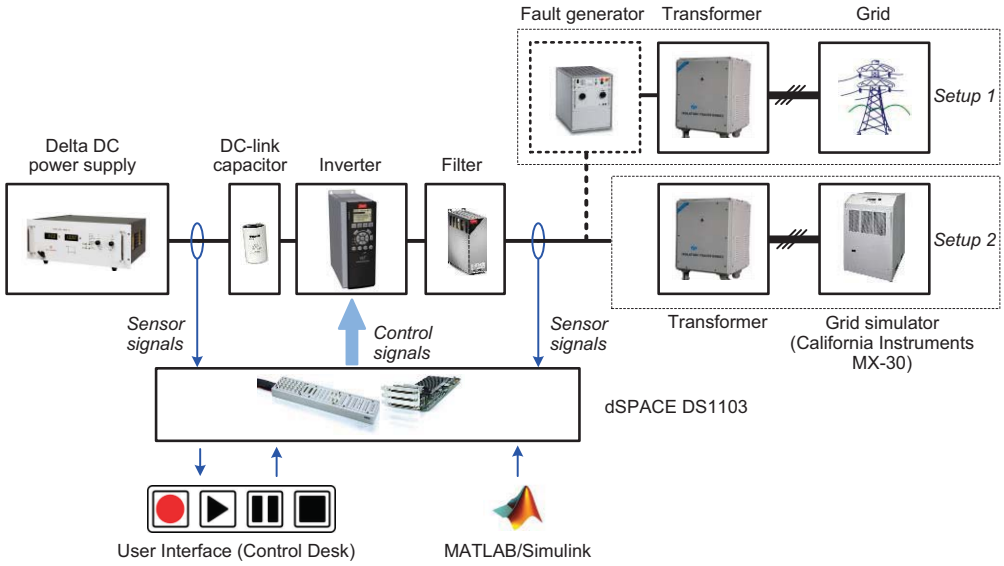

Figure B.1: *Setup configurations of a single-phase grid-connected full-bridge system.*

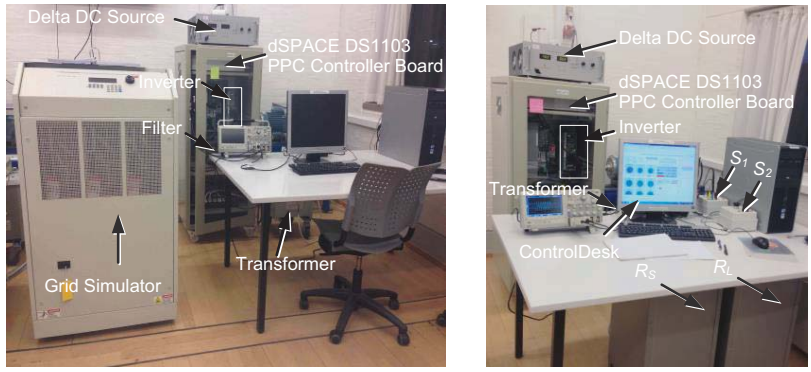

Figure B.2: *Experimental setups of a single-phase grid-connected full-bridge system: (a) with a fault generator (Setup 1 in Figure B.1) and (b) with the grid simulator (Setup 2 in Figure B.1).*

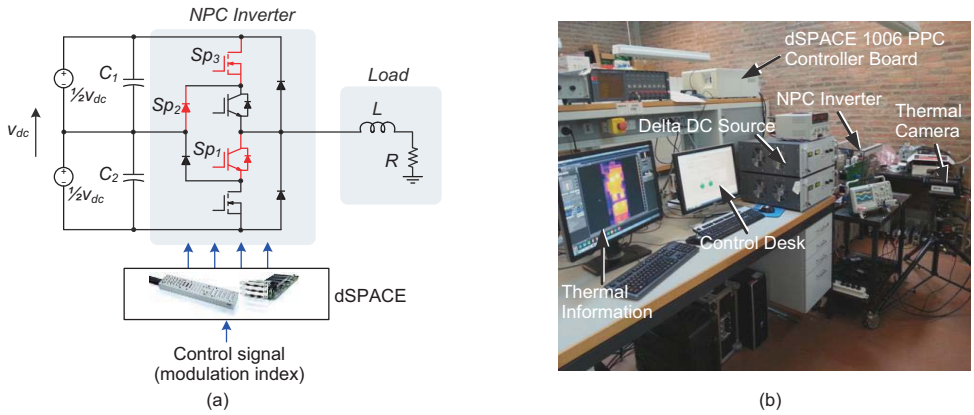

Figure B.3: *Experimental setup of a three-level NPC PV inverter: (a) open-loop control diagram with resistive-inductive load and (b) photo of the test setup.*

Table B.1: *System parameter of a three-level NPC PV inverter.*

Parameter	Symbol	Value	Unit
Modulation index	m	0.81	-
DC-link voltage	v_{dc}	400	V
DC-link capacitor	C_1, C_2	2700	μF
Switching frequency	f_{sw}	20	kHz

Table B.2: *Load parameters for the thermal tests on a three-level NPC PV inverter.*

Test no.	Power factor	Inductor L (mH)	Resistor R (Ω)
1	0.4538	100	16
2	0.8955	50	31.6
3	0.9996	3	31.6

Selected Publications

Journal Papers

There are eight journal papers and three contributed book chapters published (accepted) till now. Five journal papers were evaluated by the PhD Thesis Assessment Committee. One co-authored journal paper submitted to IEEE Transactions on Power Electronics is in review.

Publication 1

(*Journal Paper*)

Low-voltage ride-through capability of a single-stage single-phase photovoltaic system connected to the low-voltage grid

Yongheng Yang and Frede Blaabjerg

The paper has been published in the
International Journal of Photoenergy, vol. 2013, pp. 1–9, Feb. 2013.
Open Access. Available at: http://www.hindawi.com/journals/ijp.

DOI:10.1155/2013/257487

Publication 2

(*Journal Paper*)

Benchmarking of grid fault modes in single-phase grid-connected photovoltaic systems

Yongheng Yang, Frede Blaabjerg, and Zhixiang Zou

The paper has been published in the
IEEE Transactions on Industry Applications, vol. 49, no. 5, pp. 2167–2176, Sept.-Oct. 2013.

DOI:10.1109/TIA.2013.2260512

Publication 3

(*Journal Paper*)

Low voltage ride-through of single-phase transformerless photovoltaic inverters

Yongheng Yang, Frede Blaabjerg, and Huai Wang

The paper has been published in the
IEEE Transactions on Industry Applications, vol. 50, no. 3, pp. 1942–1952, May-Jun., 2014.

DOI:10.1109/TIA.2013.2282966

Publication 4

(*Journal Paper*)

Suggested grid code modifications to ensure wide-scale adoption of photovoltaic energy in distributed power generation systems

Yongheng Yang, Prasad Enjeti, Frede Blaabjerg, and Huai Wang

The paper has been accepted in the
IEEE Industry Applications Magazine (also presented in part at the 48th Annual Meeting of the IEEE Industry Applications Society, IAS Annual Meeting 2013, Orlando, FL, USA), in press, Sept.-Oct. 2015.

DOI:10.1109/IAS.2013.6682485

Publication 5

(*Journal Paper*)

Reduced junction temperature control during low-voltage ride-through for single-phase photovoltaic inverters

Yongheng Yang, Huai Wang, and Frede Blaabjerg

The paper has been published in the
IET Power Electronics, vol. 7, no. 8, pp. 2050-2059, Aug. 2014.

DOI:10.1049/iet-pel.2013.0734

Publication 6

(*Journal Paper*)

Reactive power injection strategies for single-phase photovoltaic systems considering grid requirements

Yongheng Yang, Huai Wang, and Frede Blaabjerg

The paper has been accepted in the
IEEE Transactions on Industry Applications (also presented in part at the 29th Applied Power Electronics Conference and Exposition, APEC 2014, Fort Worth, TX, 2014), vol. 50, no. 6, in press, Nov.-Dec. 2014.

DOI:10.1109/TIA.2014.2346692

Publication 7

(*Journal Paper*)

A hybrid power control concept for PV inverters with reduced thermal loading

Yongheng Yang, Huai Wang, Frede Blaabjerg, and Tamas Kerekes

The paper has been published in the
IEEE Transactions on Power Electronics (also presented in part at the 29th Applied Power Electronics Conference and Exposition, APEC 2014, Fort Worth, TX, 2014), vol. 29, no. 12, pp. 6271-6275, Dec. 2014.

DOI:10.1109/TPEL.2014.2332754

Conference Contributions

There are more than ten conference papers published (accepted) till now as the main author. Besides, there are more than twelve co-authored conference contributions published (accepted) till now, and some of them have been submitted to journals for peer review. Four conference papers were evaluated by the PhD Thesis Assessment Committee, and two of them have been published (accepted) in journals.

Publication 8

(*Conference Contribution*)

Harmonics suppression for single-phase grid-connected photovoltaic systems in different operation modes

Yongheng Yang, Keliang Zhou, and Frede Blaabjerg

The paper has been published in the
Proceedings of the 28th *Annual IEEE Applied Power Electronics Conference and Exposition (APEC 2013)*, pp. 889–896, Mar. 2013.

DOI:10.1109/APEC.2013.6520316

Publication 9

(*Conference Contribution*)

Mission profile based multi-disciplinary analysis of power modules in single-phase transformerless photovoltaic inverters

Yongheng Yang, Huai Wang, Frede Blaabjerg, and Ke Ma

The paper has been published in the
Proceedings of the 15^{th} *Conference on Power Electronics and Applications (EPE'13 ECCE Europe)*, pp. 1–10, Sept. 2013.

DOI:10.1109/EPE.2013.6631986

TRYK: UNIPRINT AAU

ISBN 978-87-92846-40-2